A study of the physics of sea-land breezes with particular applications to Hong Kong

NGAN Shiu Fai

A Thesis Submitted in Partial Fulfillment
of the Requirements for the Degree of
Master of Philosophy
in
Physics

The Chinese University of Hong Kong
August 2000

Abstract

Sea-land breeze circulation can be regarded as a kind of forced inertio-gravity oscillation, thermally driven by the spatially uneven distribution of heating which varies in time in the course of a day.

In light of this, a three-dimensional linear atmospheric model is developed, which starts with the different heating rates over land and sea, and attempts to capture the influence of the coastline pattern on the circulation system.

Using the model, we have performed a semi-analytic harmonic analysis, in which the sea-land breeze circulation is viewed as a resultant flow of modes with different time and length scales.

From the model, we see that the basic structure of the circulation is determined by the fundamental spatial mode. Furthermore the model reveals that the sinking of the return flow results in the onset of a breeze phase. It also reveals that the time of onset of the sea-breeze phase over an island is related to the island size.

When we apply the model to the case of Hong Kong, the following conclusion are drawn.

According to the meteorological statistics, Hong Kong is often subject to the influence of sea-land breezes, with the highest frequency in winter and autumn. The modeling result confirms that in the sea-breeze phase, there are three wind branches, leading to various convergence zones. Both the sun-facing slopes and the urban heat islands effects are also studied.

A statistical study on the association of the spatial rainfall distribution in

Hong Kong with the average vertical motion due to sea-land breeze circulation is performed. It shows that they are correlated in autumn and in winter.

The treatment and the mathematical approach of the model go beyond the sea-land breeze application; it can be used to study other thermally driven secondary circulation.

Submitted by NGAN Shiu Fai

for the degree of Master of Philosophy in Physics

at The Chinese University of Hong Kong in August 2000

Acknowledgements

I would like to express my wholehearted gratitude to Prof. Kenneth Young. He has given me invaluable guidance, countless comments and encouragement throughout the project. Without his patience and encouragement, the work would definitely never be finished.

I would like to thank Prof. Zhang Ming, Institute of Atmosphere Science, the Chinese Academy of Science, and for his marvelous guidance and suggestions in this work. I acknowledge my special debt to his guidance on the meteorology and numerical methods. In addition, I would like to thank Prof. Zhang Lifeng for her valuable discussions on the phenomenon and other meteorological events.

I would also like to thank Mr Lam Chiu Ying and Mr Poon Hoi To of the Hong Kong Observatory for their valuable advice and discussions. Special thanks are due to Mr Wong Wai Kin, Mr Lee Kwok Lun, Mr Armstrong Cheng Yuen Chung, all of the Hong Kong Observatory and Mr Lam Wun Yuen. They have provided me with much help and support.

Last of all, I would like to express my gratefulness Dr Chu Ming Chung and Dr Lee Kai Ming for their inspiring discussions on many topics in physics; and to Miss Yip Ching Wa, Mr Cheung Hong Yung and Mr Lai Chi Wai for their warm encouragement throughout the study. Their sincerity is greatly appreciated.

Contents

List of Figures

List of Tables

Chapter 1

Introduction

Coastal areas often experience a wind flow pattern which reverses on a diurnal cycle, in addition to the seasonal cycle. Bodies of water gain and lose heat much more slowly than the land. Consequently, over any 24-hour period the water temperature will remain relatively constant, while the land may be much warmer during the day than the water and somewhat cooler at night. In such cases, air rises over the land during the day, and the cooler air over the sea flows landward (Figure 1.1). At night the air over the water is warmer and rises, and the cooler air over the land flows seaward.

The daytime wind from sea to land is called the *sea breeze*; its reverse is called the *land breeze*. In the tropics sea breezes may occur throughout the year, but

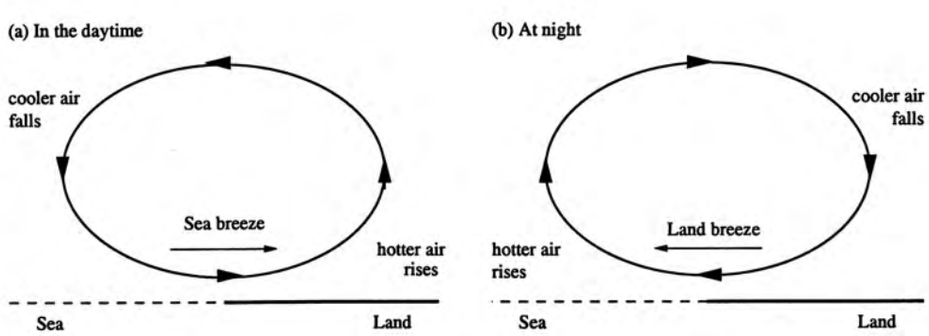

Figure 1.1. Simple diagram showing how a sea-land breeze forms over the coastline: (a) sea breeze in the daytime, and (b) land breeze at night. In the daytime, the land, with a smaller heat capacity, heats up more than the sea. As a result, the air above the land surface is hotter with a lower pressure. Wind then blows from sea to land. At night the situation is reversed, giving rise to the land breeze.

at higher latitudes they are mostly confined to the summer. Sea breezes may generate much rain, more often also foggy conditions as the moisture condenses upon meeting the cooler air near the shore or inland, particularly in the morning when the sea breeze first onsets (Chan and Ng, 1993). The sea breeze phenomenon in summer often makes the coast much cooler than farther inland.

1.1 Observations in Hong Kong

Hong Kong is a small territory of just over 1000 km^2, located at about 22 °N, 114 °E on the south China coast (Figure 1.2). It is bounded to the north by the great land mass of mainland China, to the south and east by the South China Sea, and to the west by Pearl River (Zhujiang) Estuary. Within the territory itself, numerous small hills dominate the landscape, the highest reaching 1000 m above mean sea level.

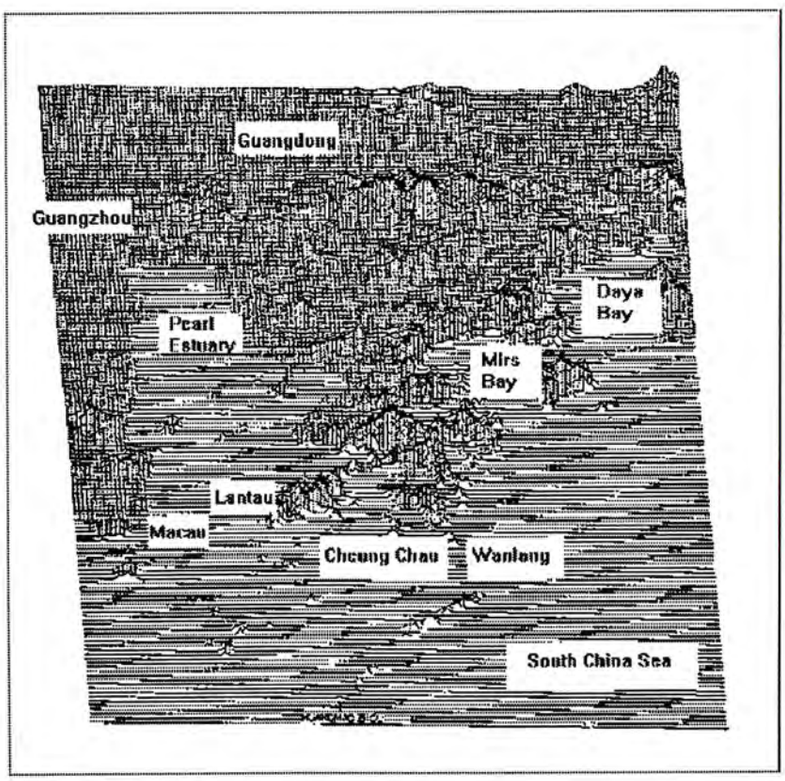

Figure 1.2. Location of the meteorology stations. Three locations were selected for the study: Cheung Chau, Macau and Guangzhou.

There are about 70 sea-land breeze days in a year in Hong Kong, and their importance on local weather forecasting and the study of air pollution is well recognisied (Chan and Ng, 1993; Wai, 1993). However, the phenomenon has received only limited attention so far (Chin, 1963). We are not aware of any comprehensive attempt, in terms of either spatial coverage and record over time, to summarise the systematic characteristics of sea-land breezes observed in Hong Kong. Observations of the breezes usually appear in the literature in connection with more general studies. The number of reports is so few that we may list them all here (Chin, 1963; Jackson and Hsu, 1996; Wai, 1993; Zhang and Zhang, 1997; Chan and Ng, 1993; Wai et al., 1995).

Zhang and Lam (1996) have carried out an observational study, investigating the sea-land breeze system in the Pearl River Estuary over a ten-year period 1980–1989, using daily meteorogram prepared by the Hong Kong Observatory. Unfortunately the project was not completed and only a brief summary has been published as a section of an article (Zhang and Zhang, 1997; 1999). The study, however, covers the longest period and has collected the richest information among the earlier observational studies in Hong Kong. In order to improve the knowledge of the circulation in the area of Hong Kong, the findings are reported and discussed below.

Data selection

Three locations were selected for the study: Cheung Chau, Macau and Guangzhou. Cheung Chau is a tiny rural island in the south of Hong Kong. Several kilometres to its north-west lies Lantau island, the largest island in the territory. Meteorological data are recorded by the automatic station on Cheung Chau. The station is chosen as the representative of Hong Kongi since it is well known that the wind direction at Cheung Chau station is heavily influenced by sea-land breezes (Zhang and Zhang, 1997). Macau sits on the western corner of the Pearl River

Delta. The station is situated on the top of a hill in the eastern part of Taipa Island, near Macau International Airport. Guangzhou station is located 100 km inland from the vertex of the Delta.

The study was concerned with the development of sea-land breezes in this region with a complicated topography. The definition of the breezes used in that study therefore differs slightly from that normally used for a straight coastline.

The principal criterion used to recognize sea-land breezes is the occurrence of a distinct reversal of the surface wind direction within a 24-hour period which cannot be attributed to synoptic-scale circulation features. Diurnal changes in temperature corresponding to the arrival of air from the sea were also monitored. According to the forecasters' experience, it is proposed that the wind speed observed should be within 7 m s^{-1} for sea breeze, and less than 5 m s^{-1} for land breeze in the area. In a period with these diurnal variations, winds starting to blow onshore mark the onset of the sea breeze, while winds offshore signal the arrival of the land breeze. For each day that a sea-land breeze is indicated by this criterion, a closer study was carried out in order to ensure that the observed changes in wind direction and other features are not the result of large-scale synoptic activities.

Annual average

In Hong Kong, sea-land breezes are on average observed 69 days in a year (one day in five). The most frequent occurrence was in 1980, with about three days in ten. The fewest was in 1988, with sea-land breezes reported only one day in ten. The statistics on annual changes of sea-land breezes in Hong Kong for the period of 1980-1989 is presented in Table 1.1.

In general, sea breezes in Hong Kong onset at about noon, and last for about 9 hours (Table 1.2). The time of onset shows little variation from year to year; however, the duration of the sea-breeze phase shows large fluctuations from year

Table 1.1. Number of occurrence of sea-land breezes in Hong Kong for 1980–1989

Sea-land breeze	1980	1981	1982	1983	1984	1985	1986	1987	1988	1989	**Mean**
Frequency[a]	104	69	80	52	64	57	91	53	35	81	**69**

[a]Frequency: Number of sea-land breeze days

Table 1.2. Features of sea breezes in Hong Kong for 1980–1989

Sea breeze	1980	1981	1982	1983	1984	1985	1986	1987	1988	1989	**Mean**
Onset[a]	1100	1148	1142	1206	1224	1148	1142	1218	1148	1124	**1142**
Duration[b]	8.0	8.5	10.9	8.8	6.8	9.2	10.5	7.2	10.1	9.9	**9.0**
MaxSpeed[c]	4.7	3.7	3.5	4.0	3.8	4.1	4.6	4.0	4.2	4.6	**4.1**

[a]Onset: Mean time of onset (LST)

[b]Duration: Mean duration of the breeze phase (hours)

[c]MaxSpeed: Mean maximum strength (m s^{-1})

to year. The longest sea-breeze phase survives an average of about 11 hours in 1982, 25% above the mean, while the shortest annual average is only about 7 hours, 25% below the long-term average.

Sea breezes in Hong Kong are mostly moderate in strength, with fresh winds observed only rarely. The mean maximum speed is found to be about 4 m s^{-1}, ranging from 3.5 m s^{-1} in 1984 to 4.7 m s^{-1} in 1980. Although sea breezes in Hong Kong are not very strong, it is found to play an important role in triggering local rainfall storms under particular conditions (Wai et al., 1995).

The statistics of the land breezes are, unfortunately, not available.

Seasonal distribution

In Hong Kong sea-land breezes occur throughout the year, but most frequently in December and January. These two months account for over a quarter of the annual total. About two-thirds of the breezes are found from September to January,

and about 86% within the months of August to March. The monthly mean number of days in which sea-land breezes are observed in the territory is tabulated in Table 1.3.

Sea-land breezes occur most prominently under clear sky conditions with a weak synoptic wind. In winter, Hong Kong is often influenced by a weak ridge of high pressure over the south China coast and the sky is clear without strong turbulence. Bright sunshine and an absence of clouds (Table 1.4) favour the development of the breezes. In summer, especially in July, Hong Kong is often disturbed by unsettled conditions with low pressure troughs and active southwest monsoon conditions. Spells of rainy weather generally hinder the occurrence of sea-land breezes.

Table 1.3. Monthly mean number of sea-land breeze day for 1980–1989 observed at Cheung Chau (CCH), Macau (MAC) and Guangzhou (GUZ)

	Jan	Feb	Mar	Apr	May	Jun	Jul	Aug	Sep	Oct	Nov	Dec	**Annual**
CCH	9.6	5.2	5.2	3.5	2.7	1.4	1.7	6.1	7.1	7.8	8.6	9.7	**68.6**
MAC	4.0	5.1	6.0	2.2	0.5	0.5	2.5	5.1	7.1	6.0	7.1	9.0	**55.1**
GUZ	0.2	1.0	0.0	0.0	0.2	0.0	0.0	0.0	0.2	0.2	0.2	0.4	**2.4**

Table 1.4. Monthly means of selected meteorological elements observed at Hong Kong for the 30-year period 1961-1990

	Jan	Feb	Mar	Apr	May	Jun	Jul	Aug	Sep	Oct	Nov	Dec	
Sunshine													
Duration[a]	153	98	96	109	154	161	231	207	182	195	182	182	hours
Percentage[b]	45	30	26	29	38	40	56	52	49	54	55	54	%
Cloud[c]	58	73	76	78	74	75	65	66	63	56	53	49	%
SolarRad[d]	11.6	10.7	11.2	13.1	16.1	16.6	19.2	17.6	16.5	15.5	13.4	12.0	MJ m^{-2}

[a]Duration: Total bright sunshine duration [b]Percentage: Percentage of possible bright sunshine duration

[c]Cloud: Amount of cloud [d]SolarRad: Mean daily solar radiation

Element (a), (b) and (c) are observed at King's Park while (d) is obtained at the Hong Kong Observatory.

Sea-breeze phase

In this part, three aspects of the seasonal features are highlighted: the time of onset, the maximum strength and the duration of the phase.

Onset. — The time of onset of sea breezes, averaged over the year, is noon. However, with an earlier sunrise and stronger solar radiation, the onset time is earlier in the summer, e.g., 1000 LST in July. Here LST stands for local standard time. In winter, the later sunrise and weaker solar radiation cause the onset to be delayed, e.g., to 1300 LST in January.

Maximum strength. — The maximum strength of the sea breeze, averaged over the year, is about 4.1 m s^{-1}, occurring at about 1500 LST. The maximum strength is larger in summer than in winter, on account of the longer duration and higher intensity of the solar radiation, which is the driving force for the sea-land breeze circulation. For example, the average maximum strength is 5.4 m s^{-1}in July, versus 2.4 m s^{-1}in January.

Duration. — Again, the intensity and duration of solar radiation cause the duration of the sea-breeze phase to change with the seasons, averaging 8 hours in January versus 12 hours in July.

These and other statistics are recorded in Table 1.5.

Land-breeze phase

We now turn to the land breezes in Hong Kong, concentrating on two aspects: the time of onset and the duration of the phase. The statistics of the wind strength are, unfortunately, not available.

Onset. — The time of onset of land breezes, averaged over the year, is about 2100 LST. In summer, owing to the later sunset, the onset time is delayed, e.g., to 2300 LST in July. In winter, however, the earlier sunset allows the breeze to start an hour earlier in general.

Duration. — In Hong Kong, land breezes last longer than sea breezes re-

Table 1.5. Monthly mean of sea-land breeze elements observed at Cheung Chau for the 10-year period 1980–1989

Sea breeze	Jan	Feb	Mar	Apr	May	Jun	Jul	Aug	Sep	Oct	Nov	Dec	**Annual**
Onset[a]	1300	1300	1200	1200	1100	1200	1000	1100	1200	1200	1300	1300	**1200**
PeakHour[b]	1418	1430	1354	1500	1530	1624	1530	1730	1542	1430	1530	1400	**1511**
Duration[c]	8.0	7.0	8.0	9.0	10.0	11.0	12.0	12.0	9.0	9.0	7.0	7.0	**9.1**
MaxSpeed[d]	2.4	3.0	3.5	5.2	5.2	4.9	5.4	4.6	4.8	4.2	3.4	3.8	**4.2**
Land breeze	**Jan**	**Feb**	**Mar**	**Apr**	**May**	**Jun**	**Jul**	**Aug**	**Sep**	**Oct**	**Nov**	**Dec**	**Annual**
Onset[a]	2100	2000	2000	2100	2100	2300	2200	2300	2100	2100	2000	2000	**2105**
Duration[c]	16.0	15.0	16.0	15.0	14.0	13.0	12.0	12.0	15.0	15.0	17.0	17.0	**14.8**

[a]Onset: Time of onset (LST)
[b]PeakHour: Time of maximum strength (LST)
[c]Duration: Mean duration of the breeze phase (hours)
[d]MaxSpeed: Mean maximum strength (m s^{-1})

gardless of the season. The duration of the land-breeze phase is 14.8 hours on average, ranging from 12 hours in July to 16 hours in January. The statistics shows that land breezes survive longer in winter than in summer, which agrees with the seasonal variation in the length of the night.

These statistics are also presented in Table 1.5.

Spatial variations in the Estuary region

The seasonal distribution of sea-land breezes at Macau is found to be similar to that in Hong Kong, but the occurrence is about 20% less compared to Hong Kong. In Guangzhou, however, only 2–4 occurrences are reported over a year in the last decade, since the station is located about 100 km inland, far from the main coast. (For a discussion on the horizontal extent of sea-land breeze systems, see Chapter 3.) This phenomenon agrees with the earlier observation that there should be fewer instances where sea breezes reach stations far inland (Simpson,

1994). The statistics reported from these two stations are given in Table 1.3 for reference.

Sea and land breezes in Macau on average onset about an hour later than in Hong Kong. The duration of the sea-breeze phase in Macau is 2 hours longer; however the duration is about 3.5 hours shorter for the land-breeze. The seasonal features of the breezes in Macau, as revealed in Table 1.6, are similar to those found in Hong Kong.

Table 1.6. Monthly mean of sea-land breeze elements observed at Macau for 1980–1989

Sea breeze													
	Jan	Feb	Mar	Apr	May	Jun	Jul	Aug	Sep	Oct	Nov	Dec	**Annual**
Onset[a]	1400	1300	1200	1300	1200	1200	1300	1300	1300	1400	1400	1400	**1305**
PeakHour[b]	1600	1430	1330	1530	1548	1600	1800	1830	1530	1830	1812	1736	**1636**
Duration[c]	9.1	9.2	12.0	14.0	14.0	13.0	12.0	11.7	12.0	10.8	10.9	9.7	**11.5**
MaxSpeed[d]	1.2	1.8	2.0	2.3	2.7	3.0	3.0	2.8	2.5	2.0	2.0	1.5	**2.2**
Land breeze													
	Jan	Feb	Mar	Apr	May	Jun	Jul	Aug	Sep	Oct	Nov	Dec	**Annual**
Onset[a]	2300	2300	2400	0100	0200	0100	0000	0100	0000	0000	0000	2300	**2415**
MaxSpeed[c]	15.0	15.0	12.0	10.0	10.0	11.0	12.0	12.0	12.0	13.0	13.0	14.0	**12.4**

[a]Onset: Time of onset (LST)

[b]PeakHour: Time of maximum strength (LST)

[c]Duration: Mean duration of the breeze phase (hours)

[d]MaxSpeed: Mean maximum strength (m s^{-1})

1.2 Review of analytical approach

Studies of the sea-land breeze circulation can be classified into observational studies, analytical studies and numerical modeling. In the following discussion, we shall stress the analytical works.

The phenomenon of sea-land breezes is one of the oldest subjects studied by meteorologists (Halley, 1686). The sea-land breeze circulation has attracted attention from early days[1].

Although the sea-land breeze has been mentioned in the literature since the 17th century, the earliest quantitative study is that of Davis (1889). According to Rotunno (1983), at least two aspects of the report deserve notice. First, the conventional model of sea-land breezes (see the paragraph above and the discussion in Chapter 2) was put into a clear mathematical formulation. Second, the typical rotation of the wind direction was attributed to the rotation of the earth.

An attempt to study sea-land breezes by means of a linear theory began with the work of Jeffreys (1922). However, owing to a significant underestimate of the horizontal scale of the sea breeze, Jeffreys wrongly concluded that the rotation of the earth was not relevant to the dynamics of the sea-land breezes. In his work, Jeffreys took the horizontal scale to be 15 km only, whereas Neumann (1984) noted that the horizontal scale should be about 50 to 150 km[2]. (See Chapter 3.)

The first linear theory that included the effect of the earth's rotation, i.e., the Coriolis effect, is that of Haurwitz (1947). His treatment is generally recognized as an important milestone in sea-land breeze theory. This is a fundamental paper showing that the inclusion of the Coriolis effect can explain the diurnal change in wind direction in a sea-land breeze system. (Rotunno, 1983)

[1]In fact, an attempt to understand the phenomenon at least began with the ancient Greeks. An explicit discussion of the nature of the sea-land breeze is found in the tract *Problemata* attributed to Aristotle (384–322 BC). (Neumann, 1973)

[2]Neumann has also pointed out that Jeffreys's value of 10 m s^{-1} for the wind speed of the sea-land breeze was an overestimate. The wind speed is nearly 5 m s^{-1}, rather than 10 m s^{-1}. However we argue that this inaccuracy is insignificant to the problem at stake.

Since then, many other investigations have been carried out (Niino, 1987; Rotunno, 1983; Smith et al., 1982; Sun and Orlanski, 1981; Yan and Anthes, 1987). Recent attention is also related to the dispersal of air-borne pollutants, which is important for coastal industrial areas (Lu and Turco, 1994).

To model the sea-land breeze realistically in the atmosphere, one has to consider various complex processes, such as heat balance at ground level, heat transfer from the ground, and so on.

Numerical models give a realistic simulation of the actual sea-land breeze circulation in the atmosphere; however they may not help to obtain a physical understanding of the circulation (Simpson, 1994). Despite the necessary simplifications, analytic models are important for the insights they provide.

An excellent historical review of the analytical works that have contributed to the development of the linear theory has been given by Rotunno (1983). Many results of observational, analytic and numerical studies have also been reviewed by Simpson (1994). Here, we only review several works that have direct links with the present study.

In his fundamental report mentioned above, Haurwitz (1947) assumed that the pressure gradient force perpendicular to a straight coastline can be expressed as $-\partial\phi/\partial x$, which remains uniform in space and varies in time periodically with frequency $\omega = 2\pi/T$, where T is one day, and is independent of height. Based on these assumptions, the solution of a linear homogeneous sea-land breeze model was found.

Schmidt (1947) attacked the problem in almost the same way, but instead of assuming the pressure gradient force $-\partial\phi/\partial x$ as a function of t only, he prescribed it as a sinusoidal function of x and t and an exponentially decaying function of the height z. The spatial scale of the solution is thus expected to be prescribed by the assumed behaviour for $\phi(x, z, t)$.

Defant (1951) introduced a more reasonable treatment of the driving force.

Instead of specifying the pressure gradient, he assumed that the perturbation of the surface potential temperature can be written as

$$\theta(x, z = 0, t) = \theta_{max} e^{i\omega t} \sin lx \tag{1.1}$$

where x is the coordinate perpendicular to the coast and z is the vertical height. This parameterisation of the x-dependence is somewhat unphysical. Clearly the surface potential temperature would not be periodic in x, though Defant stressed that the overall flow would be obtained when a number of such harmonics resulting from the Fourier series with different values of l are superimposed.

Walsh (1974) assumed the perturbation of the temperature to be

$$\theta(x, z = 0, t) = \sin \omega t \times \begin{cases} \theta_{max}, & x > 0 \\ -\theta_{min}, & x < 0 \end{cases} \tag{1.2}$$

The step-function profile in x is more realistic, and solutions were found within a linear homogeneous sea-land breeze model. Both of these models start from the temperature, whereas more realistically one should start with the heating rate as the driving force; the time lag between the heating and the temperature rise should be part of the outcome of the model, and important for understanding the time of onset of sea and land breezes.

As mentioned above, Rotunno (1983) has reviewed the development of analytic solutions of linear sea-land breeze models within the context of the shallow, incompressible approximation to the equations of motion (Ogura and Phillips, 1962). By ignoring the frictional force but incorporating the heating rate in an inhomogeneous sea-land breeze model, an analytic solution was obtained.

However, because he ignored the frictional force, the solution has an infinite horizontal scale at latitude 30 °N, where the Coriolis parameter is the same as the diurnal frequency ω. This does not happen in reality (Smith et al., 1982; Niino, 1987; Yan and Anthes, 1987).

Dalu and Pielke (1998) have analyzed a model with both heating and friction (but with the latter assuming the same value on land and on sea). They showed

how friction contributes in controlling the horizontal scale of the circulation, and how the horizontal scale is related to the vertical one.

Young and Zhang (1999) presented a model which starts with different heating rates over the land and the sea, and also incorporates different frictional forces on land and sea. The result reveals that the former drives the entire effect, and all measures of the sea-land breeze circulation is proportional to the differential heating; the latter plays some role in accounting for the difference in the extent of the penetration landwards and seawards.

The models reviewed above all attack the problem of an infinite long straight coastline. Up to now, there have been very few analytical models that attempt to address the effect of an irregular coastline. Only some numerical studies have considered the effect, as well as the non-linear effects (McPherson, 1970).

Our work attempts to develop a model that may reveal the effect of the coastal irregularity on the sea-land breeze circulation. We present the semi-analytical solution as a combination of spatial and temporal harmonics.

The treatment and the mathematical approach, presented below, go beyond the sea-land breeze application (Zhang et al., 1997). For example, it can be used to study the enhancement of convective precipitation by mesoscale variations in vegetative covering (Anthes, 1984), or to study the modification of the mesoscale atmospheric flow due to irregular irrigation patterns.

The rest of this thesis is orgainized as follows. Chapter 2 develops the mathematical model, with a brief discussion of its physical interpretation and an analysis of the general properties of the solution. Chapter 3 applies the model to the case with a straight coastline, which gives a general picture of the basic structure of the sea-land breeze circulation and its dependence on the model parameters. Chapter 4 studies the effect of the coastline geometry, paying special attention to the cases with curved coastlines and islands. Chapter 5 applies the model to the case of Hong Kong. Chapter 6 studies the association of the sea-land breeze

circulation with spatial rainfall patten in Hong Kong. Concluding remarks are given in Chapter 7.

Chapter 2

Mathematical model

Sea-land breezes are mesoscale, secondary circulation forced by thermal gradients, and occur prominently under conditions of weak prevailing winds. The shape of the coastline is an important factor that determines the structure of the sea-land breeze system. However, conventional linear models usually deal with the case of a straight coastline only. This chapter presents a simple model which attempts to capture the effect of an irregular sea-land distribution on sea-land breeze circulations. The model can also be applied to any thermally driven periodic secondary circulations[1]. The work is an extension of that of Young and Zhang (1999).

2.1 Semi-analytical approach

For the sake of simplicity we shall consider the circulation under no prevailing wind and over a flat terrain. The model domain consists of an infinite horizontal plane, on which the coastline is specified. The air motion is assumed to be confined within the inversion layer, bounded by at the bottom by the sea-level $z = 0$ and at the top by $z = H$. The flow is treated as three dimensional.

As the vertical scale of motion of sea-land breezes is observed to be limited to 1–2 km above ground, which is small compared to the tropopause extent of about 10 km, the Boussineq approximation is employed to simplify the primitive equations.

[1]The model developed in this chapter has been published (Zhang et al., 1997; 1999).

The Boussineq approximation treats the density as a constant except where it is coupled with gravity in the buoyancy term of the vertical momentum equation. Thus in this approximation the atmosphere is considered to be incompressible and local density variations are assumed to be small perturbations of the constant basic state field (Holton, 1992).

In the following, we take a Cartesian system of coordinates in which z denotes the vertical direction, and x and y span the horizontal plane. The plane where $z = 0$ represents the sea-level. In contrast to usual treatments, we emphasize that there is no assumption of a straight coastline. The three components of the velocity field are represented by (u, v, w), where u, v and w are in x-direction, y-direction and z-direction, respectivly .

From Rotunno (1983), the linearized equations describing the sea-land breeze flow are[2]

$$\begin{aligned}
\partial_t u - fv + \partial_x \Phi &= -ku \\
\partial_t v + fu + \partial_y \Phi &= -kv \\
\partial_t w - \theta + \partial_z \Phi &= -kw \\
\partial_t \theta + N^2 w &= -\kappa\theta + Q \\
\partial_x u + \partial_y v + \partial_z w &= 0
\end{aligned} \tag{2.1}$$

where f is the Coriolis parameter (assumed to be constant[3]), θ is the potential temperature, Φ is the geopotential, k^{-1} and κ^{-1} are the damping times due to Rayleigh friction and Newton's cooling respectively, N is the Brunt-Väisälä frequency, and Q is the diabatic forcing to be specified, which warms the air during the day and cools it during the night.

The Brunt-Väisälä frequency N is a measure of the vertical stability of the atmosphere due to density stratification, and expresses the natural frequency

[2]Derivation of the linearized set of the basic equations is presented in Appendix A.

[3]The Corilois parameter is assumed to be constant because the horizontal extent of sea land breeze is limited. Also, Coriolis terms is omitted in equation specifying the vertical motion because w is relatively small in sea-land breezes so that the Corilois effect on w is negligible(Holton, 1992).

of oscillations when the vertical equilibrium between buoyancy and gravity is disturbed. This is given by $N^2 = g\mathrm{d}\theta_0/\mathrm{d}z$, where g is the acceleration due to gravity, θ_0 is the mean potential temperature and z is the height.

Constant θ corresponds to an atmosphere in neutral equilibrium. If ρ_0 is the ambient density at a lower level, one may regard $\rho_0 N^2$ as the effective force constant of a 'spring' restoring the vertical movement of a unit volume of air mass. In this case, both N^2 and ρ_0 are assumed to be constant in time and space. Strictly speaking, N^2 cannot be exactly constant if ρ_0 is constant. However, for shallow disturbances, the variation of N^2 with height is unimportant.

Following Defant (1951), we see that the conventional understanding[4] suggests (a) that the system is set in an oscillation with a period of a day if the weather permits, and (b) that the the most essential function of irreversible processes is the transfer of heat from the ground to the air above it.

However, the actual process by which heat is transferred to the air is very complicated, so that in first approximation we consider the diabatic forcing Q to be a known function of space and time, which may be assumed to take the factorised form

$$Q = \tilde{Q}(x, y) Q_z(z) \sum_n q_n e^{in\omega t} \tag{2.2}$$

where $\tilde{Q}(x, y)$ describes the horizontal variation and $Q_z(z)$ describes the vertical variation, assuming to be

$$Q_z(z) = e^{-\delta z} \tag{2.3}$$

over both land and sea, characterized by the same scale δ^{-1}.

The time variation, assumed to be periodic with period $T = 2\pi/\omega = 1$ day, is expanded in harmonics. We shall implicitly take the real part, so that $t = 0$

[4]Namely, Buchan's description (1860): the cause of the sea-land breeze is that the land 'heated to a much greater degree than the sea during the day, by which the air resting on it being also heated, ascends, and the cooler air of the sea breeze flows in supply its place. But during the night the temperature of the land the air above it falls below that of the sea, and the air thus becming heavier and denser flows over the sea as a land breeze.'

corresponds to midnight. The circulation for the fundamental harmonic ($n = 1$) is exactly reversed in the two halves of a diurnal cycle. The higher harmonics break this symmetry, so that the land breeze and the sea breeze phases are no longer mirror images with equal strengths. The static mode ($n = 0$) represents the average flow over a day.

Within this approximation, all quantities vary in a diurnal cycle as the diabatic forcing, so we also expand them in harmonics, e.g.,

$$u = \sum_n \widehat{u}_n e^{in\omega t} \tag{2.4}$$

where the phases of the amplitudes (e.g., $\widehat{u}_n$) represent possible time lags in the response for each mode.

The flow is assumed to be confined between two horizontal 'solid' surface, so that the upper and lower boundary conditions are

$$w\big|_{z=0} = w\big|_{z=H} = 0 \tag{2.5}$$

Thus w can be expanded in a Fourier series involving $\sin(m\pi z/H)$, $m = 1, 2, \cdots$, so all the functions can also be expanded in Fourier series in z. As the boundary conditions on w demand that it is expanded in a sin series, Eq. (2.1) specifies how each function is expanded, whether in sine or cosine series:

$$\begin{aligned}
\widehat{u}_n &= \sum_{m=1}^{\infty} \widetilde{U}_{mn} \cos(m\pi z/H) \\
\widehat{v}_n &= \sum_{m=1}^{\infty} \widetilde{V}_{mn} \cos(m\pi z/H) \\
\widehat{w}_n &= \sum_{m=1}^{\infty} \widetilde{W}_{mn} \sin(m\pi z/H) \\
\widehat{\theta}_n &= \sum_{m=1}^{\infty} \widetilde{\Theta}_{mn} \sin(m\pi z/H) \\
\widehat{\Phi}_n &= \sum_{m=1}^{\infty} \widetilde{\Phi}_{mn} \cos(m\pi z/H)
\end{aligned} \tag{2.6}$$

Here m is a spatial mode index, and the characteristic height scales as m^{-1}. In particular, for the z-dependence of the heating term, we have

$$Q_z(z) = \sum_{m=1}^{\infty} \gamma_m \sin(m\pi z/H) \tag{2.7}$$

In this case, using the explicit form $Q_z(z) = e^{-\delta z}$, we find[5]

$$\gamma_m = \frac{2}{m}\left[1 + \left(\frac{\delta H}{m\pi}\right)^2\right]^{-1}\left(1 - e^{-\delta H}\right) \tag{2.8}$$

Hence, by expanding the quantities in spatial and temporal harmonics, the equations become

$$\begin{aligned}
\chi\tilde{U}_{mn} - f\tilde{V}_{mn} + \partial_x\tilde{\tilde{\Phi}}_{mn} &= 0 \\
\chi\tilde{V}_{mn} + f\tilde{U}_{mn} + \partial_y\tilde{\tilde{\Phi}}_{mn} &= 0 \\
\chi\widetilde{W}_{mn} - \tilde{\Theta}_{mn} - \frac{m\pi}{H}\tilde{\tilde{\Phi}}_{mn} &= 0 \\
\zeta\tilde{\Theta}_{mn} + N^2\widetilde{W}_{mn} &= q_n\gamma_m\tilde{Q} \\
\partial_x\tilde{U}_{mn} + \partial_y\tilde{V}_{mn} + \frac{m\pi}{H}\widetilde{W}_{mn} &= 0
\end{aligned} \tag{2.9}$$

for each mode (m, n), where

$$\chi = in\omega + k \qquad \text{and} \qquad \zeta = in\omega + \kappa$$

From the first two equations in (2.9), we get

$$\begin{aligned}
\tilde{U}_{mn} &= -\frac{1}{\chi^2 + f^2}\left(\chi\partial_x\tilde{\tilde{\Phi}}_{mn} + f\partial_y\tilde{\tilde{\Phi}}_{mn}\right) \\
\tilde{V}_{mn} &= \frac{1}{\chi^2 + f^2}\left(f\partial_x\tilde{\tilde{\Phi}}_{mn} - \chi\partial_y\tilde{\tilde{\Phi}}_{mn}\right)
\end{aligned} \tag{2.10}$$

and from the last two equations of (2.9), we get

$$\begin{aligned}
\widetilde{W}_{mn} &= \frac{1}{\chi\zeta + N^2}\left(\zeta\frac{m\pi}{H}\tilde{\tilde{\Phi}}_{mn} + q_n\gamma_m\tilde{Q}\right) \\
\tilde{\Theta}_{mn} &= \frac{1}{\chi\zeta + N^2}\left(\chi q_n\gamma_m\tilde{Q} - N^2\frac{m\pi}{H}\tilde{\tilde{\Phi}}_{mn}\right)
\end{aligned} \tag{2.11}$$

Putting the above into the incompressible condition in (2.9), we get

$$\left[\nabla^2 - \alpha_{mn}^2\right]\tilde{\tilde{\Phi}}_{mn}(x, y) = \alpha_{mn}^2\beta_{mn}\tilde{Q}(x, y) \tag{2.12}$$

[5]In fact, the Fourier series does not converge to the right values at $z = 0$ and at $z = H$. All the series above should be understood to be evaluated for $0 < z < H$ only, and the limits $z \to 0$ or $z \to H$ taken afterwards if necessary. This may be understood by using an analogy. Consider the case of a charged string, which is fixed at the two end points, and driven by an arbitary transverse electric field E. The displacement φ of the string from the equilibrium position thus satisfies $\partial^2\varphi/\partial x^2 + b\varphi = \rho E$, where ρ is the charge distribution on the string (per unit mass). The boundary condition demands that the displacement of the string is expanded by a sin series. Obviously, this and the governing equation together demands that the diving force is also expanded in a sin series, even though $E \neq 0$ at the end points.

where $\nabla^2 = \partial_x^2 + \partial_y^2$,

$$\alpha_{mn} = \frac{m\pi}{H}\left(\frac{\chi^2 + f^2}{\chi\zeta + N^2}\right)^{\frac{1}{2}}\left(\frac{\zeta}{\chi}\right)^{\frac{1}{2}}$$

$$\beta_{mn} = \frac{q_n\gamma_m}{\zeta}\left(\frac{m\pi}{H}\right)^{-1}$$

Once $\widetilde{\Phi}_{mn}$ is solved for a specific heating distribution, the entire field is known. Note that the function $\widetilde{\Phi}$ remains continuous physically even when $\widetilde{Q}$ has a step discontinuity. The conservation of momentum ensures the continuity of the normal wind component across shorelines.

2.2 Physical interpretation

The inhomogeneous Helmholtz equation, (2.12),

$$\left[\nabla^2 - \alpha_{mn}^2\right]\widetilde{\Phi}_{mn}(x,y) = \alpha_{mn}^2\beta_{mn}\widetilde{Q}(x,y)$$

hints that the sea-land breeze circulation undergoes some kind of forced oscillation, thermally driven by the uneven distribution of heating source which varies in time with a period of a day. Both the buoyancy force (vertical) and the Coriolis force (horizontal) are the restoring forces responsible for the oscillation.

In the former case the resistive force is opposite to the direction of air parcel displacement, but in the latter it is at right angles to the horizontal air parcel velocity. This resulting elliptical oscillation is known as inertio-gravity oscillation.

Furthermore, we eliminate $\widetilde{\Phi}_{mn}$ in term of $\widetilde{W}_{mn}$ by virtue of the relation (2.11), so that $\widetilde{W}_{mn}$ satisfies the following inhomogeneous Helmholtz equation.

$$\left[\nabla^2 - \alpha_{mn}^2\right]\widetilde{W}_{mn}(x,y) = \frac{q_n\gamma_m}{\chi\zeta + N^2}\nabla^2\widetilde{Q}(x,y) \tag{2.13}$$

for a mode with vertical and temporal indices m and n.

The physical meaning of the equation is as follows. It suggests that the horizontal distribution of the vertical motion is determined by the heating rate gradient for each mode.

Under the influence of the differential heating, convective currents flow across the heating and cooling sources. The flow can be obtained by solving the Helmholtz equation for the $\tilde{\Phi}$ field. This result is based on linearization, which is due to the assumption that no horizontal momentum is transferred by advection and diffusion, and therefore the motion is completely determined by the distribution of the heating source.

2.3 General properties of the solution

Distribution of vertical modes

The vertical structure is expressed as a sum of harmonics $\sin(m\pi z/H)$ or $\cos(m\pi z/H)$, with wavelengths $\lambda_m = 2H/m$. The adiabatic forcing of each mode is determined by the coefficient γ_m in (2.8), which is proportional to m^{-1} asymptotically. From (2.12) we see that the solution for $\tilde{\Phi}_{mn}$ goes as $\beta_{mn} \propto \gamma_m/m$. Therefore $\tilde{\Phi}_{mn}$ goes as m^{-2}.

The relative magnitudes of γ_m are shown on Figure 2.1. The odd modes die out monotonically as δH increases. The even modes behave somehow differently when the δH is small: the magnitudes rise from zero as δH increases, then attain their maxima, and again drop. Here the dimensionless parameter $1/\delta H$ is a measure of the vertical scale of the heating rate.

The $m = 1$ term is a barotropic mode, which has no node within the model domain $(0, H)$; the $m \geq 2$ modes, however, are baroclinic.

Horizontal penetration

The horizontal scale of the motion in a mode with vertical index m and temporal index n is characterised by $D_{mn} = 1/\mathrm{Re}(\alpha_{mn})$, which defines the distance over which the mode decays by a factor of e. The reciprocal $1/\mathrm{Im}(\alpha_{mn})$ represents the wavelength of the amplitude oscillation. For typical values describing the

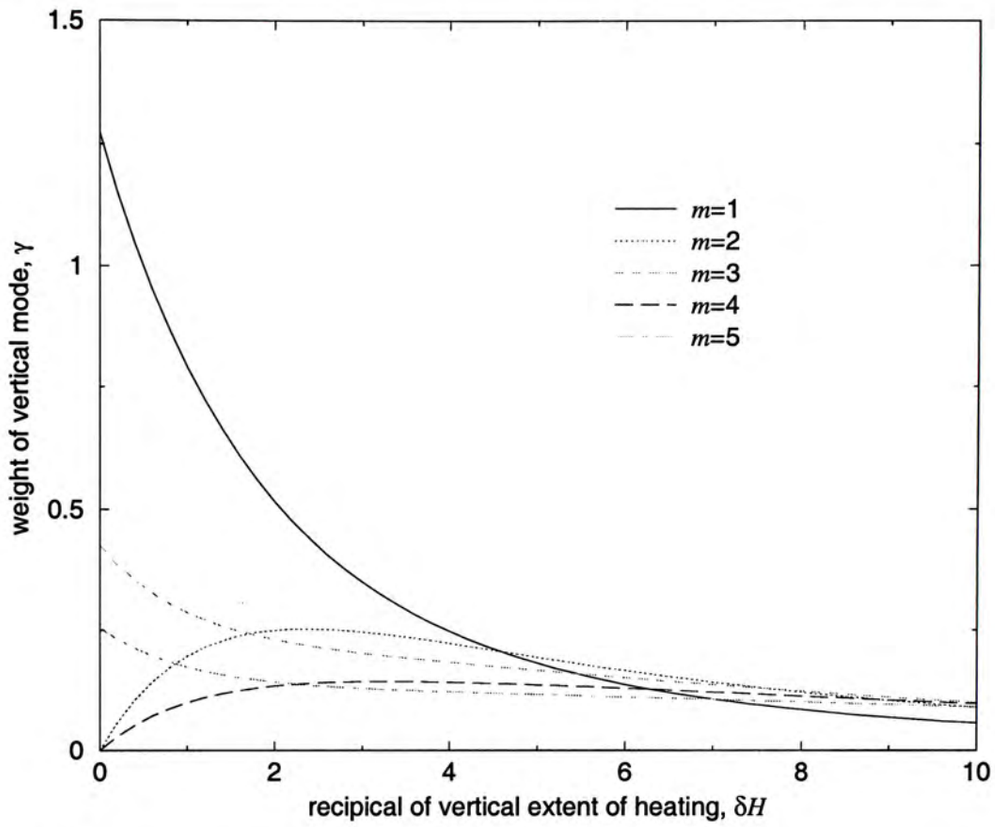

(a)

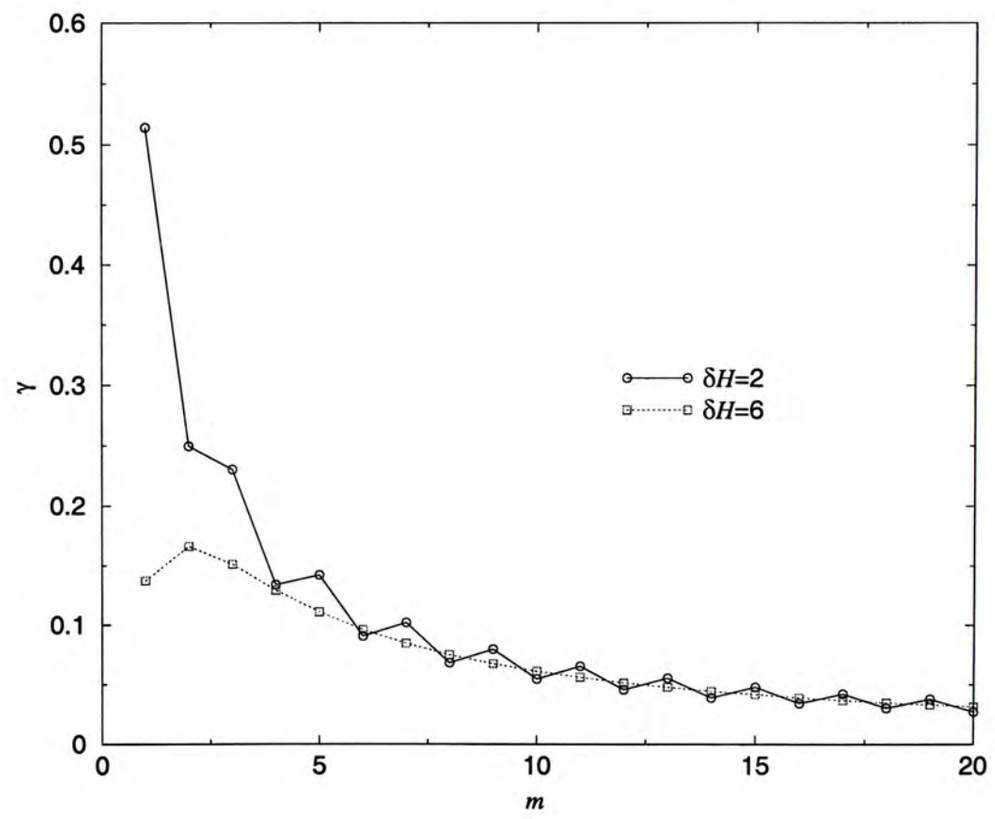

(b)

Figure 2.1. The relative weights γ_m of the heating rate. (a) The coefficient γ_m for each mode m is plotted against the δH, which is a measure of the vertical extent of the heating rate. (b) The Fourier coefficient for different values of δH. The barotropic mode ($m = 1$) dominates when δH is small.

atmosphere, $|N| \gg |\chi| \approx |\zeta|$, so

$$\begin{aligned} \alpha_{mn} &= \frac{m\pi}{H}\left(\frac{\zeta}{\chi}\right)^{\frac{1}{2}}\left(\frac{\chi^2+f^2}{\chi\zeta+N^2}\right)^{\frac{1}{2}} \\ &\approx \frac{2\pi}{\lambda_m N}\left(\frac{\zeta}{\chi}\right)^{\frac{1}{2}}\left(\chi^2+f^2\right)^{\frac{1}{2}} \end{aligned} \tag{2.14}$$

so that $D_{mn} = 1/\mathrm{Re}(\alpha_{mn}) = \lambda_m N\tau_n/2\pi$, where τ_n denotes the characteristic time of penetration, defined as

$$\begin{aligned} (\tau_n)^{-1} &= \mathrm{Re}\left[\left(\chi^2+f^2\right)^{\frac{1}{2}}\left(\frac{\zeta}{\chi}\right)^{\frac{1}{2}}\right] \\ &= \mathrm{Re}\left[\left((k^2+f^2-n^2\omega^2)+i\,2n\omega k\right)^{\frac{1}{2}}\left(\frac{\zeta}{\chi}\right)^{\frac{1}{2}}\right] \end{aligned} \tag{2.15}$$

It is useful to interpret $N\tau_n/2\pi$ as the aspect ratio (i.e., the ratio of horizontal to vertical extent) and λ_m as the vertical extent of the mode. The aspect ratio is in fact the ratio of the time scale of the horizontal motion to that of the vertical oscillation. At a given latitude, the characteristic time τ_n is constant, so that the horizontal scale is proportional to $N\lambda_m$. The breeze penetrates farther for larger convective depths and when the atmosphere is more stable. The horizontal scale is suppressed for higher spatial modes m as $\lambda_m \propto m^{-1}$. For the temporal harmonics, the dependence of D_{mn} on n is contained in the square bracket in (2.15), which is rather complicated but in general increasing with n.

Wind direction

In general the geopotential isobars do not follow the contours of the heating rate. The sensitivity of the geopotential isobars to the distribution of the heat source is different for different modes. It is more sensitive in the higher vertical modes to the shape of the coastline than the lower vertical modes, because the higher vertical modes have a shorter penetration from the coast, and hence depend more on the local coastal topography.

The horizontal velocity (2.10) consists of two parts: the first one is directly driven by the thermal gradient across the shore and the second part can be

regarded as a geostrophic response along the shore. In order to illustrate the geostrophic response by the Coriolis force, let us consider a case with a straight and infinite shoreline.

For each mode, the ratio of the wind speeds along and normal to the coastline is given by

$$\frac{\tilde{V}_{mn,l}}{\tilde{U}_{mn,l}} = -\frac{f}{\chi_l} = -f\left(\frac{k - in\omega}{k^2 - n^2\omega^2}\right) \tag{2.16}$$

It is worth noting that the ratio is independent of m, so that the overall wind components $\hat{u}$ and $\hat{v}$ for each temporal mode (the sum over all vertical modes) have the same ratio in (2.16).

The magnitude of the ratio given by $f/\sqrt{n^2\omega^2 + k^2}$ is larger (i.e., the wind is more inclined along the coastline) for higher latitudes and lower temporal modes; it also increases as the frictional force decreases, with an upper limit of $2\sin\varphi/n$, where φ is the latitude, since $f = 2\omega\sin\varphi$. This shows that the along-shore speed v becomes larger than the normal component u for higher latitudes.

The strengths of the two components oscillate diurnally with a phase difference of $\tan^{-1}(n\omega/k)$. The difference is larger for higher temporal harmonics. Assuming $k \sim \omega$ (i.e., the frictional damping time is on the order of one day), u leads v by 3 hours in the fundamental harmonic ($n = 1$) and by about 4.2 hours in the second harmonic. The phase difference increases as k decreases, with a maximum of 6 hours if the frictional force is neglected.

Chapter 3

Typical sea-land breezes

In Chapter 2, we have developed a linear model for examining sea-land breeze systems, and discussed the general properties of the solution. Within the model, we employed a harmonic analysis to reduce the four-dimensional (x,y,z,t) initial-boundary value problem to a two-dimensional boundary value problem. The time dimension is replaced by the temporal harmonics n. The vertical dimension is replaced by the mode m. The horizontal boundary value problem in (x, y) is then ready to be solved analytically or numerically when the heating source distribution is specified.

However, before we do so, in this chapter we give a general picture of the basic structure of sea-land breezes, with special attention paid to the dependence on the model parameters, by a study of the case of an infinite straight coastline. The following discussion basically follows that given by Young and Zhang (1999).

3.1 Circulation over a straight coastline

The treatment below is slightly different from that mentioned above. We begin with the entire three-dimensional flow in (x, y, z) instead of a horizontal boundary value problem in (x, y).

Consider a Cartesian system of coordinates in which the ground plane is at $z = 0$, with an infinitely long straight coastline at $x = 0$, along the y-axis separating the land ($x > 0$) from the sea ($x < 0$).

It is assumed that the motion vanishes either far inland or far offshore. The motion is assumed uniform along the coastline and independent of y, so that the problem reduces to two dimensions in the x-z plane.

The time and vertical dimensions are then replaced by the temporal harmonics n and the spatial mode m. The governing equation for $\tilde{\Phi}_{mn}$ in a mode of vertical index m and temporal index n then becomes

$$\left[\partial^2 - \alpha_{mn}^2\right] \tilde{\Phi}_{mn}(x) = \alpha_{mn}^2 \beta_{mn} \tilde{Q}(x) \tag{3.1}$$

where

$$\alpha_{mn} = \frac{m\pi}{H} \left(\frac{\chi^2 + f^2}{\chi\zeta + N^2}\right)^{\frac{1}{2}} \left(\frac{\zeta}{\chi}\right)^{\frac{1}{2}}$$

$$\beta_{mn} = \frac{q_n \gamma_m}{\zeta} \left(\frac{m\pi}{H}\right)^{-1}$$

The heating rate $\tilde{Q}$ and the frictional coefficients k and κ assume different forms over land and sea; we take

$$\left(\tilde{Q}, k, \kappa\right) = \begin{cases} (Q_s, k_s, \kappa_s), & x < 0 \\ (Q_\ell, k_\ell, \kappa_\ell), & x > 0 \end{cases} \tag{3.2}$$

which are constants, with larger values for land than sea, e.g., $k_\ell > k_s$.

The solution is[1]

$$\tilde{\Phi}_{mn}(x) = q_n \gamma_m \left(\frac{m\pi}{H}\right)^{-1} \times \begin{cases} C_s\, e^{\alpha_{mn,s} x} - Q_\ell/\zeta_s, & x < 0 \\ C_\ell\, e^{-\alpha_{mn,l} x} - Q_s/\zeta_\ell, & x > 0 \end{cases} \tag{3.3}$$

where

$$C_s = - \Delta Q \frac{a_s}{a_s + a_\ell}$$

$$C_\ell = \Delta Q \frac{a_\ell}{a_s + a_\ell}$$

and

$$\Delta Q = Q_\ell/\zeta_\ell - Q_s/\zeta_s$$

[1]The equation is invalid at the coastline, where the step singularity of α_{mn} appears. The value of $\tilde{\Phi}_{mn}(x = 0)$ at the coastline is taken as $\lim_{x \to 0} \tilde{\Phi}_{mn}$ if neccessary.

$$a_s = \alpha_{mn,s}\zeta_\ell(\chi_s\zeta_s + N^2)$$

$$a_\ell = \alpha_{mn,l}\zeta_s(\chi_\ell\zeta_\ell + N^2)$$

Here we note that both $\tilde{\Phi}$ and its first derivative are continuous across the coastline, since the former is essentially the pressure and the latter is the onshore wind component. The coefficients C_s and C_ℓ are determined by matching the solutions and their derivatives across the coastline.

Hence we obtain, under the assumption that $|N| \gg |\chi|$ and $|N| \gg |\zeta|$, the entire field of the flow as follows.

$$\tilde{U}_{mn} = \left(\frac{m\pi}{H}\right)\frac{q_n\gamma_m\Delta\mathcal{Q}}{N^2}\left(\frac{\alpha_s}{\zeta_s}+\frac{\alpha_\ell}{\zeta_\ell}\right)^{-1}\times\begin{cases} e^{\alpha_{mn,s}x}, & x<0 \\ e^{-\alpha_{mn,l}x}, & x>0 \end{cases} \tag{3.4}$$

$$\tilde{V}_{mn} = \left(\frac{m\pi}{H}\right)\frac{q_n\gamma_m\Delta\mathcal{Q}}{N^2}\left(\frac{\alpha_s}{\zeta_s}+\frac{\alpha_\ell}{\zeta_\ell}\right)^{-1}\times\begin{cases} \dfrac{f}{\chi_s}e^{\alpha_{mn,s}x}, & x<0 \\ \dfrac{f}{\chi_\ell}e^{-\alpha_{mn,l}x}, & x>0 \end{cases} \tag{3.5}$$

3.2 Structure of sea-land breezes

In this section, we discuss the general properties of the solution found for the sea-land breeze circulation, using the typical values of parameters listed in Table 3.1[2]

The series solution consists of two kind of harmonics/modes, i.e., the temporal harmonics n and the spatial modes m. In this section we first concentrate on the contributions of various spatial modes to the sea-land breeze system. To do this, only the fundamental harmonic ($n = 1$) is kept for the temporal series, or in other words, a sinusoidal differential heating with period of a day is taken.

The contribution of higher temporal harmonics will be discussed in Section 3.4.

[2]The diabatic heating is usally expressed as J/c_p in K day^{-1}, where J is the rate of heating per unit mass owing to radiation, conduction, and latent heat release, and c_p is the heat capacity per unit mass with constant pressure. The quantity Q in the model has under a certain scaling: $Q = gJ/c_pT_o$, where T_0 is the base state temperature. In this case, the equivalent heating rate $J/c_p \approx 1$ K d^{-1} when $Q_l = 6 \times 10^{-6}$ m s^{-3}, T_0 is about 300 K and $g = 10$ m s^{-2}.

Table 3.1. The standard values of model parameters (I)

Parameter	Value	Unit	Comments
Q_l	6×10^{-6}	m s^{-3}	
Q_s	1.5×10^{-6}	m s^{-3}	$Q_s = 0.25\, Q_l$
k_l	5	day^{-1}	
k_s	1.25	day^{-1}	$k_s = 0.25\, k_l$
κ_l	5	day^{-1}	
κ_s	1.25	day^{-1}	$\kappa_s = 0.25\, \kappa_l$
N^2	1×10^{-4}	s^{-2}	
f	0.54484×10^{-5}	s^{-1}	at latitude 22 °N
H	1	km	
δ	2×10^{-3}	m^{-1}	

As mentioned in Chapter 2, the amplitude of Φ goes asymptotically as m^{-2}, and thus decreases rapidly with m. In practice, all numerical results reported are calculated by truncating the sum at $m = 20$.

Driving force

We see that the wind components u and v and the gradients of other quantities across the shore are all directly proportional to the difference in the diabatic forcing $\Delta\mathcal{Q}$, where $\Delta\mathcal{Q} = Q_l/\zeta_l - Q_s/\zeta_s$, and ζ_l and ζ_s are determined by the damping time due to Newton's cooling κ_l and κ_s over land and sea. In other words, if $\kappa_l \neq \kappa_s$, there is a sea-land breeze even if the land and the sea are subjected to the same diurnal heating. This is an important feature of the model, which Young and Zhang (1999) overlooked.

Horizontal extent

The horizontal extent in a mode is characterized by $D_{mn} = 1/\mathrm{Re}(\alpha_{mn})$. With the assumed parameters, the barotropic mode ($m = 1$) has a horizontal extent

of about 50 km inland but 160 km out to the sea, because friction is smaller over the sea. When all modes are summed, the overall wind field has a shorter horizontal length scale, of about 30 to 50 km inland, and 80 to 120 km out to the sea, broadly consistent with observations (Atkinson, 1984; Abbs, 1986; Fisher, 1960).

Wind hodograph

The diurnal changes in the sea-land breeze can be summarised in a wind hodograph, from which the wind direction and the strength at any time of the day can be read off.

Figure 3.1 gives the wind hodograph 1 km inland, at latitudes 22 °N and 60 °N respectively, and is labelled by hours according to the local sun time (LST). The heating rate is assumed to be maximum at 1200 LST.

These figures show that the wind speed is minimum at about 0900 and 2200 LST, and maximum at about 0400 and 1600 LST (near sunrise and sunset), with some small variations with latitude. The wind component v is larger at higher latitudes, as is also evident from the dependence on f. See (2.16) below. The major axis of the ellipse tilts more toward the shore at higher latitudes so that the wind component v is larger.

Assuming the coast runs along the east-west direction with the sea to the south, the strongest sea breeze is from the SW and strongest land breeze from the NE. The result agrees with observations (Atkinson, 1984).

In this model the wind hodograph for each vertical mode is elliptical. In fact it can be shown that within the approximation the wind hodographs should be ellipses, and its sense of rotation is always clockwise (in the northern hemisphere).[3]

[3]For a wind vector (u, v), whose components vary with time as $u(t) = \cos(\omega t+\phi_0)$ and $v(t) = \xi\cos(\omega t+\phi_0+\phi)$, where ξ is real. By noting that $v = \xi\left[\cos(\omega t + \phi_0)\cos\phi - \sin(\omega t + \phi_0)\sin\phi\right] = \xi\left[u\cos\phi - \sqrt{1-x^2}\sin\phi\right]$ and squaring it, we get $\xi^2u^2 - 2uv\xi\cos\phi + v^2 = \xi^2\sin\phi$, which is in a form of $Au^2 + 2Buv + Cv^2 = F$, with $B^2 - AC = \xi^2(\cos^2\phi - 1) < 0$. The locus is therefore in the shape of an ellipse, and the angle α between the x-axis and its major axis satisfies $\tan 2\alpha = (A - C)/B$.

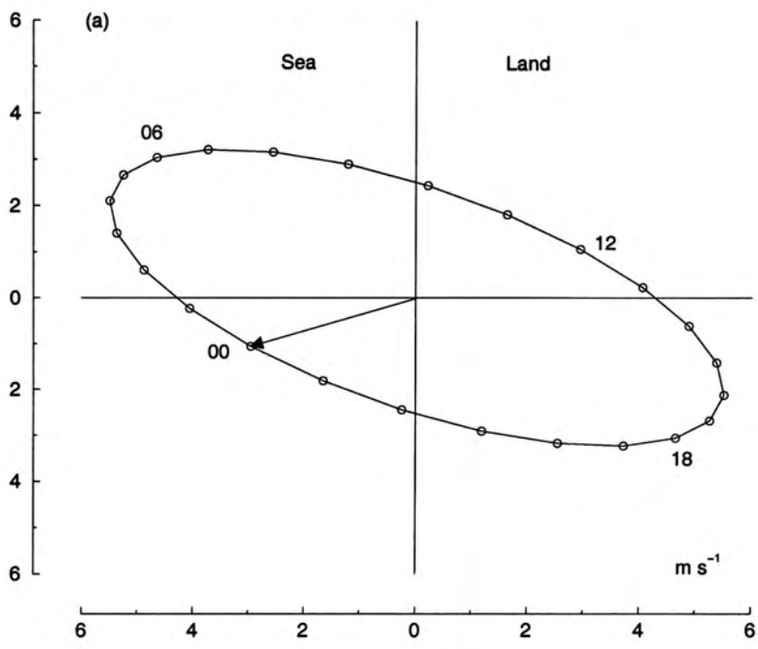

(a)

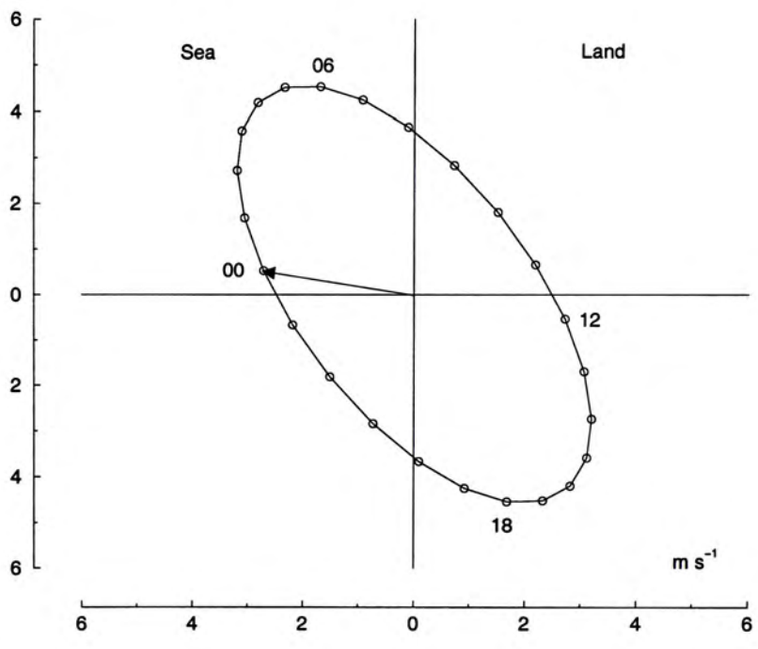

(b)

Figure 3.1. Wind hodographs at latitudes (a) 22 °N and (b) 60 °N, 1 km inland. The time (hour LST) of measurement is indicated near the data ponts. The diurnal variation of the sea-land breeze is clearly shown in the wind hodographs, which summarize the changes in intensity and direction during a day. It is noted that the breeze becomes more parallel to the coast at higher latitudes.

The wind hodograph appears as an ellipse with clockwise rotation. The coastal topography among other reasons affects the forms of the wind hodographs, which may then appear very different when modes are summed up, even though they are elliptical for individual modes. The forms of the wind hodographs would vary considerably if the coastline departs from linearity. More discussion can be found in Chapter 4.

Diurnal variation

Figure 3.2 gives the diurnal variation of the surface wind field at latitude 22 °N, using the parameters in Table 3.1. The horizontal axis x is the distance from the coastline, and the vertical axis is time in hours LST.

As both the sea and the land begin to heat up after sunrise, the sea breeze develops and the wind speed increases as the heating rate increases. The wind, which blows rather tangential to the coastline at first, is then gradually directed towards the sea in a clockwise sense. At 1200 LST the sea-land heating difference is at a maximum and the wind speed follows, with a value of about 6 m s^{-1}. The differential heating then decreases and changes sign after sunset, so that the sea breeze weakens and dies, and the land breeze starts to develop. The cooling rates have a maximum difference at midnight and the land breeze reaches its maximum about 3 hours later. The land breeze then decays until the sea breeze arrives.

Figure 3.3 gives the time history of the surface wind components u and v 1 km inland from the coast over a 24-hour period, and illustrates how they vary with the change of ΔQ during the day. The values of the parameters used are as shown in Table 3.1.

The most noticeable feature is the phase difference between the wind components and the differential heating. The across-shore wind component u attains its maximum intensity about 4 hours after ΔQ does, and the along-coast component v gradually develops as a geostrophic response to the mesoscale pressure gradient. The component v leads u, as shown by the clockwise rotation of the wind vectors in Figure 3.2 above.

Spatial profile

Figure 3.4 shows the x-z profile of the flow on the vertical plane at 1600 LST (maximum sea breeze) and 2200 LST (transition from sea breeze to land breeze), respectively, using the same parameters as for Figure 3.3.

From Figure 3.4, the sea-land breeze extends further out to the sea than into

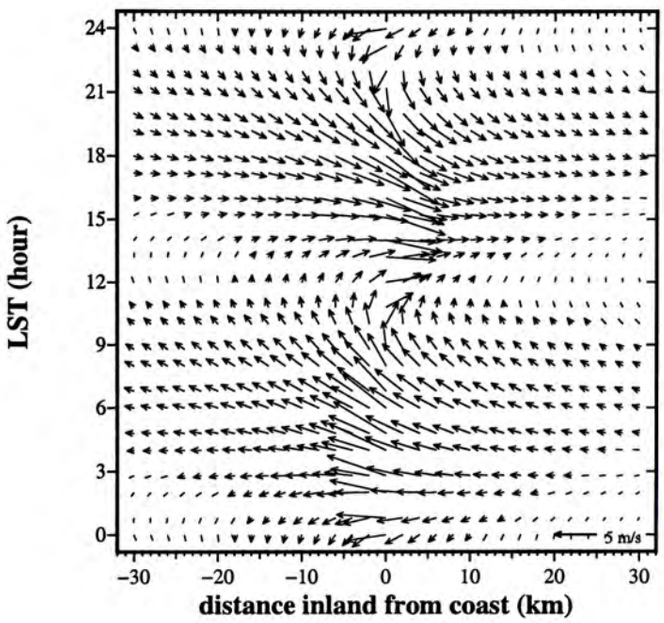

Figure 3.2. Changes in the surface wind field during a sea-land breeze day, at at latitude 22 °N. The horizontal axis is the distance from the coastline, where positive values denote the distance out to the sea and negative values represent locations inland. The vertical axis is time in hours LST. The wind strength decays as it spreads inland and out to the sea. The wind is directed to the sea before the sun rises and to the land after midday, rotating in a clockwise sense.

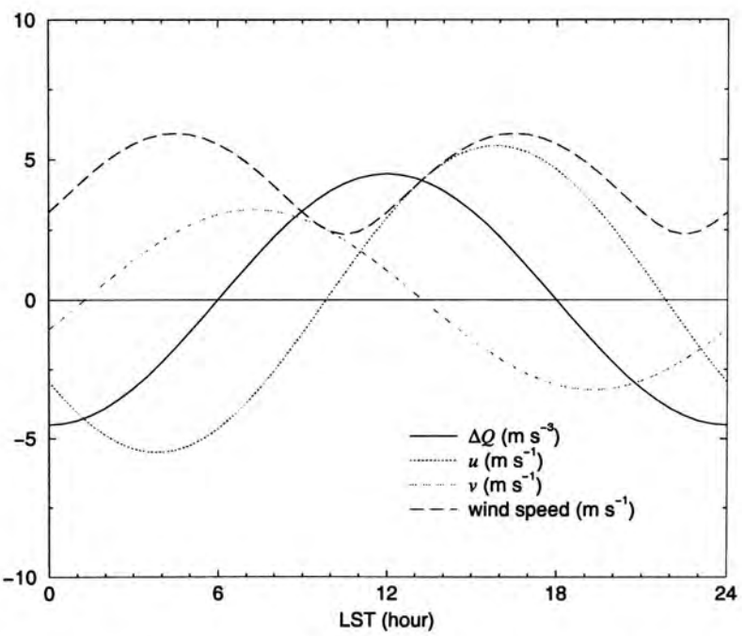

Figure 3.3. A graph showing the time history of the surface wind components u and v 1 km inland from the coast over a 24-hour period, which illustrates how they vary with the change of ΔQ during the day. There is a phase difference of about 3 hours between the across-shore component u and the differential heating.

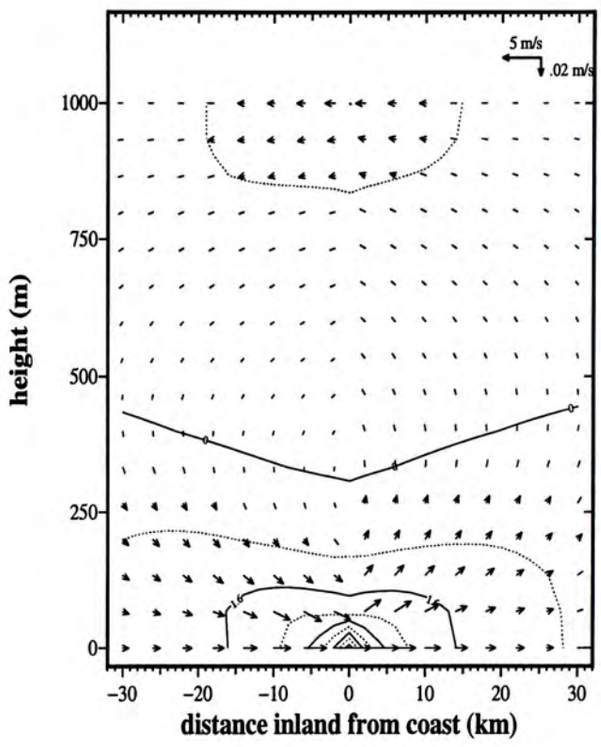

(a)

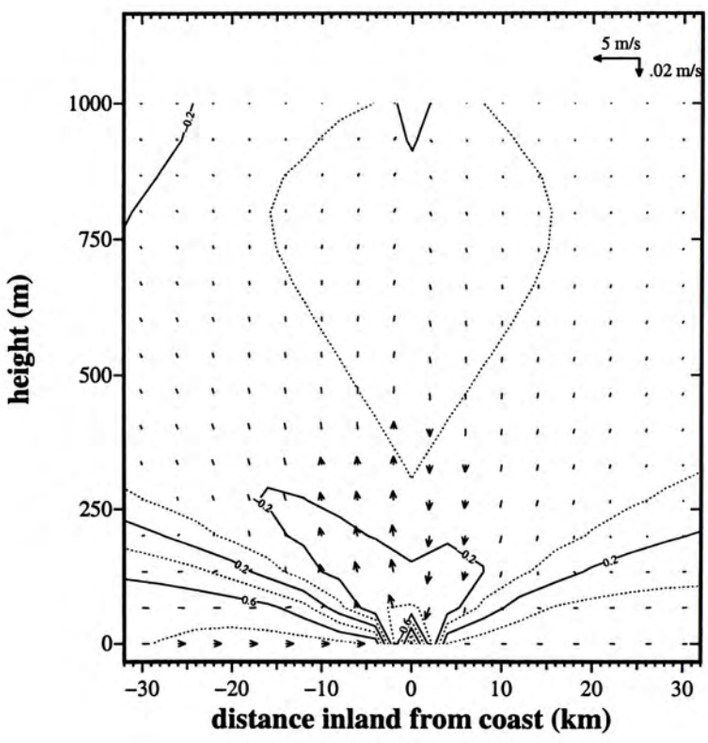

(b)

Figure 3.4. Vertical profile of the flow field (a) at 1600 LST, the time that the sea breeze attains its maximum strength. The contour shows the onshore wind component u in m s^{-1}. Note the contour of $u = 0$. The onshore flow rises over the land and reverses at a height about 300 m; (b) at 2200 LST, when the land breeze begins to replace the sea breeze after the sun sets. The wind turns onshore over the coast, while it still blows offshore far from the shore. This indicates that the sea-land breeze develops and changes direction starting from the coast.

the land, essentially because different values of the frictional parameter have been used. Convergence occurs over the land while divergence occurs over the sea during the sea-breeze phase. This situation reverses for the land-breeze phase.

The wind speed decreases vertically until a height of about 300 m, and reverses above that height. A weaker return flow aloft is necessary to balance the system as shown in Figure 3.4, since the atmosphere is assumed incompressible. The flow pattern is qualitatively the same as shown in Atkinson's analysis (1984) on the cross-section of the circulation.

At 2200 LST, the pattern of the circulation is quite different from that at the sea-breeze phase. Away from the coast, the wind still blows onshore ($u > 0$), implying that it is in the sea-breeze phase. Over the coast, however, a narrow land-breeze circulation is developed, which indicates the beginning of the land-breeze phase. In short, this suggests that the sea-land breeze develops and changes direction starting from the coast, and is seen inland only later.

Figure 3.5 gives the wind components u and v respectively, 1 km inland at various heights. The horizontal axis is time in hours. The vertical axis is height in metres. These two figures show that the sea breeze occurs in the lower parts of the atmosphere, decreasing in amplitude vertically. At a height of 300 m, the direction of the circulation is reversed.

The height at which the circulation reverses depends physically on the height of the inversion layer (represented by H) and the vertical heating profile (represented by δ^{-1}), and can range from 100 m (the present model) to over 1 km. In fact the product δH determines the distribution of the vertical modes. The higher modes, in which the flow returns at lower heights, become significant when δH is large.

The contribution of the spatial modes

Figure 3.6 shows the x-z profiles of the flow on the vertical plane at 1600 LST

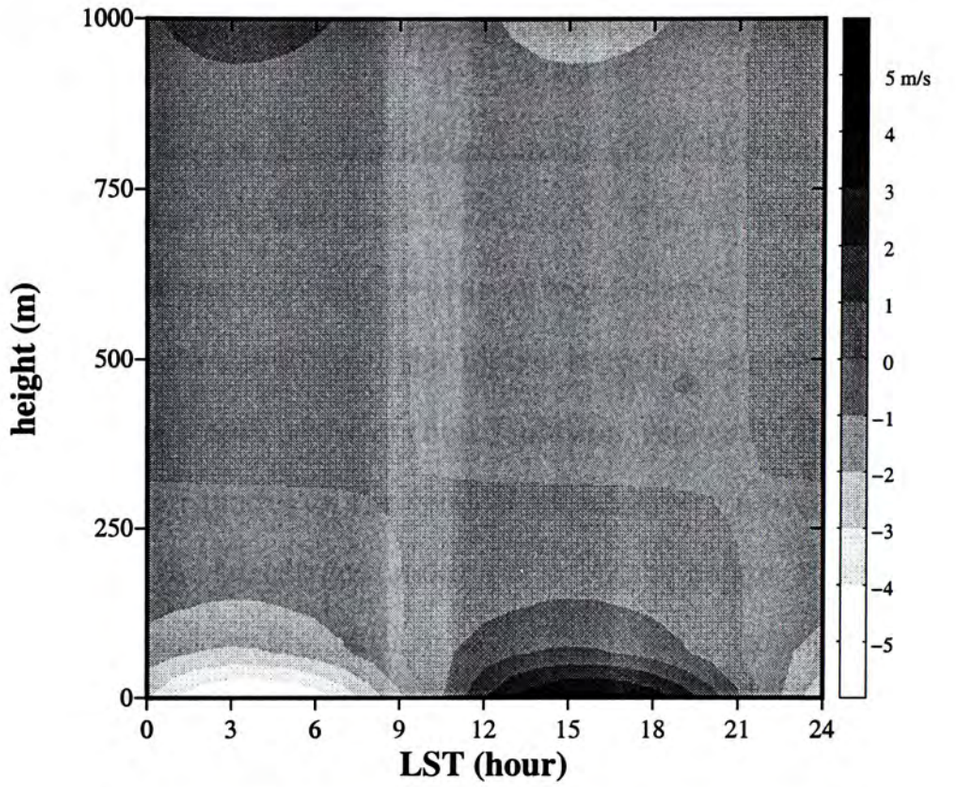

(a)

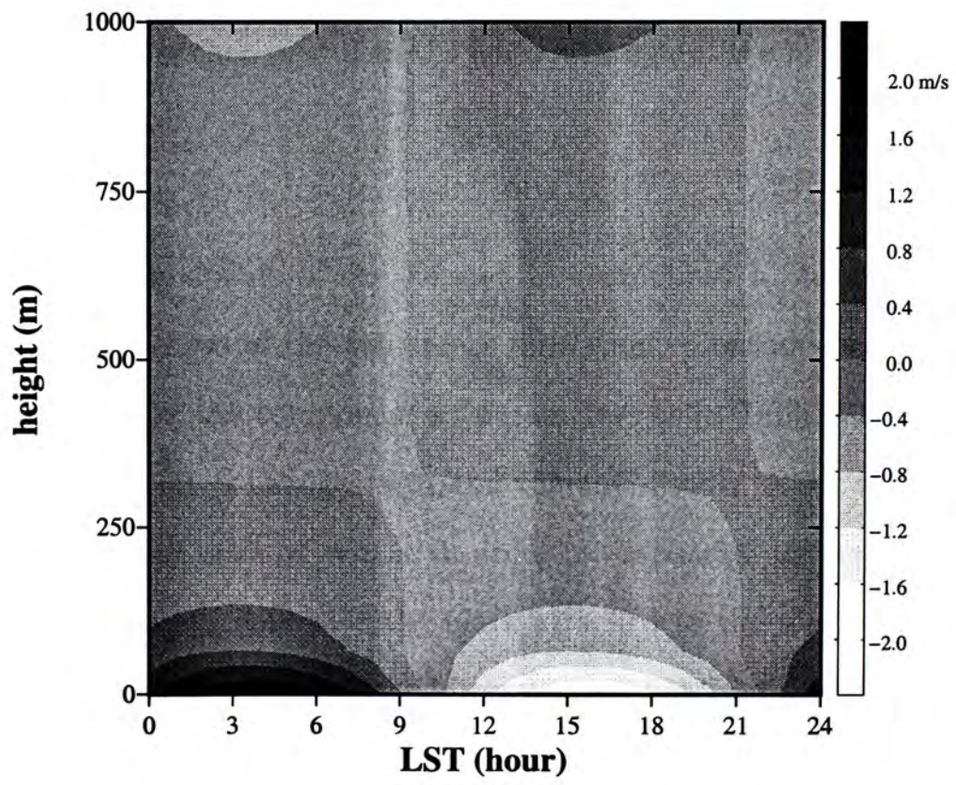

(b)

Figure 3.5. Changes during a day of (a) the wind components u and (b) the wind components v (both in m s^{-1}), 1 km inland at various heights. The horizontal axis is time in hours. The vertical axis is height. The figures show that sea-land breeze has only a shallow extent. A weak return flow aloft is induced to balance the system.

(sea-breeze phase), using the same parameters as for Figure 3.4, summed up to different spatial modes m. The profile (a) is up to $m = 1$, while (d) is up to $m = 4$.

From Figure 3.6, we see that barostropic mode ($m = 1$) primarily determines the spatial structure of the sea-breeze circulation. The air flows seawards near the surface, rises over the land and returns at higher levels.

Besides affecting the amplitude, the higher baroclinic modes ($m = 2, 3, \cdots$) are also related to the length scales of the circulation, especially the vertical scale. The effect of the higher modes on the vertical extent is very noticeable. As higher modes are added to the barostropic mode ($m = 1$), the height at which the flow reverses decreases considerably, until $m = 3$. The vertical extent is nearly fixed after the $m = 3$ mode.

The horizontal extent is however dominated by the $m = 1$ mode. The contribution of modes higher than $m = 2$ on the horizontal extent is not very significant.

Onset of sea breeze

Figure 3.7 shows the change of the horizontal component u on the x-z cross-section during the course of the sea-breeze formation. Contours on the graphs represent the values of the component u (parameters as in Table 3.1). We highlight the contour where u changes sign and thereby divides zones with onshore winds from those with offshore winds, in order to emphasise its vertical motion as the sea breeze onsets. Following the mark attached to the $u = 0$ contour, we see that the return flow sinks as time advances, and finally reaches sea level, so that the surface wind changes from a land breeze to a sea breeze.

Since the vertical extent over coastal areas is the shortest, the return flow reaches sea-level there earlier than in regions far from the coast, so that the sea breeze starts to develop close to the coast, and then extends out to the sea and penetrates inland.

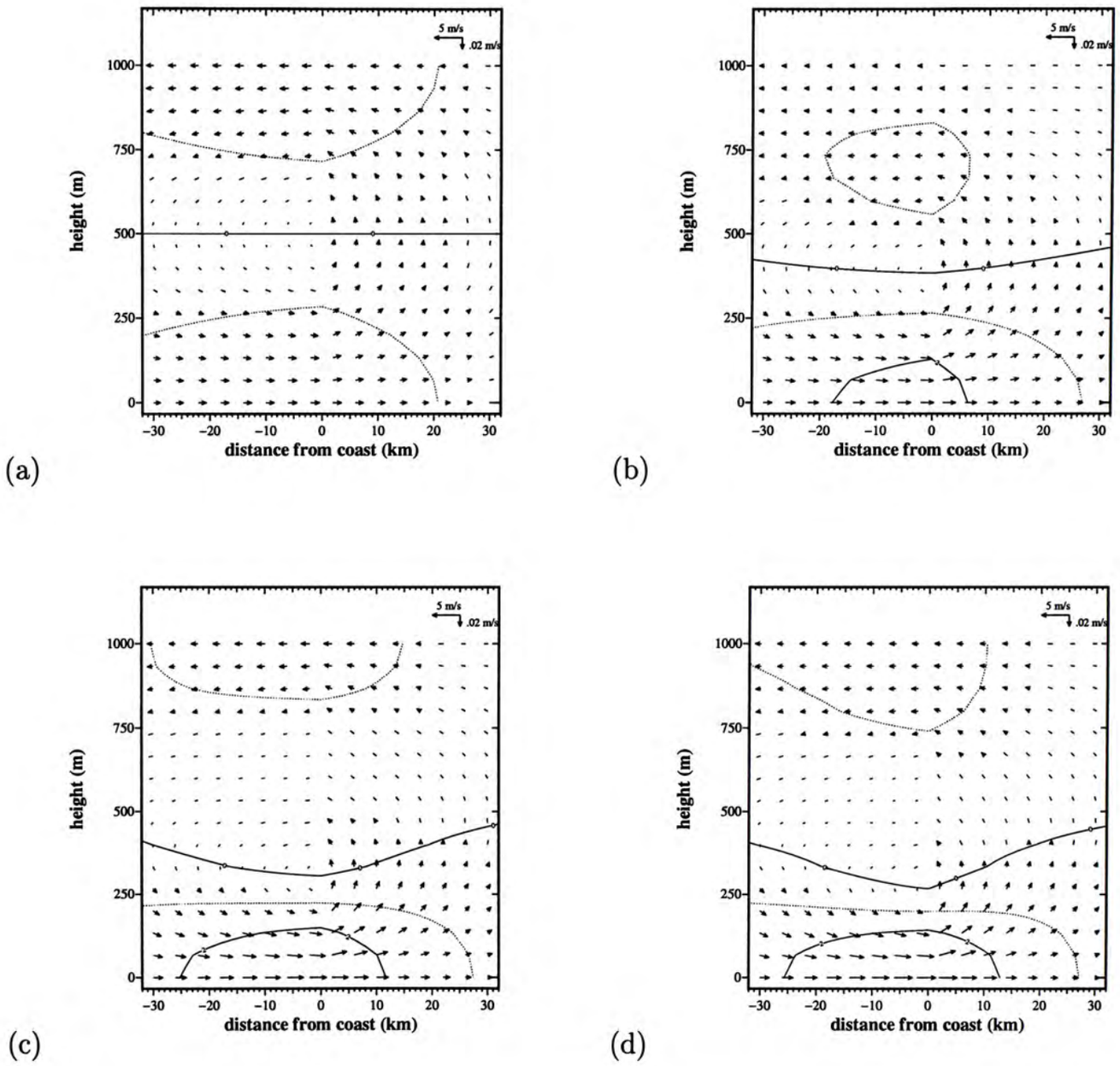

Figure 3.6. Vertical profiles of the flow field in sea-breeze phase, at 1600 LST, showing the contribution of spatial modes m. The profiles show the resultant flow summed (a) up to $m = 1$, (b) up to $m = 2$, (c) up to $m = 3$, and (d) up to $m = 4$. The contour is the onshore wind component u in m s^{-1}.

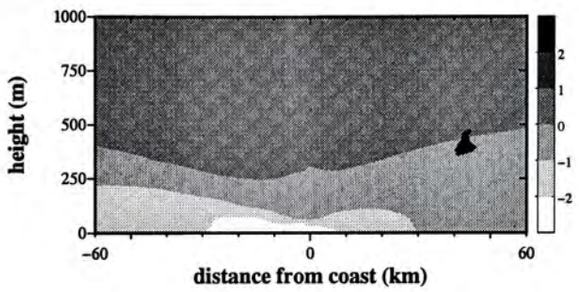

(a)

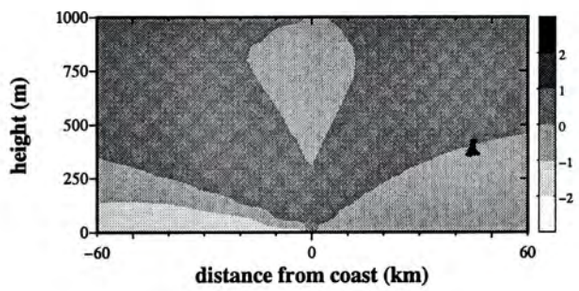

(b)

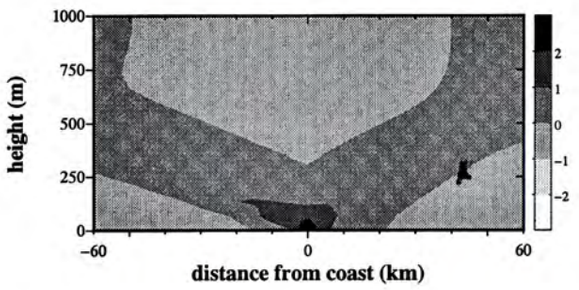

(c)

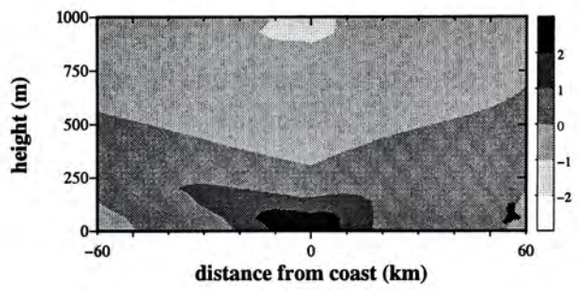

(d)

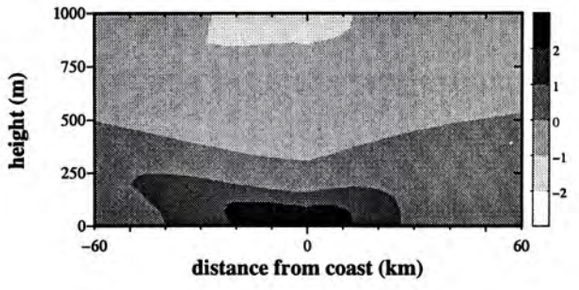

(e)

Figure 3.7. Vertical profiles showing the change in the wind speed u during the course of the sea-breeze formation. The profile (a) is taken at 0800 LST, and at two hour intervals for (b)–(e). Contours on the graphs represent the values of the component u in m s^{-1}, where a mark is attached to the one where $u = 0$. The trace of the mark shows that the return flow sinks as time goes on and finally reaches sea level, so that the surface wind changes from a land breeze to a sea breeze.

From the above results, the output of this analytic model agrees with data qualitatively and can represent the structure and evolution of sea-land breeze very well.

3.3 Dependence on the parameters

Heating rate

The variations of the heating rate in fact determine the structure of the breeze. The horizontal variation is characterized by the distribution of landmass and water, and by the width of the transition region. The vertical variation is characterized by the length scale δ^{-1}, at which height the heating rate drops by a factor of e.

The strength of the breeze is proportional to the horizontal gradient of the heating rate as mentioned above. An abrupt change has been assumed in our case, so that no information is revealed about the effect of the width of the transition region. However one may expect that the breeze disappears if the width is much larger than the horizontal scale of the breeze. The effect is discussed in the next section.

The influence of the vertical scale of Q on the sea-land breeze is interesting. Together with the height of the inversion layer H, they form a dimensionless parameter δH, which indicates the portion of the layer affected. The parameter turns out to be a factor determining both the vertical and the horizontal scale of the motion.

As an example, we use the parameters as in Table 3.1, except that δ is doubled to 4×10^{-3} m^{-1} (then $\delta H = 4$ instead of 2). The surface wind field (Figure 3.8) remains more or less the same as before (Figure 3.2), but the wind speed is smaller. The vertical profile at 1600 LST (Figure 3.9) shows a lower vertical extent of the sea-land breeze circulation. When δ is further increased to 10^{-2} m^{-1} ($\delta H = 10$), the speed of the sea-land breeze not only decreases but its

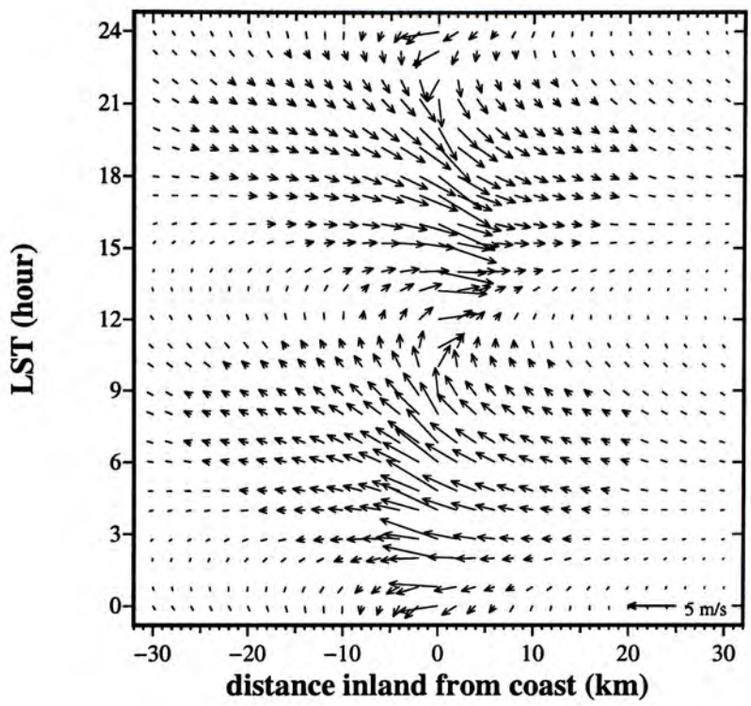

Figure 3.8. Surface wind field with δ doubled to 4×10^{-3} m^{-1}. The surface wind field is more or less the same as that with the standard value, but the wind speed is smaller.

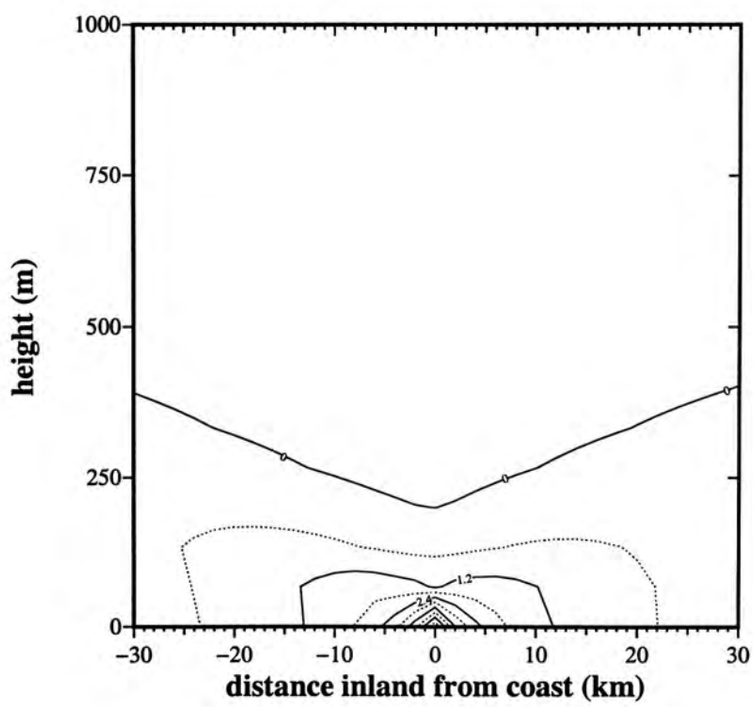

Figure 3.9. Vertical profile of u at 1600 LST with δ doubled to 4×10^{-3} m^{-1}. The drop of vertical extent when δ is doubled indicates that the vertical extent of sea-land breezes varies roughly with δ^{-1}.

vertical extent also decreases, to about 100 m. This indicates that the vertical extent of sea-land breezes varies roughly with δ^{-1}.

Latitude

The model shows that sea-land breezes are easier to establish at mid-latitudes with larger wind speed and horizontal extent. This result agrees with observation.

The horizontal extent D_{mn} is $1/\mathrm{Re}(\alpha_{mn}) \sim 1/\mathrm{Re}(\chi^2 + f^2)^{1/2}$, so that D_{mn} is shorter at higher latitudes.

Figure 3.10 gives the values of $D_{11,l}$ and $D_{11,s}$ at different latitudes, using parameters as in Table 3.1. The subscripts l and s denote the extents over land and sea, respectively. From the figure, as the latitude increases, $D_{11,l}$ and $D_{11,s}$

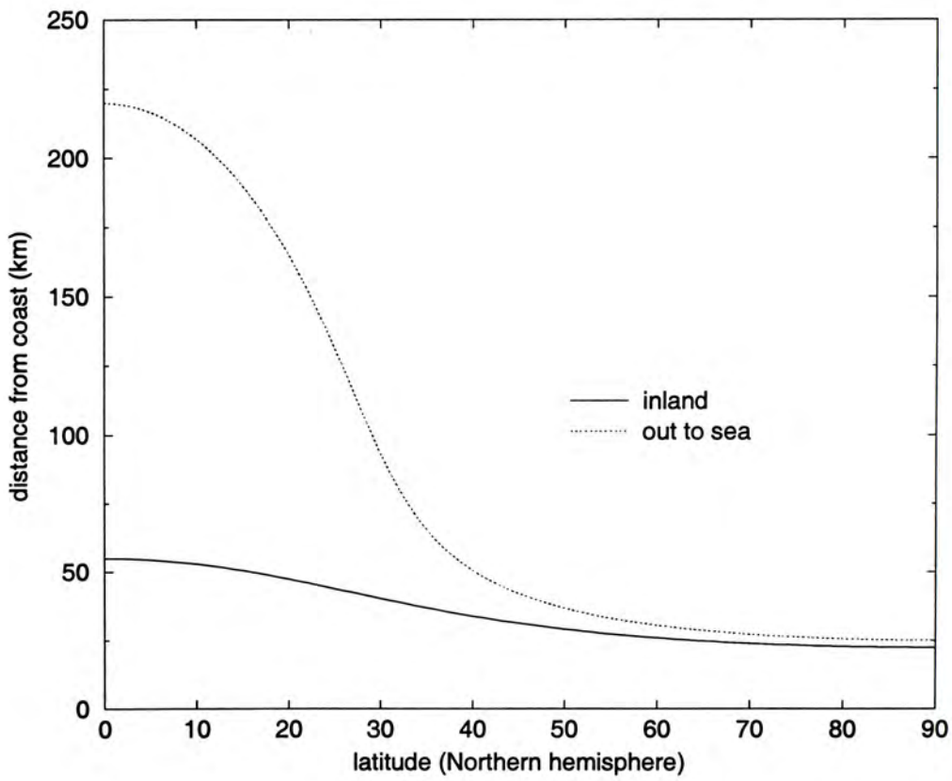

Figure 3.10. The graph showing the horizontal extent of sea-land breezes at different latitudes. The solid line represents the distance of penetration inland, and the dashed line denotes the distance out to sea. In general, the horizontal scale shrinks as the latitude increases. The extent over the sea is larger than over land, primarily due to the different values of friction in each domain.

decrease, more rapidly at lower latitudes.

With the same heating rate, a weaker and shallower sea-land breeze is developed at higher latitudes because the Coriolis force is larger. The force turns the wind much more, so that it cannot penetrate as much inland. The same applies to the land breeze. Actually, there are fewer sea-land breezes at higher latitudes, not only because of the above reason, but also because the heating rate is smaller.

Stratification

Figure 3.11 gives the values of $D_{11,l}$ and $D_{11,s}$ at 22 °N, but with various values of the stratification N^2, with other parameters as in Table 3.1. As the stability of stratification increases, both horizontal extents also increase, but u decreases.

Figure 3.12 gives the diurnal variation of the surface wind at 22 °N, using parameters as in Figure 3.11 and $N^2 = 10^{-5}$ s^{-2} instead of 10^{-4} s^{-2}. Comparing Figure 3.2 with Figure 3.12, we find that the wind speed is doubled: the former is about 5 m s^{-1}, while the latter is about 10 m s^{-1}. In fact, sea breezes seldom reache a strength of over 8 m s^{-1}, so the latter case is artificial, and is included only to illustrate the effect of the stratification.

With weaker stratification stability, the speed of sea-land breezes is higher but the winds decay more rapidly with the distance from the coast.

The horizontal wind speed is higher along the coastline and by continuity, so is the vertical wind speed. Thus rainfall or thunderstorms tend to occur when the stratification stability is weaker. This result should be of interest in weather forecasting.

Frictional parameter

Many studies (Defant, 1951; Haurwitz, 1947; Rotunno, 1983; Dalu and Pielke, 1998) use the same frictional parameter for the sea and the land; however, in reality the roughness is not the same in the two cases.

Young and Zhang (1997) suggested using different values of the frictional

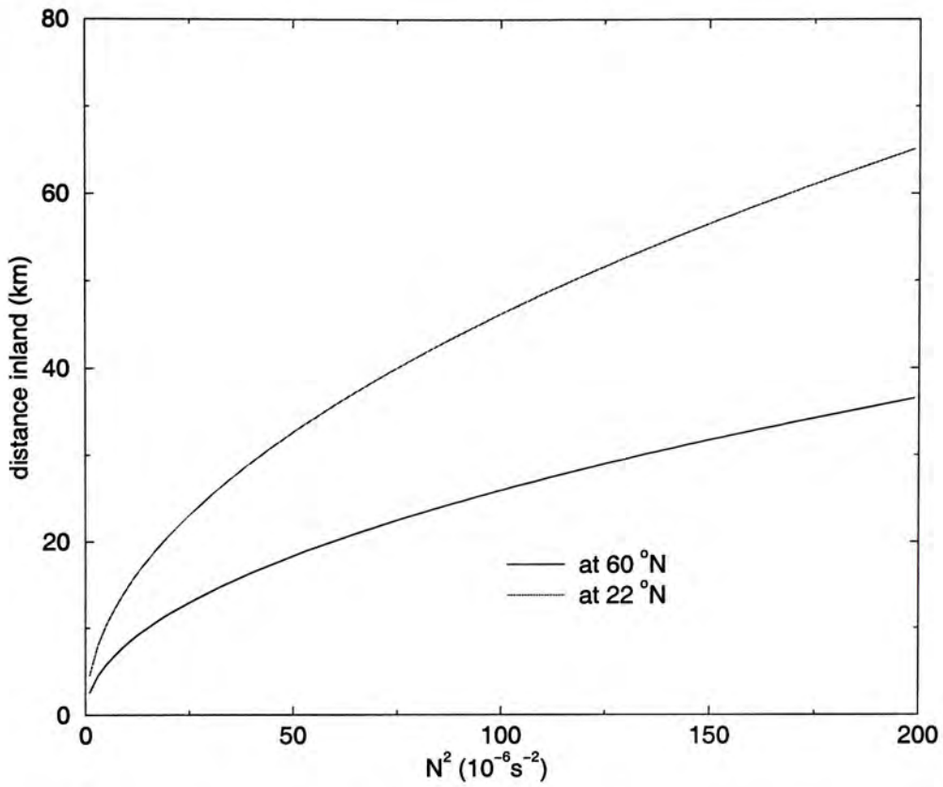

Figure 3.11. Effect of the horizontal extent on the stability of a stratified atmosphere. The solid line shows the distance of influence inland at 22 °N, and the dashed line denotes the distance at 60 °N. A more stable atmosphere allows the breeze to extend farther both inland and out to the sea.

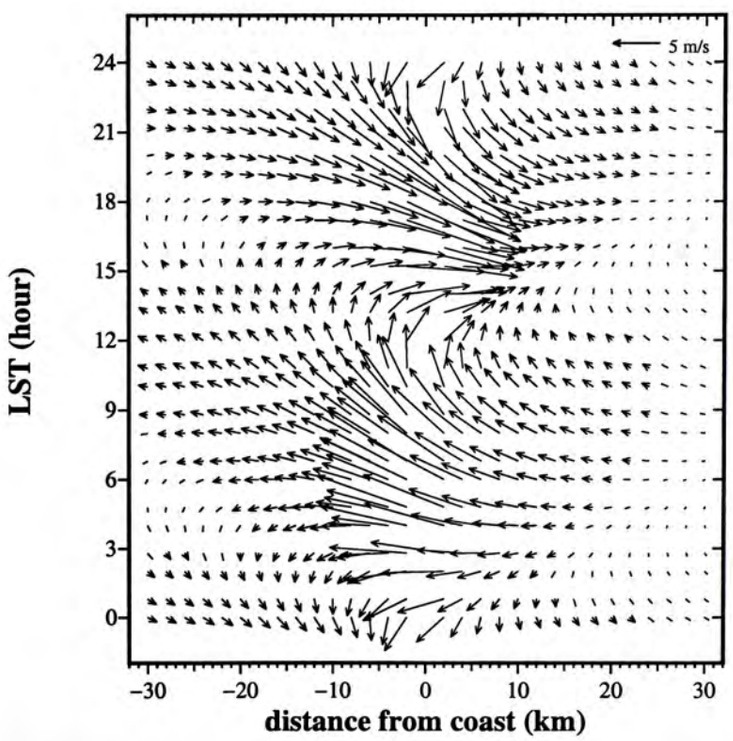

Figure 3.12. Surface wind field with $N^2 = 10^{-5}$ s^{-2}. The parameter used here is less than the standard values by an order-of-magnitude. With a weaker stratification stability, the sea-land breeze is intensified so that the wind speed is nearly doubled compared to the standard atmosphere.

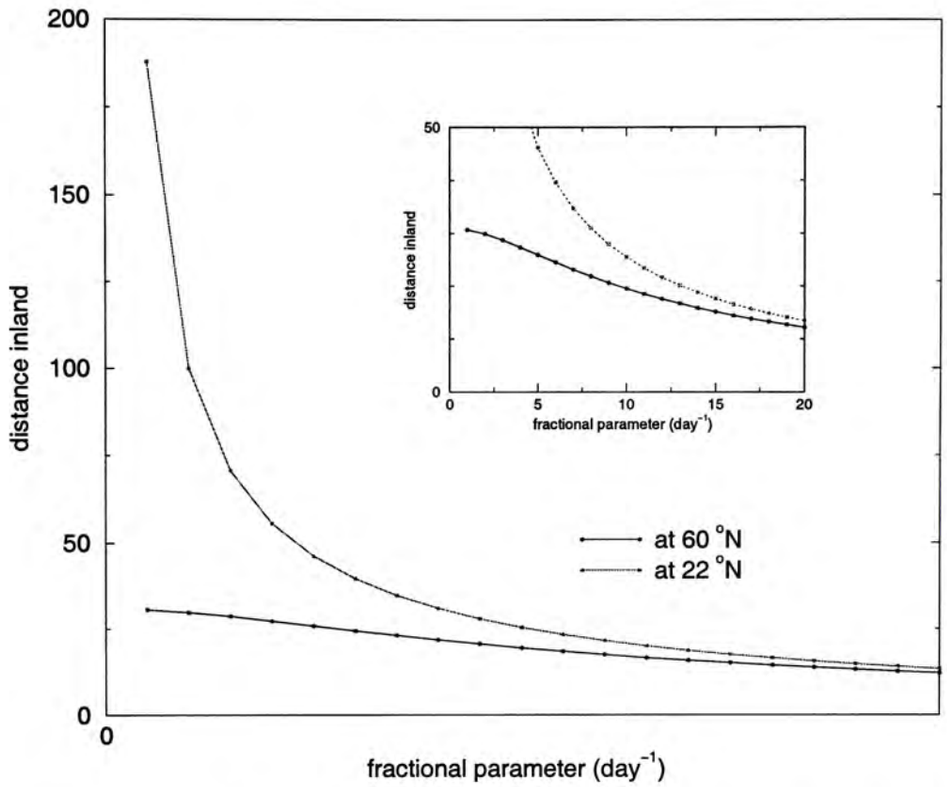

Figure 3.13. Effect of the frictional parameter on the horizontal extent. The solid line represents the distance of inland penetration at 22 °N, and the dashed line shows the distance at 60 °N. The graph indicates a significant reduction in the horizontal extent of the sea-land breeze at lower latitudes due to friction, while at higher latitudes it does not affect the breeze as much.

parameter, and those of the land and the sea can be assumed to be constants in each domain, since the vertical extent of the sea-land breeze circulation is not too high. In the following discussion, we keep $k_s = 0.25\, k_l$, and vary the two together.

Figure 3.13 shows the values of $D_{11,l}$ and $D_{11,s}$ at latitudes 22 °N and 66 °N respectively with different values of the frictional parameters in unit of day^{-1}, using other parameters as in Table 1.

From Figure 3.13, we see that the friction significantly reduces the horizontal extent of the sea-land breeze at lower latitudes, while at higher latitudes it does not affect the breeze as much. It can therefore be said that the horizontal extent at lower latitudes is more sensitive than at higher latitudes to changes in the frictional parameter. The frictional force also slows down the breeze as more kinetic energy is lost.

For the above reason, it can be seen that if we use different frictional parameters over the land and the sea, the horizontal extent will be different in the two cases: larger over the sea and smaller over the land. The sea-land breeze circulation is thus not symmetrical. From the previous figures, this situation can be clearly observed.

3.4 Discussion

Transition region

In the last sections we have assumed that the heating rates are different over the land and the sea, and changes abruptly across the coastline. This assumption is not realistic. There is a region over which the heating rate gradually changes from one value to the other. The width L of such a region enters as an external length scale which affects the system. In order to investigate the effect of this length scale, we modify the horizontal variation of the heating rate as

$$\tilde{Q} = \frac{1}{2}\left[(Q_l + Q_s) + \Delta Q \tanh\left(\frac{x}{L}\right)\right] \tag{3.6}$$

where $\Delta Q = Q_l - Q_s$ and L characterizes the width of the transition region; the meanings of the other parameters remain unchanged.

The domain now consists of a straight uniform coast with a transition region. The heating rate drops gradually from Q_l over the land ($x > 0$) to Q_s over the sea ($x < 0$). The previous setting is thus a special case where $L \to 0$. For the sake of simplicity the frictional parameter, however, is assumed to be the same across the coastline.

The Green's function for the governing equation (3.1), which satisfies the boundary condition $\tilde{\Phi}(x \to \pm\infty) = 0$, is

$$g_{mn}(x, x') = -\frac{1}{2\alpha_{mn}} e^{-\alpha_{mn}|x-x'|}$$

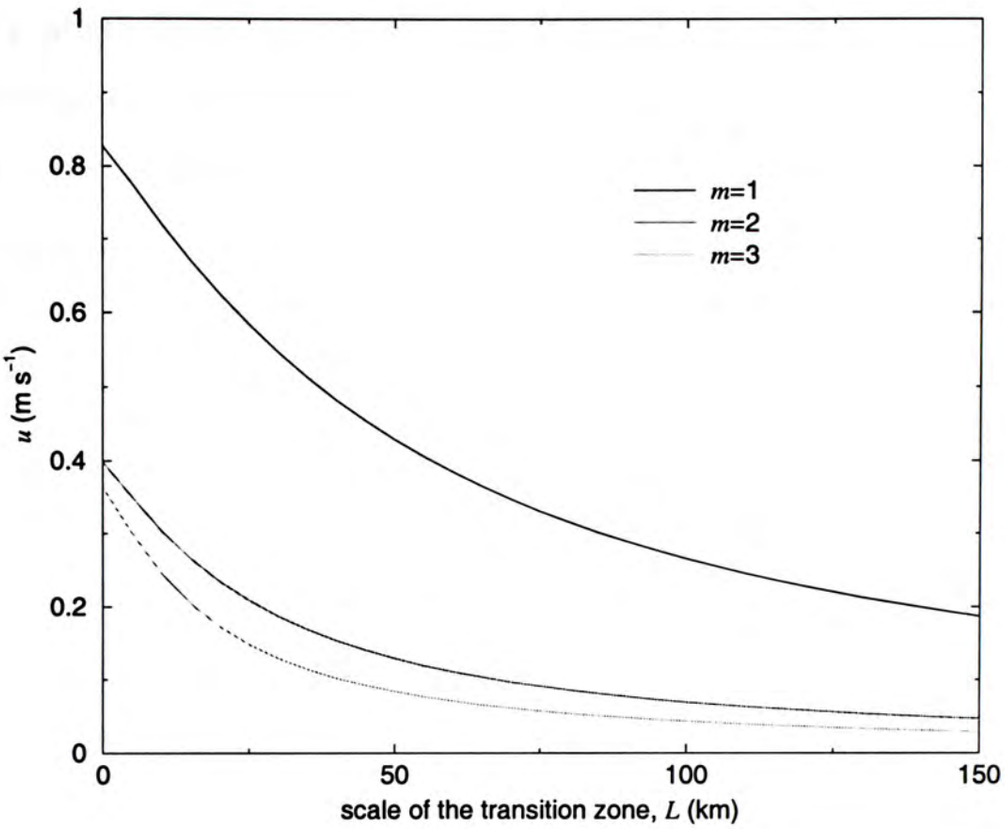

Figure 3.14. Effect of the width of the transition region on vertical modes. The figure shows the amplitudes of u versus L for the first three vertical modes ($m = 1, 2, 3$; $n = 1$). The spread of the transition zone reduces the wind strength rapidly, especially when the horizontal extent of the breeze is within the length scale L.

The solution $\tilde{\Phi}_{mn}$ is obtained by performing numerically the integral

$$\alpha_{mn}^2 \beta_{mn} \int_{-\infty}^{\infty} g_{mn}(x, x') \tilde{Q}(x') \, \mathrm{d}x'$$

$$= -\frac{\beta_{mn}}{2} (Q_t + Q_s) - \frac{\alpha_{mn} \beta_{mn} \Delta Q}{2} \int_{-\infty}^{\infty} \tanh\left(\frac{x'}{L}\right) e^{-\alpha_{mn}|x - x'|} \, \mathrm{d}x'$$

Figure 3.14 shows the amplitude of u as a function of the width L for the first three vertical modes ($m = 1, 2, 3$; $n = 1$). The spread of the transition zone reduces the wind strength rapidly, especially when the horizontal extent of the breeze is within the length scale L. The wind dies off for $L \ll D$.

The length scale $1/\mathrm{Re}(\alpha)$ therefore not only characterises the spread of the breeze, but also the system's spatial resolution of the heating source variation.

More realistic heating rate

The heating rate adopted in the above study is a sinusoidal function of time with a period of a day. This has the effect that the two halves of the day are mirror images, so that the land breeze and the sea breeze have equal strengths and opposite directions. This feature is not realistic. In reality, the cooling rate at night is much less than the heating rate in daytime. The excess heat influx is advected to the poles so that the global heat budget is balanced.

The actual process of heat transfer that gives the diurnal variation of the heating rate is very complicated. But we can think of it essentially as a balance between the solar radiation S and the radiation from the heated ground. This may be assumed to take the form

$$Q \sim S - e\sigma T^4 \tag{3.7}$$

where the radiation from the ground is modelled by the black body radiation σT^4 with an emissivity e. The solar radiation peaks at noon and dies out at night. And in days with weak sea-land breezes, the temporal variation of the ground temperature is often mild. Figure 3.15 shows a conceptual model of the heating heat with these assumption.

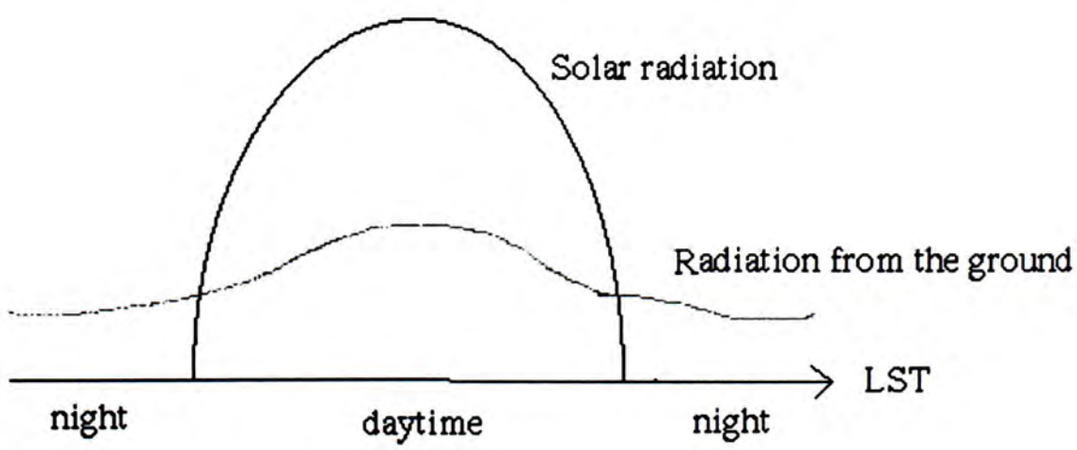

Figure 3.15. A conceptual model explaining the temporal variation of the realistic heating rate. The actual heating rate is essentially a balance between the solar radiation S and the radiation cooling $e\sigma T^4$ of the heated ground.

In light of these, we now employ a temporal function of the heating rate as shown in Figure 3.16 in order to obtain a more realistic simulation. The function is basically the difference between the two curves in Figure 3.15. For simplicity here we assume the diabatic function in time is essentially sinusoidal, chopped off from below, so that there is a period of constant cooling. The ratio of the amplitude of the heating and the cooling rate is taken to be 1 : 0.26 (Mass and Dempsey, 1985). The durations of the day and the night remain the same. Such a treatment is adopted by many realistic simulation models, e.g., Mass and Dempsey (1985).

In this case, the temporal variation is no longer sinusoidal; therefore, higher temporal harmonics must be kept in order to capture the characteristics of the temporal variation. Using typical values of parameters (Table 3.1), we compute the wind system again, and the time variation of the breeze is presented in Figure 3.17.

The land breeze becomes considerably weaker than the previous cases with the heating rates sinusoidal in time, as the cooling rate difference across the sea and the land is now greatly reduced[4]. The breeze is also directed more towards the normal of the shore, as shown in Figure 3.18.

Figure 3.19 shows the wind hodograph at Cheung Chau on a sea-land breeze day. The hodograph records the diurnal change in the wind direction and the strength on a typical sea-land breeze day. The prevailing wind is slightly northerly on that day. Cheung Chau lies at the opening of West Lamma Channel, facing the South China Sea. In the north are large clustered pieces of landmass (Figure 3.20). The southerly sea breeze is observed to be stronger than the northerly land breeze, and this broadly agrees with the model result.

[4]The diurnal variation in stratification (represented by N^2) also plays an important role in explaining the difference between the sea breeze and the land breeze intensity (Man and Walsh, 1976). Although in the present model, N^2 is assumed constant over time, we can still trace the effect of nighttime stability. As shown in (3.4), the amplitude of u goes as N^{-2}. The stronger stratification at night thus gives a weaker land breeze.

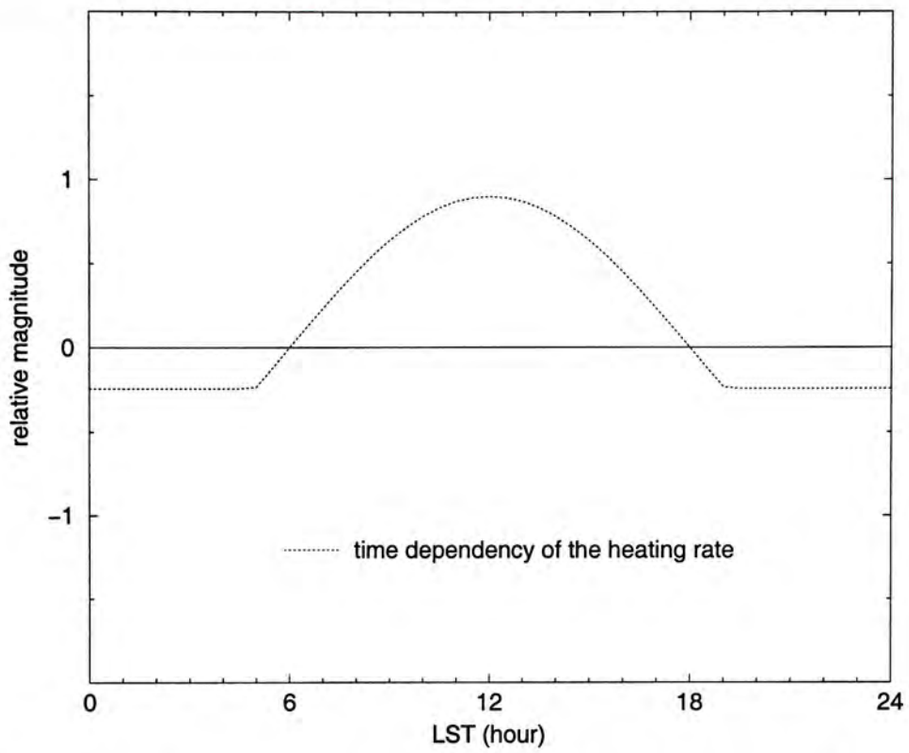

Figure 3.16. The time dependency of a more realistic diabatic forcing for 24 hours, after Mass and Dempsey (1985). The cooling rate at night, assumed constant for simiplicity, is much less than the heating rate in daytime. The excess heat influx is advected to the poles so that the globe heat flux is balanced.

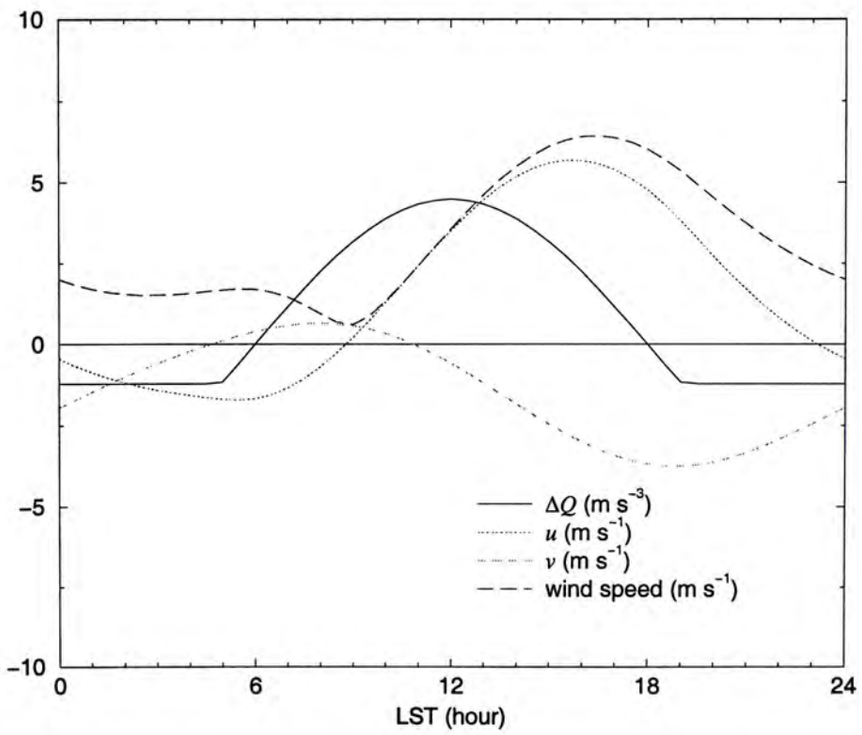

Figure 3.17. A graph showing the time history of the surface wind components u and v under a more realistic diabatic forcing, at 1 km inland from the coast for 24 hours, which illustrates the effects of the higher n-harmonics on the temporal variation during the day.

As shown in (2.14), the horizontal extent is $D = 1/\mathrm{Re}(\alpha)$ where

$$\alpha = \frac{m\pi}{H}\left(\frac{\chi^2+f^2}{\chi^2+N^2}\right)^{\frac{1}{2}}\left(\frac{\zeta}{\chi}\right)^{\frac{1}{2}} \approx \frac{m\pi}{NH}\left(\frac{\zeta}{\chi}\right)^{\frac{1}{2}}\left[\chi^2+f^2\right]^{\frac{1}{2}}$$

$$\approx \left(\frac{\zeta}{\chi}\right)^{\frac{1}{2}}\left((k+in\omega)^2+f^2\right)^{\frac{1}{2}}$$

since $|N| \gg |\chi|$ typically. The last bracket equals $(k+in\omega)^2+f^2 = (k^2+f^2-n^2\omega^2)+i\,2n\omega k$, so that the horizontal extents can be easily seen to be larger for higher harmonics.

The ratio of the wind components v and u for the barotropic mode ($m = 1$) is represented by $|\tilde{V}_{1n,l}/\tilde{U}_{1n,l}| = |f/(k+in\omega)|$, which obviously decreases as n increases, so that, when the temporal harmonics are summed up, there is overall a larger alongshore component than for the $n = 1$ alone.

Table 3.2 gives the values of the ratio $D_{1n,l}$, $D_{1n,s}$ and $|\tilde{V}_{1n,l}/\tilde{U}_{1n,l}|$ of the barotropic mode ($m = 1$) for various temporal harmonics n, with values of parameters as listed in Table 3.1. The distribution of the temporal harmonics is also shown for comparison in the Table. The horizontal extent increases rapidly, but tends to a constant as n increases; so does the ratio $|\tilde{V}_{1n,l}/\tilde{U}_{1n,l}|$. The behaviour of the lower harmonics differs significantly from each other.

Table 3.2. The effect of higher temporal harmonics on the barotropic mode ($m = 1$)

harmonic n	0	1	2	3	4	5	6	7	
$D_{1n,l}$	40.05	46.16	51.61	53.35	54.00	54.29	54.43	54.48	km
$D_{1n,l}$	56.47	152.6	204.1	212.9	215.9	217.1	217.7	217.9	km
$\lvert\tilde{V}_{1n,l}/\tilde{U}_{1n,l}\rvert$	0.941	0.586	0.348	0.241	0.184	0.147	0.124	0.106	

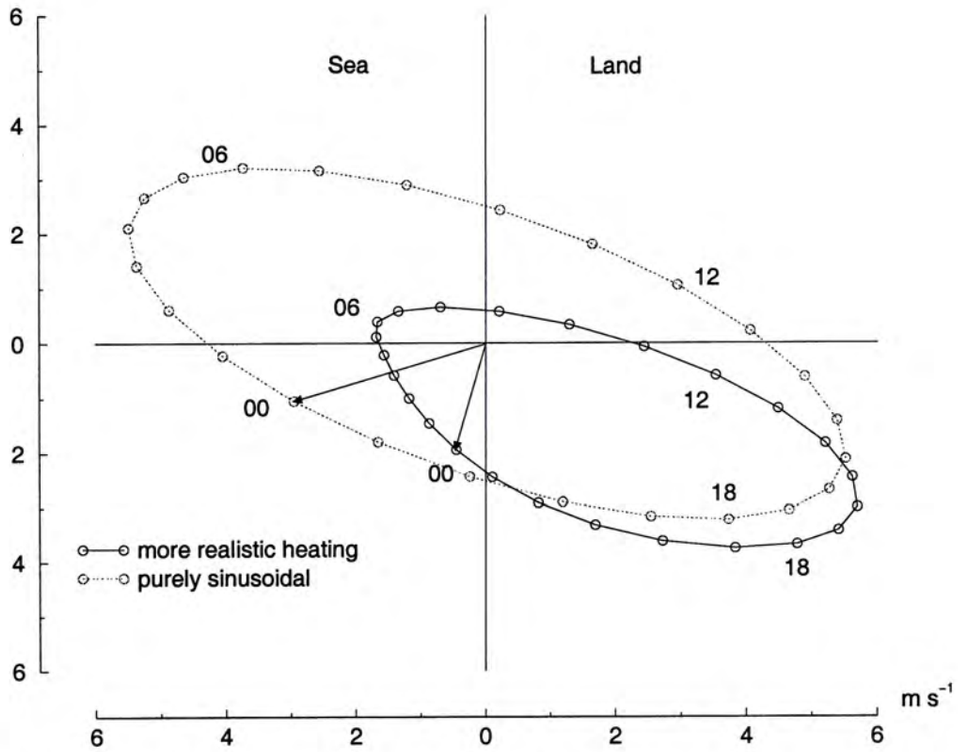

Figure 3.18. Wind hodograph under a more realistic heating. The numbers near the data points indicate the time (LST) of measurement. The land breeze becomes considerably weaker since the cooling rate difference across the sea and the land is greatly reduced. The breeze is also directed more towards the normal of the shore.

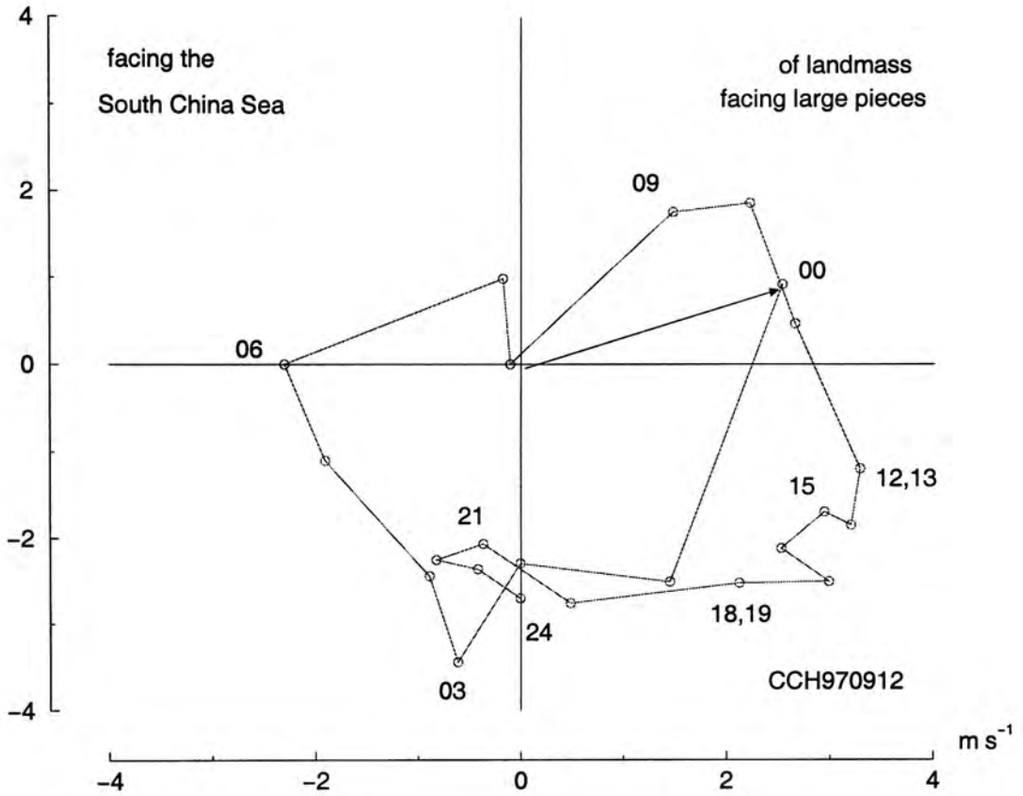

Figure 3.19. Wind hodograph at Cheung Chau on a typical sea-land breeze day, with a sight northerly prevailing wind. The hodograph records the diurnal change in the wind direction and the strength on 12 September, 1997. The southerly sea breeze is observed stronger than the northerly land breeze in agreement with the model result.

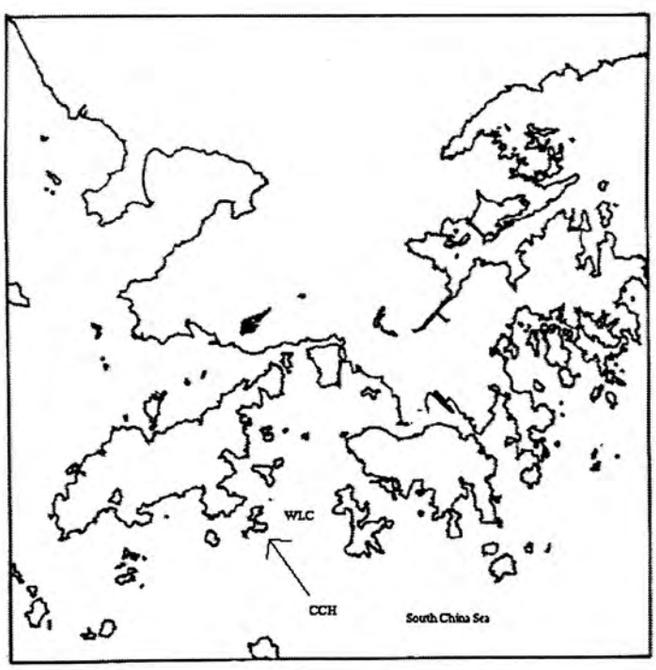

Figure 3.20. Location of Cheung Chau. Cheung Chau (CCH) lies at the opening of the West Lamma Channel (WLC), facing the South China Sea in the south. In the north are large clustered pieces of landmass.

Chapter 4

Effects of the coastline geometry

In Chapter 3, we have discussed sea-land breeze systems across a straight coastline, and the breezes in those cases are uniform along the coast. If the coast is not straight, the flow is no longer uniform along the coast, but converges or diverges according to the curvature of the coastline.

As most coastlines are curved in some way, this effect is very important in the development of the sea-land breeze, and areas of convergence and divergence are frequently formed. This phenomenon is all the more important because incoming air which must rise at the convergence line is often associated with convective clouds and rain.

4.1 Effects of coastline curvature

Simpson (1994) presented a simple diagram showing how the sea breeze converges at convex coasts (e.g., headlands) and diverges at concave ones (e.g., bays), as shown in Figure 4.1. The situation reverses in the case of land breeze, which then leads to convergence when the coast is concave and divergence when it is convex.

Bays and headlands

It is difficult to obtain an analytic solution for systems with an irregular coast. Therefore, the influence of the curvature of the coastline is studied by means of

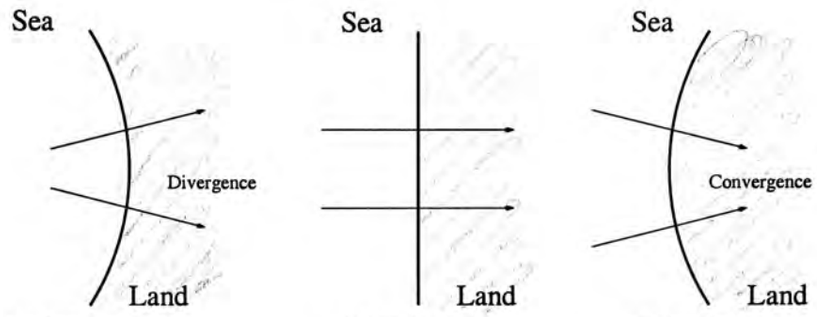

(a) Concave coast (b) Straight coast (c) Convex coast

Figure 4.1. Simple diagram showing different curved coastlines. The sea breeze diverges at concave coasts and converges at convex ones: (a) concave coast, (b) straight coast, and (c) convex coast. After Simpson (1994).

numerical solutions.

Let us first examine two typical cases, one with a semicircular bay of radius 25 km, and the other with a semicircular headland of radius 25 km, by applying the general model developed in Chapter 2. This radius was chosen because it is small enough to be within the length scale of the sea breeze as found in the straight line case, yet still large enough to be adequately resolved in the model.

Numerical Aspect. — The model configuration is three-dimensional, unlike the straight coastline case where the translational symmetry reduces the system to two dimensions. For the sake of simplicity, we assume that the frictional coefficient is the same over the land and the sea, and the temporal variation of the heating rate is nearly sinusoidal so that only the fundamental harmonic ($n = 1$) with the period of a day is kept. The values of the model parameters employed are listed in Table 4.1.

The domain is discretized into square grids of 1 km $\times$ 1 km. The equation (2.12) is replaced by a finite-difference representation (centre differencing) and solved by the simultaneous overrelaxation (SOR) method with the overrelaxation parameter set to 1.5 (Press et al., 1987). The values at the boundary is taken as if the coastline is straight, since the domain is large enough (300 km $\times$ 200 km) so that the boundary region is outside the influence of the curved part.

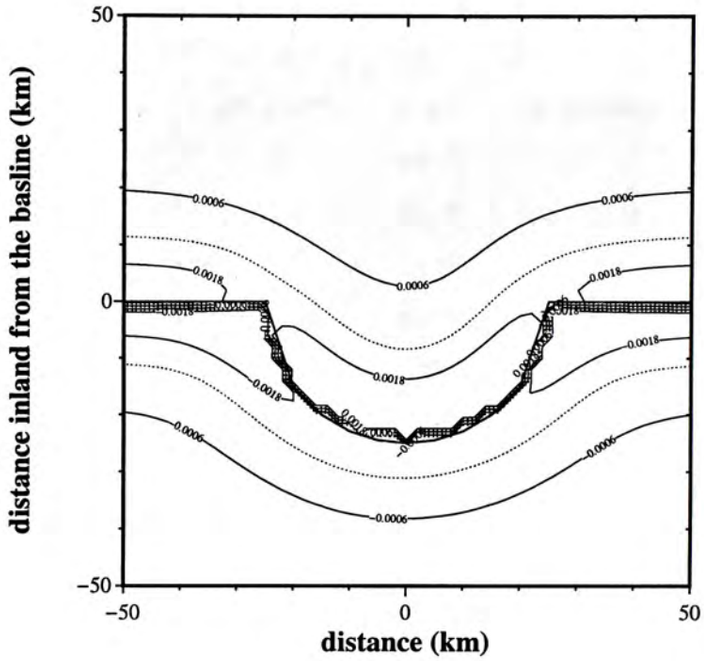

(a)

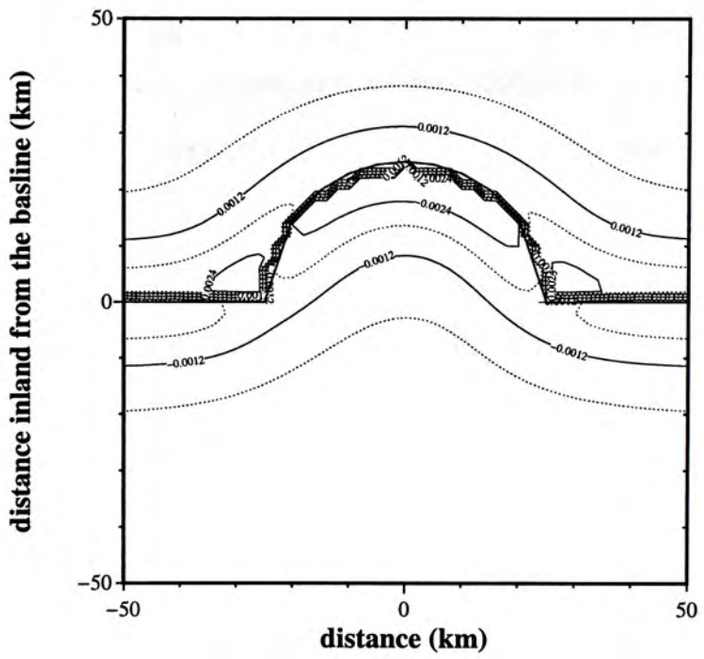

(b)

Figure 4.2. Vertical velocity in the sea breeze phase for the cases with (a) a semicircular peninsula and (b) a semicircular bay of radius 25 km. The thick solid line represents the shoreline, cutting the land in the upper half (say, North) from the sea in the lower half (South). The lines are contours of vertical velocity, at a height of 500 m at 1600 LST.

Table 4.1. The standard values of model parameters (II)

Parameter	Value	Unit	Comments
Q_l	6×10^{-6}	m s^{-3}	
Q_s	1.5×10^{-6}	m s^{-3}	$Q_s = 0.25Q_l$
k_l	5	day^{-1}	
k_s	1.25	day^{-1}	$k_s = 0.25k_l$
κ_l	5	day^{-1}	
κ_s	1.25	day^{-1}	$\kappa_s = 0.25\kappa_l$
N^2	1×10^{-4}	s^{-2}	
f	0.54484×10^{-5}	s^{-1}	at latitude 22° N
H	1	km	
δ	2×10^{-3}	m^{-1}	

Vertical motion. — The most noticeable difference between the bay and the peninsula is in the vertical velocity, as shown in Figure 4.2. Subsidence behind the sea-breeze front is slightly stronger and extends further to the sea for the concave coastline. This may enhance offshore effects such as the suppression of cloudiness (Arritt, 1989), consistent with observational evidence regarding the effect of the coastal curvature on the convergence and the divergence of sea-land breezes, and the resulting suppression or generation of thunderstorms (Neumann, 1951).

Surface wind. — Figure 4.3 shows the surface wind field in the sea-breeze phase for the two cases. These figures indicate that the effect of the coastal curvature is not symmetrical on the two sides of the headland or the bay. For convenience, we now suppose that the baseline of the coast is east-west oriented, cutting the land in the north from the water in the south. For example, in the case over a headland, winds on the west tilt more towards the coastline, while winds on the east are nearly normal to the coastline of the bulging landmass. McPherson (1970) also noticed a similar asymmetry when performing a three-dimensional simulation with a square bay, and was able to explain the asymmetry by noting

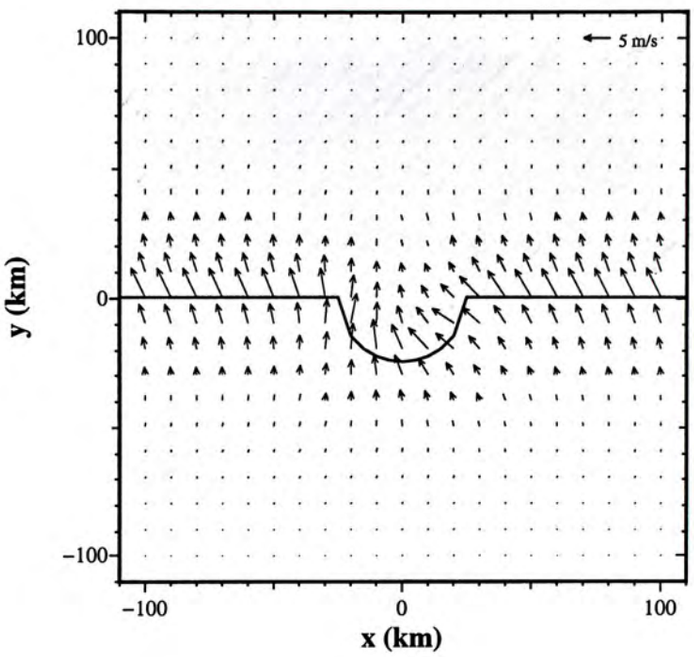

(a)

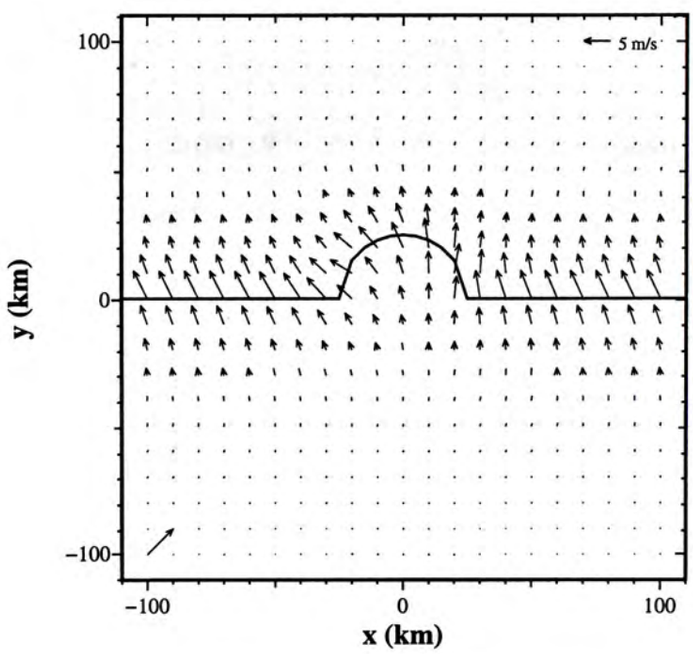

(b)

Figure 4.3. Surface wind field in the sea-breeze phase for the case with (a) a round headland and (b) a semicircular bay, both of radius of 25 km. The thick solid line represents the shoreline, cutting the land in the upper half (say, North) from the sea in the lower half (South). The wind field is taken at height of 100 m at 1600 LST. Note that in case (a), the direction of the winds on the east becomes nearly normal to the baseline, while on the west winds tilt from the bulging landmass; in case (b), the breeze deflects when passing over the bay, differently at positions along the coast.

that the Coriolis force and the overall pressure force act in the same direction on one side but in opposite direction on the other.

Coastline curvature

These features arise because the scale of the coastal irregularity is less than the extent of the sea breeze (e.g., estimated from the case with a straight coastline). As pointed out by Arritt (1989), the radius of curvature R of the coastline must be considered in the light of the other length scales. In the present model, the overall flow is treated as the composite of various spatial modes m, each with its own length scale. When R is less than the mode's distance of influence, sea breezes from different parts can interact, and thereby distort (compared with the case with a straight coastline). As R becomes large compared with the characteristic horizontal scale of the mode, the response should be nearly the same at points equidistant from the coast.

Figure 4.4 gives an example, which shows how the spatial pressure pattern of a sea breeze adjusts itself near the shore in spatial modes $m = 1, 2, 3$ for the case of a headland with radius 25 km. The horizontal length scale of the modes $m = 1, 2, 3$ are about 150, 75 and 50 km, respectively. The thick solid line represents the shoreline, cutting the land in the upper half from the sea in the lower half. In higher spatial modes, the spatial pressure patterns are seen to be very sensitive to the coastal irregularity, and nearly follow the shape of the shore, compared with that of the lower modes.

4.2 Model of circular islands

A circular island or lake can be regard as a limiting case of strongly curved coastline. We therefore proceed to investigate the effect of the radius on the sea breeze over a circular island.

We now place the origin of a cylindrical coordinate system at the centre of

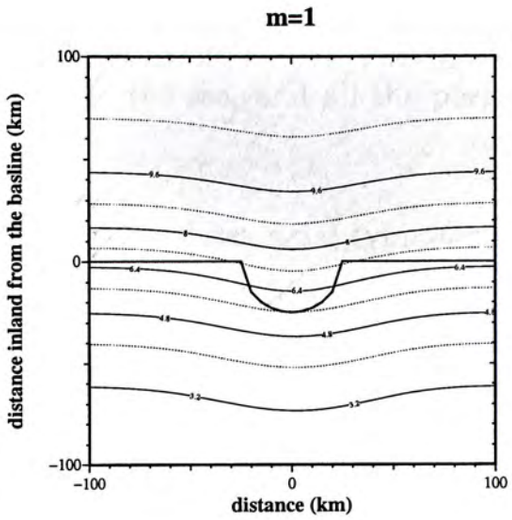

(a)

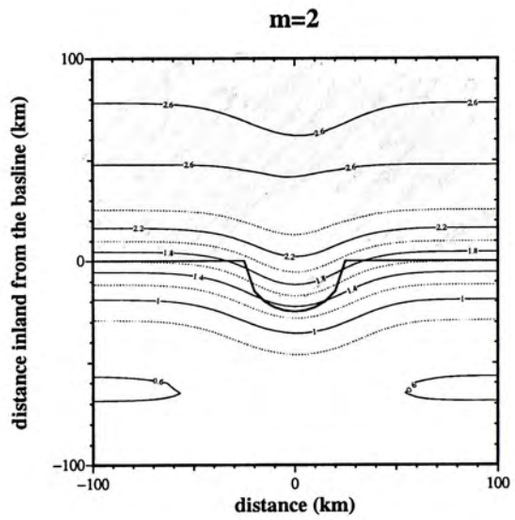

(b)

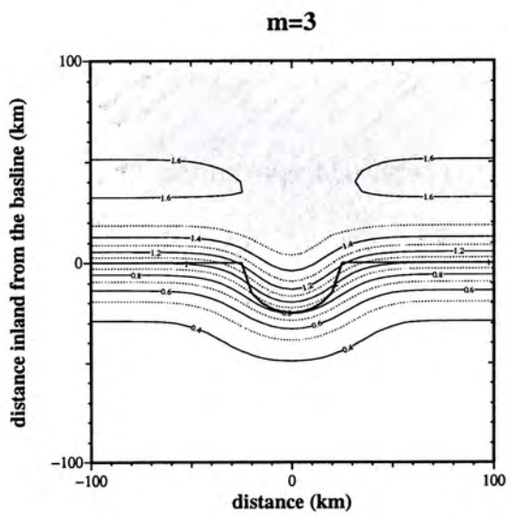

(c)

Figure 4.4. Countour plots showing the reponse of the spatial pressure pattern to the coastline curvature, in spatial modes (a) $m = 1$, (b) $m = 2$, and (c) $m = 3$, for the case with a headland of radius 25 km. The thick solid line represents the shoreline, cutting the land in the upper half from the sea in the lower half. As the radius of curvature becomes large compared with the characteristic horizontal scale of the mode, the response is nearly the same at points equidistant from the coast.

a circular island of radius R, and assume that the diabatic forcing is isotropic, higher over the land than over the sea, and all the perturbations approach zero at infinity.

Since the system obviously possesses axial symmetry, all derivatives with respect to the azimuthal angle φ about the z-axis vanish. The governing equation (2.12) then becomes

$$\left[\frac{1}{r}\partial_r(r\partial_r) - \alpha_{mn}^2\right]\tilde{\Phi}_{mn}(r) = \alpha_{mn}^2\beta_{mn}\tilde{Q}(r) \tag{4.1}$$

where

$$\alpha_{mn} = \frac{m\pi}{H}\left(\frac{\chi^2 + f^2}{\chi\zeta + N^2}\right)^{\frac{1}{2}}\left(\frac{\zeta}{\chi}\right)^{\frac{1}{2}}$$

$$\beta_{mn} = \frac{q_n\gamma_m}{\zeta}\left(\frac{m\pi}{H}\right)^{-1}$$

The model parameters k and κ are taken to be uniform over the whole plane, so that α_{mn} remains the same over the land and the sea. The horizontal variation of the heating function is assumed to be a step function across the coastline, more precisely

$$\tilde{Q}(r) = \begin{cases} Q_\ell\,, & r < R \\ Q_s\,, & r > R \end{cases} \tag{4.2}$$

which are constants, with a larger values over the land than over the sea, i.e., $Q_\ell > Q_s$. The temporal variation is taken as in Figure 3.17.

The equation (4.1) can be solved exactly. In fact the solution is given by products of the Bessel functions I and K:

$$\tilde{\Phi}_{mn}(r) = -\beta\tilde{Q} \pm \beta\Delta Q\,\alpha_{mn}R \times \begin{cases} K_1(\alpha_{mn}R)I_0(\alpha_{mn}r)\,, & r < R \\ I_1(\alpha_{mn}R)K_0(\alpha_{mn}r)\,, & r > R \end{cases} \tag{4.3}$$

By the relations in (2.10) and (2.11), the amplitudes of the velocity components are obtained as follows.

$$\tilde{U}_{mn}(r) = \frac{m\pi}{H}\frac{q_n\gamma_m\Delta Q}{N^2}R\begin{cases} K_1(\alpha_{mn}R)I_1(\alpha_{mn}r)\,, & r < R \\ I_1(\alpha_{mn}R)K_1(\alpha_{mn}r)\,, & r > R \end{cases} \tag{4.4}$$

$$\widetilde{W}_{mn}(r) = \frac{H}{m\pi}\frac{q_n\gamma_m\Delta Q}{N^2}\alpha_{mn}R\begin{cases} K_1(\alpha_{mn}R)I_0(\alpha_{mn}r), & r < R \\ I_1(\alpha_{mn}R)K_0(\alpha_{mn}r), & r > R \end{cases} \tag{4.5}$$

Hence all the flow fields as a function of time and space are readily obtained by summing the spatial and temporal modes.

All the numerical results reported below are truncated at $m = 10$ and $n = \pm 3$. The standard parameters listed in Table 4.1 are used. We shall consider the distributions of u and w in order to investigate the convergence effect at the centre.

General sea breeze

First we show an example over a sufficiently large island ($R = 100$ km) producing no strong ascending flow at its the centre. Figure 4.5 shows the plane view of the surface wind field in the sea-breeze phase. The breeze appears near the coast, blowing onshore and turning slightly anticlockwise due to the Coriolis effect. The time cross-sections of u and w at a height of 100 m are shown in Figure 4.6 and Figure 4.7. The maximum value of u is observed over the coastline at 1400 LST. The horizontal extent is broadly the same towards the land and towards the sea. Figure 4.8 and Figure 4.9 are the vertical cross-sections showing the cross-shore wind and the vertical motion of the circulation at 1400 LST, at which time w is observed to reach its maximum. Vectors in these figures represent the air flow.

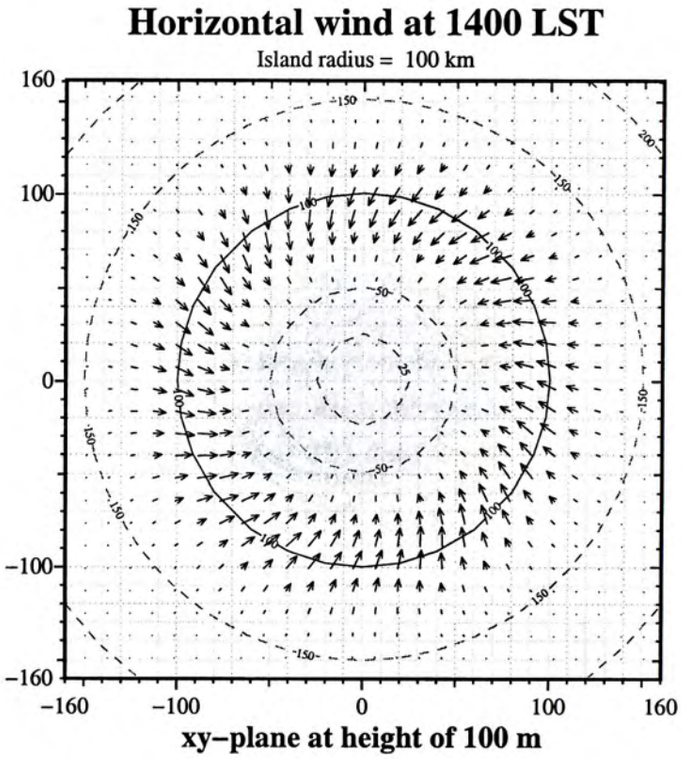

Figure 4.5. Surface wind (5 m s^{-1} per grid) in the sea breeze phase over an island of radius 100 km. The concentric circles indicate the distance from the centre of the island, while the solid line represents the coastline. The wind field is taken at a height of 100 m at 1400 LST.

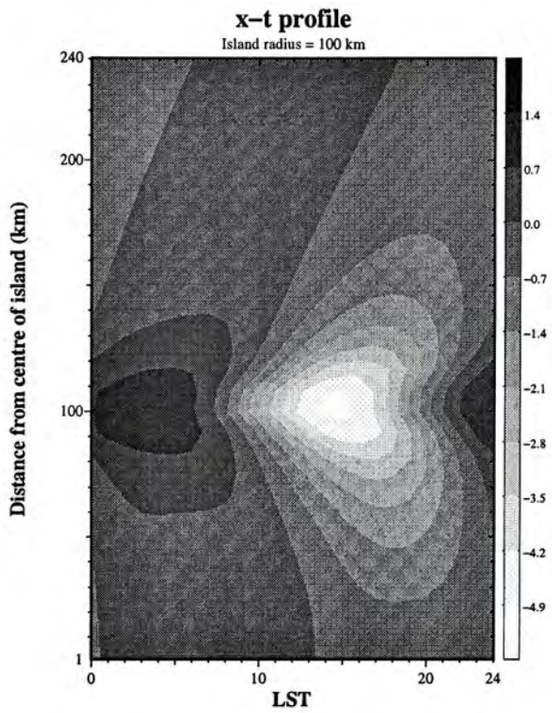

Figure 4.6. Time cross-section of surface across-shore component u in the sea-breeze phase over an island of radius 100 km. The grey scale represents the magnitude of u (m s^{-1}) and a positive value indicates an on-shore wind. The data are taken at a height of 100 m.

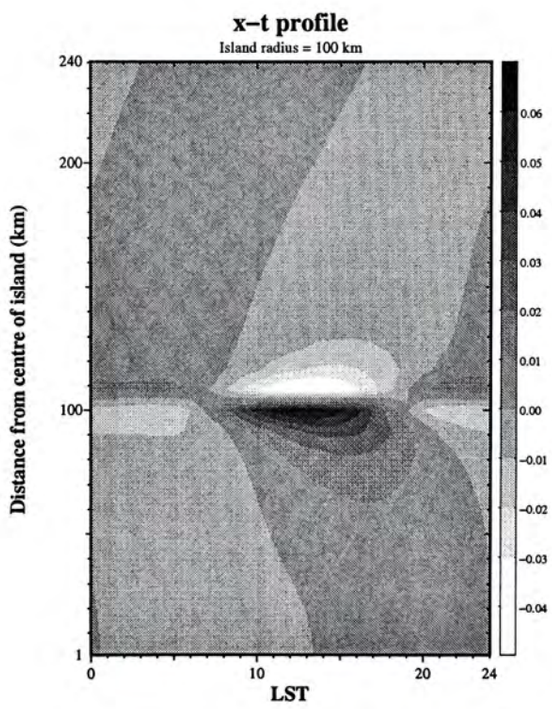

Figure 4.7. Time cross-section of vertical motion w in the sea breeze phase over an island of radius 100 km. The grey scale represents the magnitude of w (m s^{-1}) . The data are taken at a height of 500 m.

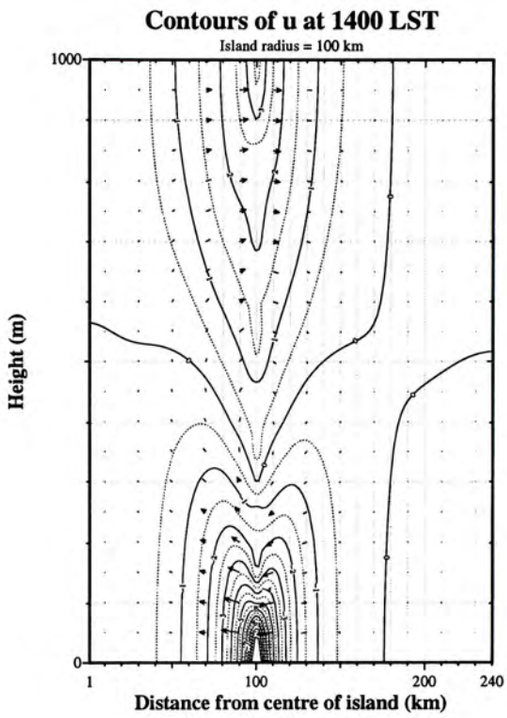

Figure 4.8. Vectical cross-section of across-shore component u in the sea breeze phase over an island of radius 100 km. The contours represent the magnitude of u (m s^{-1}), while the arrows indicate the direction of the flow.

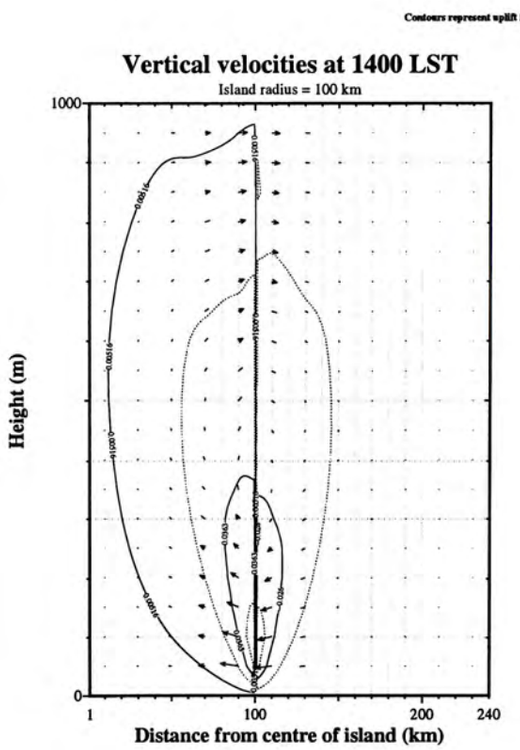

Figure 4.9. Vectical cross-section of vertical motion w in the sea breeze phase over an island of radius 100 km. The lines are contours of w (m s^{-1}), while the arrows indicate the direction of the flow.

Intensified convergence

We now examine the case of a small radius ($R = 25$ km) and compare it with the results in the last section. The plan view of the sea breeze is shown in Figure 4.10. The convergence at the centre becomes conspicuous and the vorticity is also intensified. The time cross-sections of the circulations are shown in Figure 4.11 and Figure 4.12. The maximum value of w is about 43% larger than that in the large island case. As shown in Figure 4.11, the largest onshore velocity is found a few kilometres inland, not at the shore. The breeze develops at the coastline an hour earlier and its extent is limited inland, much shorter than over the sea. Compared to the large island case, the vertical extent is also smaller over the island as shown in Figure 4.13.

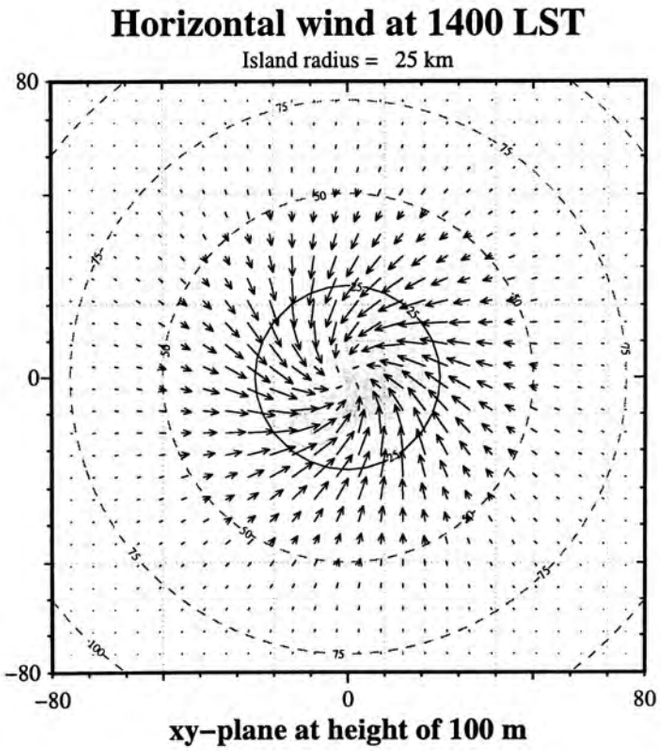

Figure 4.10. Surface wind (5 m s^{-1} per grid) in sea-breeze phase on an island of radius 25 km. The concentric circles indicate the distance from the centre of the island, while the solid line represents the coastline. The wind field is taken at a height of 100 m at 1400 LST.

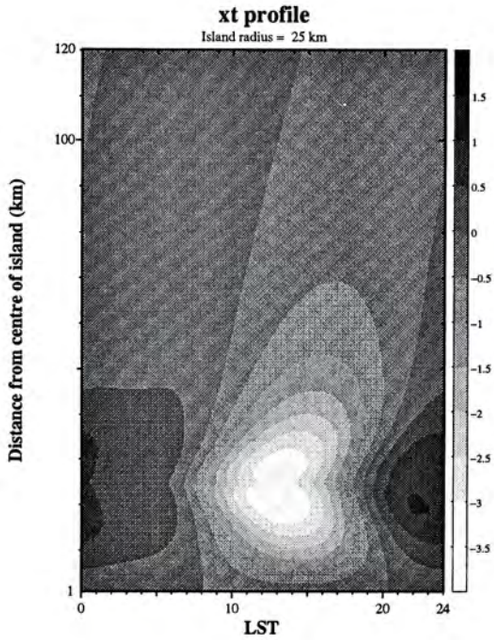

Figure 4.11. Time cross-section of across-shore component u over an island of radius 25 km. The contours represent the magnitude of u (m s^{-1}) and a positive value indicates an on-shore wind. The data are taken at a height of 100 m.

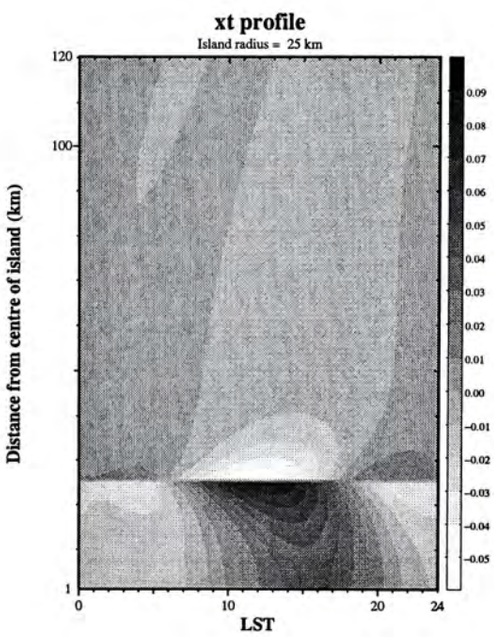

Figure 4.12. Time cross-section of vertical motion w over an island of radius 25 km. The contours represent the magnitude of w (m s^{-1}). The data are taken at a height of 500 m.

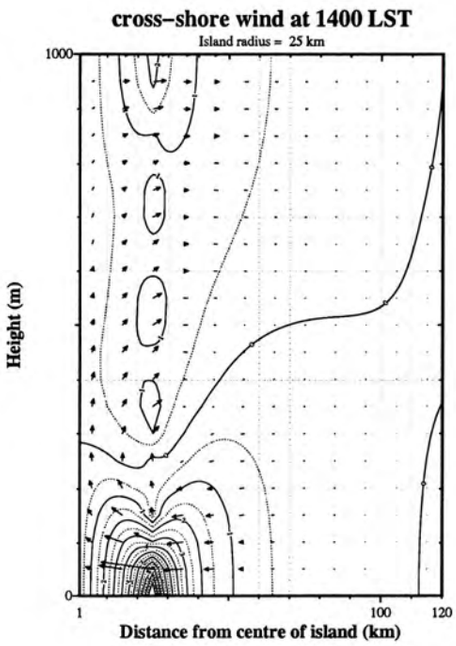

Figure 4.13. Vectical cross-section of across-shore component u in the sea breeze phase over an island of radius 25 km. The lines are contours of u (m s^{-1}), while the arrows indicate the direction of the flow.

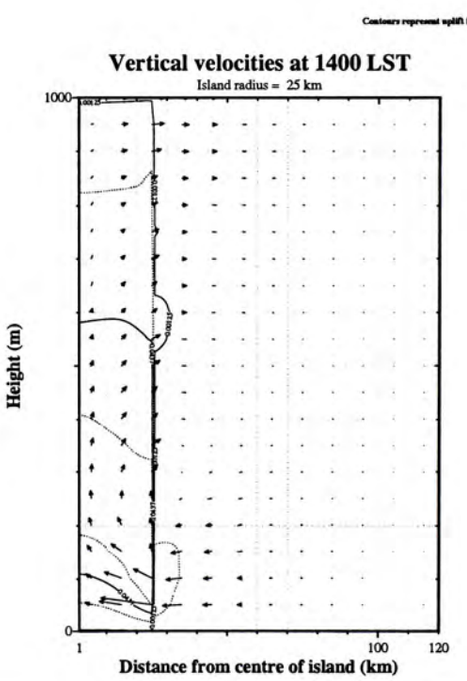

Figure 4.14. Vectical cross-section of vertical motion w in the sea breeze phase over an island of radius 25 km. The lines are contours of w (m s^{-1}), while the arrows indicate the direction of the flow.

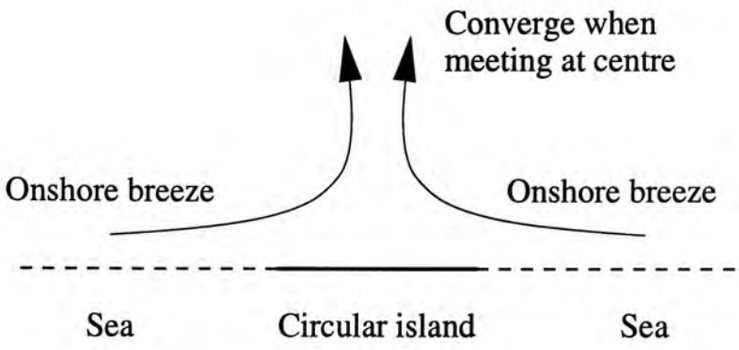

Figure 4.15. Schematic diagram showing the convergence of the onshore breezes from different directions when they meet at the centre. The intensification of the vertical motion may enhance the generation of convective clouds if the effects of latent heat or the orography are taken into account.

The intensification of the vertical motion over a small island may be explained by the convergence of the onshore breezes from different directions when meeting at the centre, as shown in the schematic diagram in Figure 4.15. One would expect the strong lifting flow to enhance the generation of convective clouds if the effects of latent heat or the orography are taken into account. This suggests that it would be worthwhile to study models making allowance for cloud formation.

Time of sea-breeze phase

Next, the time variations of $|u_{max}|$ are shown in Figure 4.16 for various island sizes. The sign convention is such that offshore winds correspond to $u > 0$, and negative values of u indicate onshore winds. The value of $|u_{max}|$ is small in the case of the comparatively small island (with Q held constant), because of the small heating surface. Earlier onset times and shorter durations are also observed. For a large island (R >100 km), their extreme values converge to the value for a straight coast and is observed near 1500 LST.

Figure 4.17 shows the time variations of $|w_{max}|$, in the same manner as Figure 4.16. The profiles of w_{max} are rather different from those of u_{max}. In the case of a large island, the value of w_{max} is, in contrast, greater. For islands of radii over 100 km, the extreme value converges to 0.75 m s^{-1} at noon, when the heating gradient

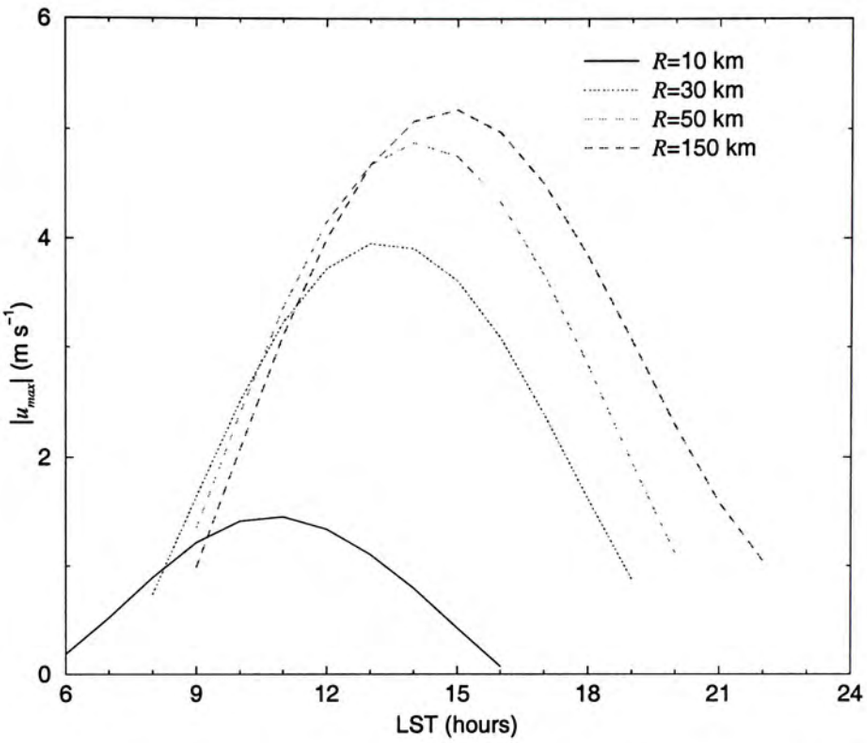

Figure 4.16. Temporal variation of surface u measured at the shore for islands of different sizes. The value of $|u_{max}|$ is small in the case of the comparatively small island (with Q held constant), because of the small heating surface. Earlier onset times and shorter durations are also observed.

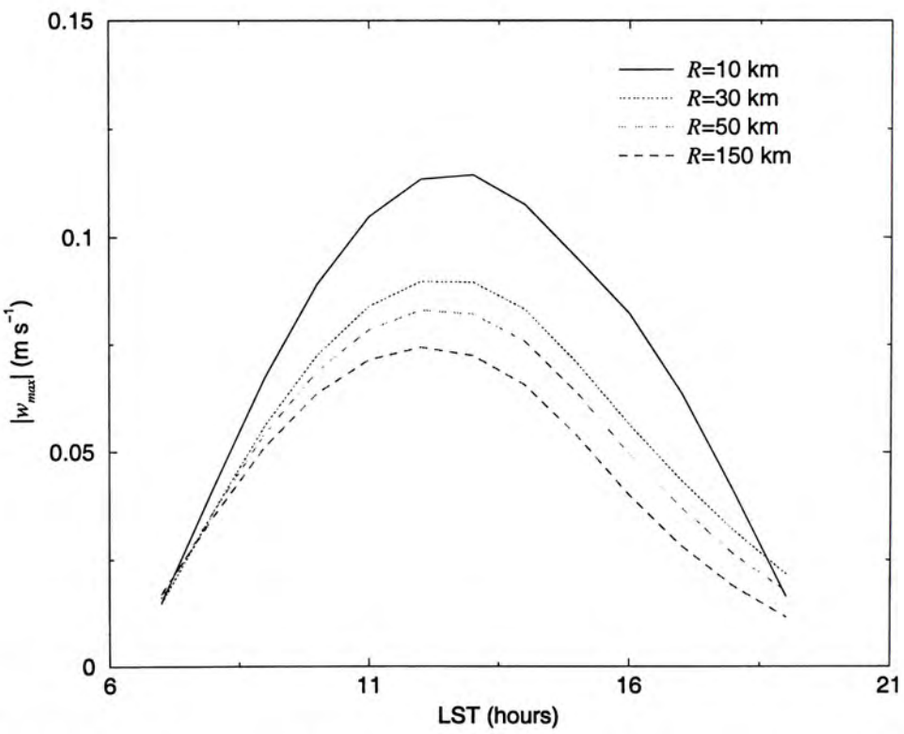

Figure 4.17. Temporal variation of surface w measured at the shore for islands of different sizes. The value of $|w_{max}|$ decreases consistently with the reduction of the heating gradient.

across the sea and the land is near its maximum. Thereafter $|w_{max}|$ decreases monotonically with the reduction of the heating gradient.

Limiting case of $R \to \infty$

Figure 4.18 and Figure 4.19 show the variation of u_{max} and w_{max} with the island size R. The vertical motion w_{max} weakens while the onshore wind $-u_{max}$ strengthens when R increases, as discussed above. In fact the limiting case of large R reduces to a straight infinite coast, which can be easily shown with the following asymptoptic formulas:

$$I_n(z) \sim \frac{e^z}{\sqrt{2\pi z}}$$

$$K_n(z) \sim \sqrt{\frac{\pi}{2z}} e^{-z}$$

as $z \to \infty$. The spatial dependence of $\tilde{U}_{mn}$ is proportional to $RI_1(\alpha_{mn}r)K_1(\alpha_{mn}r)$. If we expand r as $R + x$, where $R \gg x$, and assume that the radius R is much larger than the horizontal scale so that $|\alpha_{mn}R| \gg 1$, then by applying the asymptotic formula above,

$$\tilde{U}_{mn}(x) = \frac{m\pi}{H}\frac{\gamma_m q_n \Delta Q}{N^2} R \times \begin{cases} K_1(\alpha_{mn}R)I_1(\alpha_{mn}r), & r < R \\ I_1(\alpha_{mn}R)K_1(\alpha_{mn}r), & r > R \end{cases}$$

$$\sim \frac{m\pi}{H}\frac{\gamma_m q_n \Delta Q}{N^2}\frac{1}{2\alpha_{mn}} \times \begin{cases} e^{\alpha_{mn}x}, & r < R \\ e^{-\alpha_{mn}x}, & r > R \end{cases}$$

which reduces to the case with an infinitely long straight coastline[1].

Distribution of spatial modes

In Figure 4.18 and Figure 4.19, the cumulative contributions of the spatial modes are also shown. The graph of w_{max} indicates that the vertical flow is intensified when the island size is comparable with the horizontal scale of each mode, determined by the quantities α_m in (4.4) and (4.5). It is interesting to note that the

[1]See (3.4). Here we have assumed $k_l = k_s$ and $\kappa_l = \kappa_s$, which imply $\alpha_l = \alpha_s$ and $\zeta_l = \zeta_s$, and (3.4) gives the very expression concerned.

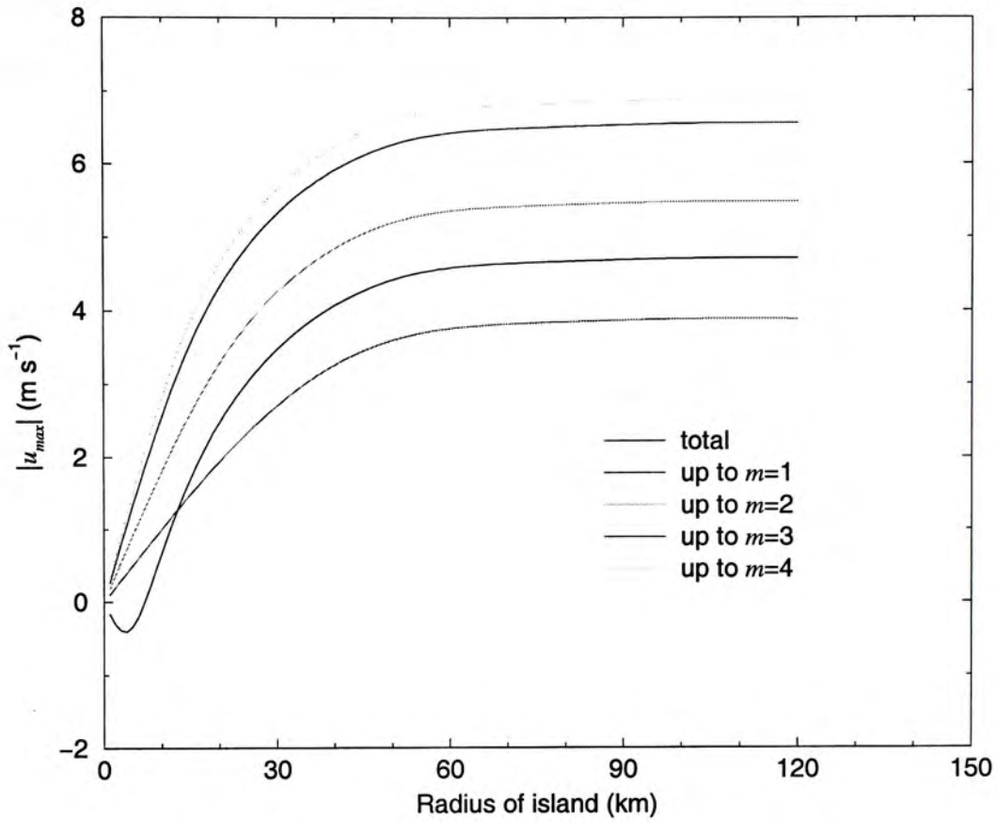

Figure 4.18. Effect of island size and contribution of different modes on surface w_{max} for islands of various sizes

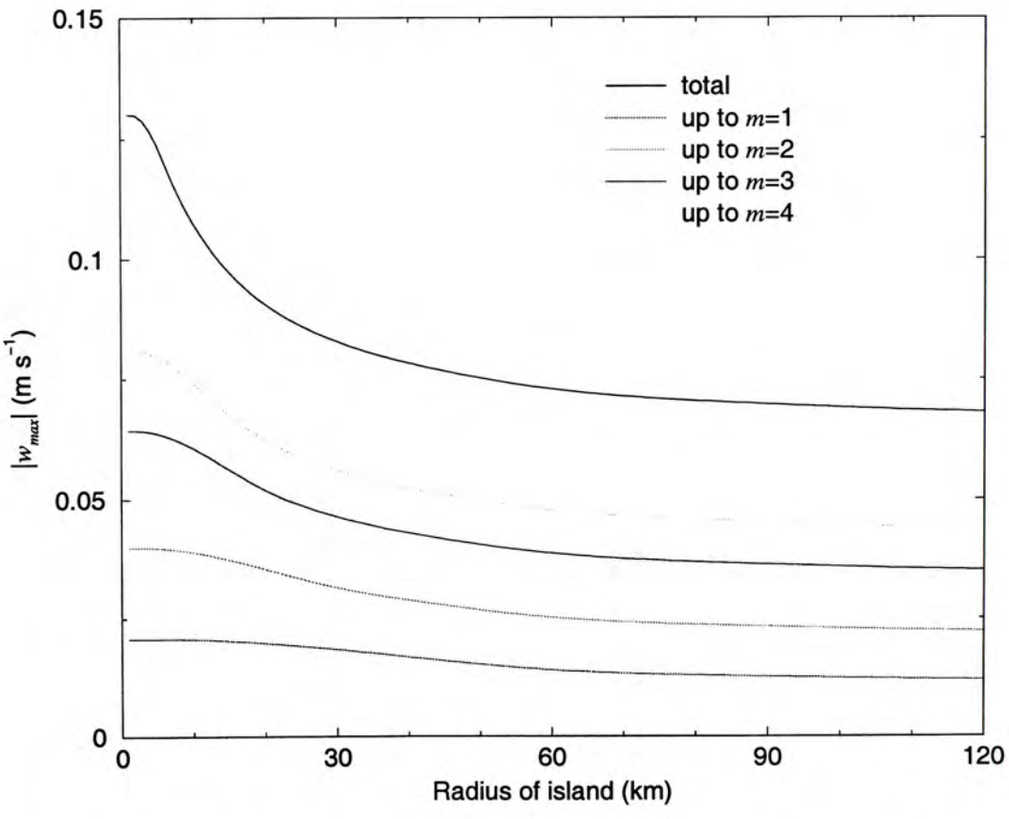

Figure 4.19. Effect of island size and contribution of different modes on surface w_{max} for islands of various sizes

cross-shore flow of the higher modes blows against the overall flow as shown in the graph of u_{max}. The cause requires further investigation.

Limiting case of $R \to 0$

From (4.4) and (4.5), for islands of radii R much smaller than the horizontal extent, we have

$$\begin{aligned}
\tilde{U}_{mn}(R_-) &= \frac{m\pi}{H}\frac{\gamma_m q_n \Delta Q}{N^2} R\, K_1(\alpha_{mn}R) I_1(\alpha_{mn}R) \\
&\sim \frac{m\pi}{H}\frac{\gamma_m q_n \Delta Q}{N^2}\frac{R}{2} \\
\widetilde{W}_{mn}(R_-) &= \frac{H}{m\pi}\frac{\gamma_m q_n \Delta Q}{N^2}\alpha_{mn} R\, K_1(\alpha_{mn}R) I_0(\alpha_{mn}R) \\
&\sim \frac{H}{m\pi}\frac{\gamma_m q_n \Delta Q}{N^2}
\end{aligned}$$

where the following asymptotic formulas for small arguments have been used:

$$\begin{aligned}
I_n(z) &\sim \frac{1}{n!}\left(\frac{z}{2}\right)^n, \qquad n \geq 0 \\
K_n(z) &\sim \frac{(n-1)!}{2}\left(\frac{z}{2}\right)^{-n}, \qquad n > 0
\end{aligned}$$

as $z \to 0$.

As the island size decreases, we see that w approaches a nonzero value, as shown in Figure 4.19, which is not realistic. When the island size becomes sufficiently small, the difference of the heating rate over the island and the surrounding waters is much reduced due to lateral diffusion. To illustrate the situation, let us assume for the case of small islands that the difference of the heating rate is an exponentially decaying function of R with a length scale L.

$$\tilde{Q}(r) = \begin{cases} Q_s + \Delta Q\left(1 - e^{-R/L}\right), & r < R \\ Q_s, & r > R \end{cases}$$

The vertical motion, instead of intensifying, vanishes as the island size shrinks, and a peak appears at a radius comparable to L, as is shown in Figure 4.20.

Abe and Yoshida (1982) in their study of sea-breeze systems on long narrow peninsulas in Japan have also pointed out (without explanation) the existence of such a 'preferable' island size, which much intensifies the uplift flow and is thus favourable for the formation of convective clouds. We therefore argue that the length scale of lateral diffusion might be a factor that determines the favourable size.

Another factor is the vertical extent of the circulation. Xian and Pielke (1991) have carried out a simulation experiment investigating the effects of the width of the landmass on the sea-breeze circulation. The hydrostatic model showed that the height of the boundary layer H varies with the island width, decreases for widths below than 100 km. From (4.5) we see that w is proportional to the model height H. As a result, the intensification is weaker for comparably small islands, which is not reflected by the model presented here, since the height of the boundary layer H is fixed as an external parameter and the model omits relevant

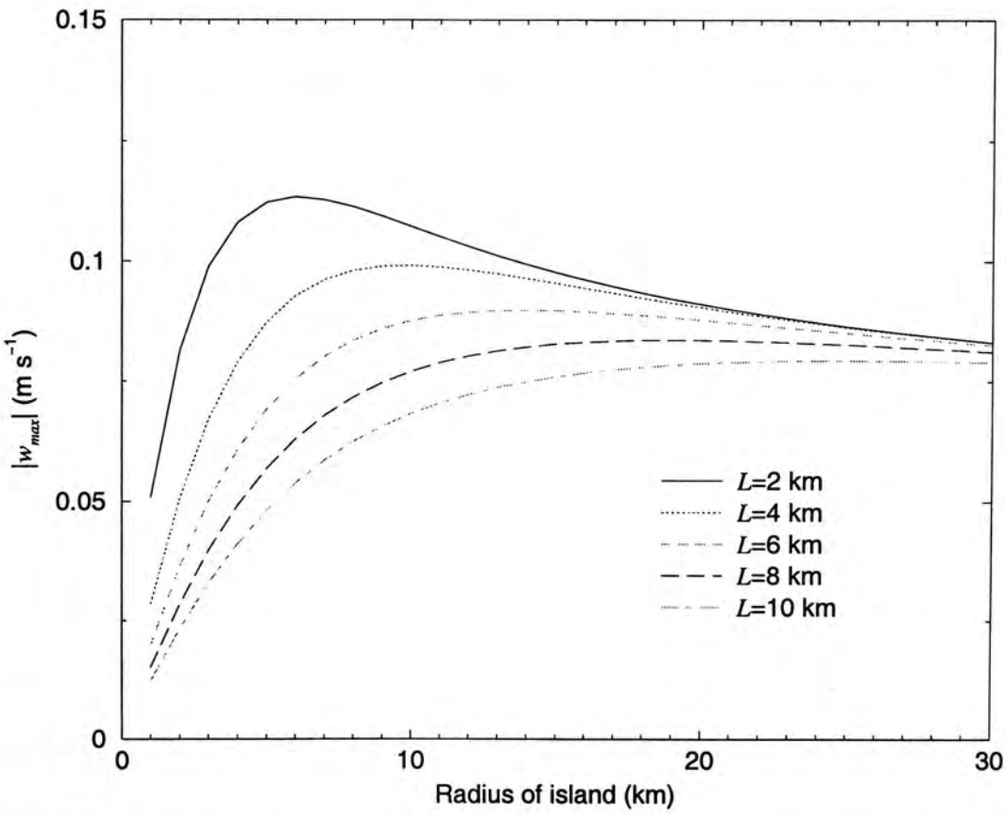

Figure 4.20. Effect of island size and horizontal diffusion on surface w_{max} for islands of various size

physical mechanisms for the self-adjustment of the height of the boundary layer.

Summary

In this section we have examined the sea-breeze circulation over circular islands of various sizes and obtained some interesting results as follows.

1. The sea-breeze phase onsets earlier for small islands.

2. Mass conservation in small and medium islands is maintained by a significant intensification of the vertical velocity as the sea breeze penetrates inland, rather than by a strong enhancement of horizontal radial flow.

3. A strong ascending flow appears in the sea-breeze phase, when the island size is comparable to the horizontal length scale of the sea-breeze circulation, and weakens rapidly as the radius increases.

4.3 Scale analysis on the effects of geometry

Even if we do not consider the effect of terrain, at least two other geometrical factors of a landmass affect the circulation: the size and the shape. In the last Section, we have examined the effect of the landmass size on sea breezes, by comparing how the intensity and other elements change with circular islands of different radii.

In this Section, we proceed to study the effect of the landmass shape, by comparing the uplifting flow intensity over a circular island and an elongated peninsula. The mechanism of the convergence over an elongated peninsula in the sea-breeze phase is the same as that over a circular island discussed in the last Section. We therefore attack the problem in a different way, instead of a numerical treatment as the last Section. For simplicity, we assume the peninsula extends to a distance of L, as shown in Figure 4.21, where $L \to \infty$.

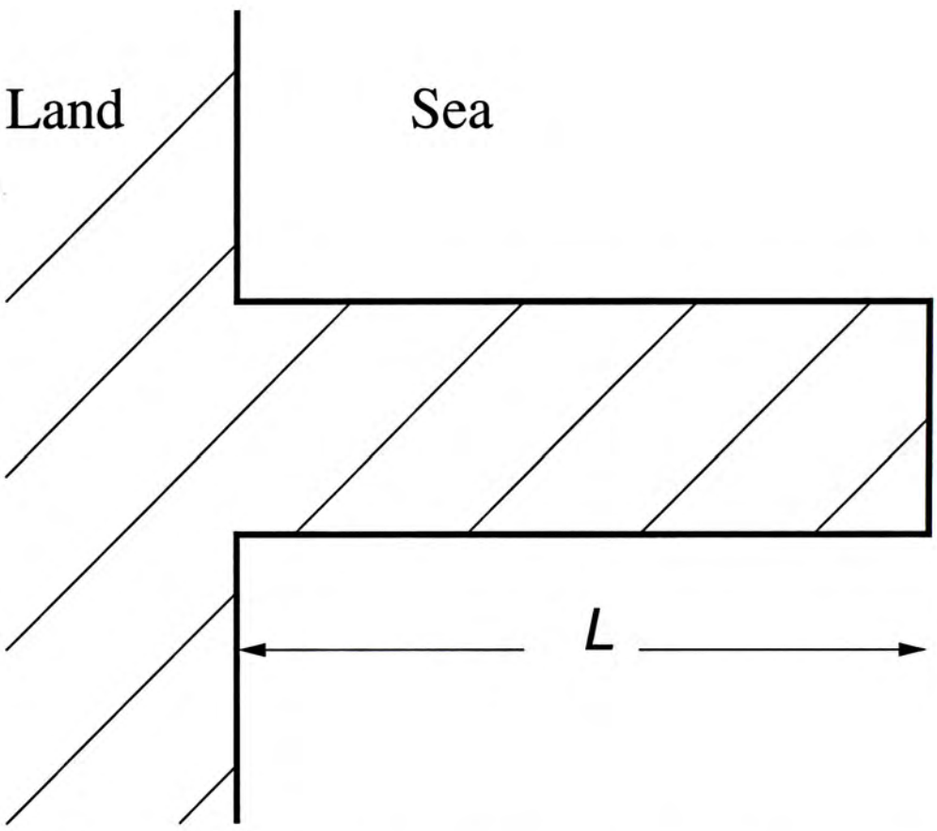

Figure 4.21. Geometry of an elongated peninsula. Its extent from the main shore $L_A \to \infty$.

Uplift flow evaluation

For circular islands, we have, from the continuity equation, for a mode of spatial index m and temporal index n,

$$\widetilde{W}_{mn,C} = -\left(\frac{m\pi}{H}\right)^{-1}\left[\frac{\partial \widetilde{U}_{mn}}{\partial r} + \frac{\widetilde{U}_{mn}}{r}\right] \tag{4.6}$$

where $\widetilde{U}_{mn}$ is the radial component of the wind and r the distance from from the centre of the island. We denote the case of a circular island by a subscript C, and the case of a peninsula by a subscript L.

In the absence of vertical motion, (4.6) suggests that the intensity of the radial wind component u is proportional to r^{-1}. Obviously, however, the sea-land breeze circulation of circular islands includes non-zero vertical velocities. Hence mass conservation should be achieved by the enhancement of both vertical and radial motions.

The above results indicate that if we assume an extreme situation, in which

$$\left(\partial \widetilde{U}_{mn}/\partial r\right)_C \approx \left(\partial \widetilde{U}_{mn}/\partial x\right)_L$$

where the subscripts C and L indicate terms related to the island and the peninsula, respectively (Mahrer and Segal, 1985), the term $\left(\widetilde{U}_{mn}/r\right)_C$ will provide additional enhancement of uplift flow over circular islands as compared to the peninsulas. In this situation, when the flow is converging at the island centre,

$$\widetilde{W}_{mn,C} = \widetilde{W}_{mn,L} - \left(\frac{m\pi}{H}\right)^{-1}\frac{\widetilde{U}_{mn}}{r}$$

By choosing typical scales of $H = 1$ km and $r = 3$ km, for example, in the fundamental mode $\widetilde{U}_{11} \sim 0.1$ m s^{-1}, and the geometry results in a difference of about 0.1 m s^{-1} in $\widetilde{W}_{11}$ over circular islands as compared to elongated ones. Hence, under supportive atmospheric conditions, one can expect that cloud triggering will be more pronounced over islands with aspect ratio close to unity than those elongated with an equivalent width.

Chapter 5

Application to Hong Kong

Hong Kong, as mentioned in Chapter 1, is a small territory of just over 1000 km^2, located at 22 °N, 114 °E on the south China coast (Figure 5.1). It can be approximately described as consisting principally of a peninsula (Kowloon and the New Territories) and two large islands (Hong Kong island and Lantau island) with over two hundred small islands scattered around. The complication of its coastal pattern thus gives rise to an interesting sea-land breeze flow pattern, which we shall set as our target of investigation by applying the model developed in Chapter 2.

5.1 Numerical aspect

The model developed in Chapter 2 is mathematically a boundary value problem. The inhomogeneous Helmholtz equation takes the form

$$\left(\nabla^2 - \alpha^2\right) \Phi(x, y) \sim Q(x, y)$$

where Q is the heating rate (the source), and Φ is geopotential, from which all other field quantities can be calculated. The parameter α may differ over land and sea.

When the model is applied to the case of Hong Kong, there are three aspects that are left to be specified: (a) the model parameters, (b) the distribution of

Figure 5.1. Hong Kong and its immediate vicinity. Hong Kong has a complex coastal pattern, which complicates the sea-land breeze circulation over it. In the map, HKI stands for Hong Kong Island, CCH for Cheung Chau, CLK for Chek Lap Kok, TH for Tolo Harbour, and WLC for West Lamma Channel. The blocked area indicates the district regarded as urban heat island in Section 5.3.

heating rate (the source) and (c) the boundary conditions at the edge of the model area.

Parameters. — The domain of interest in this investigation is an area of about 80 km × 80 km, covering Hong Kong and its immediate vicinity (Figure 5.1). Because of the small area, the Coriolis parameter and the stratification parameter are both assumed to be constant. The values of parameters used in the model are presented in Table 5.1.

Heating rate. — The heating rate over land and sea, Q_ℓ and Q_s, are assumed constant without any transition region inserted across the shore. The temporal dependence of the heating function is taken as the same as in Figure 3.16 in Section 3.4: a sinusoidal function of time with a period of a day, truncated from

Table 5.1. The values of model parameters for the case of Hong Kong.

Parameter	Value	Unit	Comments
Q_l	3×10^{-5}	m s^{-3}	
Q_s	0.75×10^{-5}	m s^{-3}	$Q_s = 0.25\, Q_l$
k	20	day^{-1}	
κ	20	day^{-1}	
N^2	1×10^{-4}	s^{-2}	
f	0.54484×10^{-5}	s^{-1}	at latitude 22 °N
H	3	km	
δ	1×10^{-3}	m^{-1}	

below.

Spatial modes and temporal harmonics are truncated as tabulated in Table 5.2. The amplitudes decrease quickly with (m,n), so that the higher modes do not alter the essential features of the breeze system.

Table 5.2. Spatial mode retained for each harmonic

harmonic n	3	2	1	0	1	2	3
highest m	3	8	20	20	20	8	3

Boundary conditions. — In dealing with numerical models in a limited area, we always face the problem of specifying the boundary conditions. The best solution, of course, is to use actual boundary data from observations. However, this is often not practical, because we usually do not have detailed observational data over the particular area with which we are concerned.

Another way to specify the boundary condition is by proposing an approximation which reflects the essential features of the average wind condition over the boundary. To do this, we first note that Hong Kong is located on the south China coast, over which the mainland and the South China Sea induce a larger scale sea-land breeze system. When we study the local wind system of Hong Kong,

the influence of this larger system cannot be neglected. Therefore in this study, the contribution of the landscape of Hong Kong is treated as a local disturbance in a larger system with a straight shoreline.

In this study, we specify the boundary conditions by two steps (Figure 5.2). First, we roughly solve the sea-land breeze system over an area of 240 km × 240 km, covering the south China coastal area, where Hong Kong is near the centre. For simplicity, we assume the coast is an infinitely long straight line, running east-west. The field quantities hence can be evaluated analytically (See Chapter 3).

Second, we embed the Hong Kong coastline pattern (over an area of 80 km × 80 km) onto the ideal south China coast system, taking the values of the fields at the boundary evaluated in the first step. (We regard the system as a fixed boundary value problem.) The treatment is justified when the disturbance concerned remains local and does not extend far to the boundary area. In our

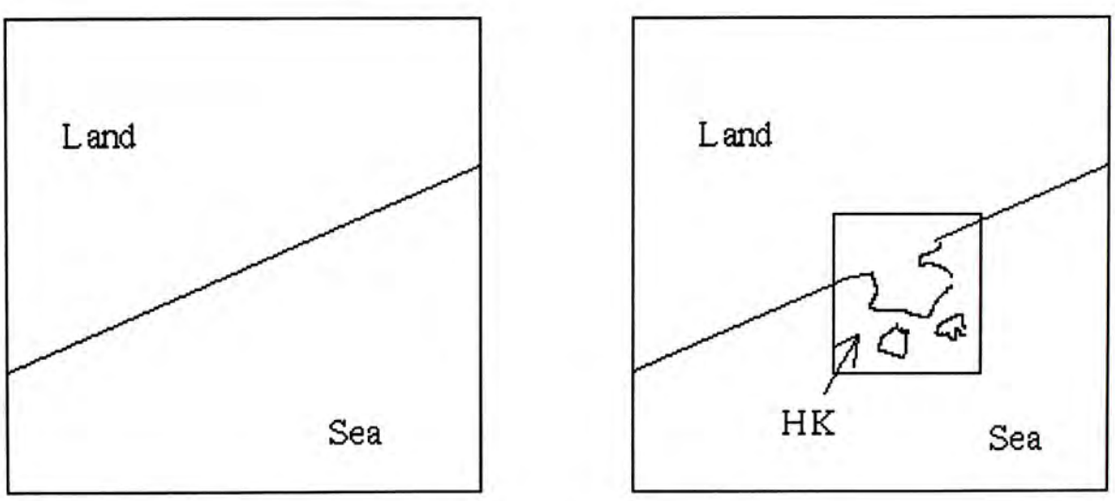

Figure 5.2. Treatment of the boundary condition. The Hong Kong coastline pattern (over an area of 80 km × 80 km) is embedded onto the ideal south China coast system of an area 240 km × 240 km. For simplicity, the south China coast is assumed a long straight line.

case, the horizontal distance of influence has a scale of only 50 km, far less than the distance from the boundary.

Numerical method. — We use a uniform 1 km × 1 km grid over the whole area (240 km × 240 km). The grid is relatively fine in order to capture the complications of the coastline pattern. The system is solved by the simultaneous overrelaxtion (SOR) method[1].

A detailed description of the numerical method is given in *Numerical Recipes* (Press et al., 1987); we shall not repeat it here. Below we only outline the main idea of how the relaxation method works.

The relaxation method, like many methods developed for solving partial differential equation, determines the solution by starting with a guess and then improving it iteratively.

The difference lies in how the improvement is carried out. In SOR, this is done by replacing the static problem by an evolution, and the solution is the final equilibrium state of the evolutionary system. As the iterations improve the solution, the result is said to relax to the true solution.

More precisely, the idea is as follows. The model equation is a second-order elliptical differential equation which takes the form

$$0 = \mathcal{D}\phi \equiv (\nabla^2\phi + \cdots)$$

Let φ be our initial guess for the solution ϕ. The expression $\mathcal{D}\phi \equiv (\nabla^2\varphi + \cdots)$ would most probably give some residual which is not zero. If we further assume the system has the property that the rate of change of φ with a "time" τ is in proportion to the residual, i.e.,

$$\frac{\partial\varphi}{\partial\tau} = \lambda(\nabla^2\varphi + \cdots)$$

then φ either exponentially increases or decays as $\tau \to \infty$, depending on the sign of λ. In this case, we take λ as positive for φ to decay. When the residual goes to zero, φ decays to the final equilibrium, namely the true solution ϕ.

[1]Taking the overrelaxation parameter to be 1.5.

This is no surprise because, in fact, the system after introducing the pseudo-time τ essentially undergoes a diffusion process, once λ is properly chosen. Ideally, the larger the coefficient λ, the faster the system reaches its final state. However, the discretization imposes limitation to the choice of λ. Large λ reduces the stability of the evolution and reliability of the solution.

The pseudo-time τ, introduced as a means of obtaining the solution, has no physical meaning, except for indicating the converging rate, and should not be confused with the physical time t (which no longer appears once we have expanded the quantities in temporal harmonics).

5.2 Wind branches

The results from the model demonstrate that the sea-breeze system depends mainly on the contrast in the diabatic heating across the coastline. Figure 5.3 shows the surface wind field during the sea-breeze phase and the divergence field described by the filled contours. The thick line on the graph indicates the shoreline. Note that negative values of divergence represent convergence.

The surface wind system in the sea-breeze phase (Figure 5.3) roughly consists of three main branches (Zhang and Zhang, 1997):

1. one with westerly winds in the northwest of the territory, flowing from Deep Bay;

2. one with southeasterly winds in the northeast of the territory, flowing inland from Mirs Bay; and

3. a weaker and broader one with southerly winds in the south and southeast of Hong Kong, forming a convergence zone on passing over Hong Kong Island and a divergence zone in the Lamma Channel.

The westerly and southerly branches develop a convergence line over Lantau Island. The southeasterly branch shows a convergence zone over Sai Kung and

is directed more easterly due to the divergence zone over Tolo Harbour. In the southerly branch when the southerly sea breeze over Kowloon meets the southwesterly sea breeze over the southern part of the New Territories, a wide and weak convergence zone is developed along the southwest coast of the peninsula.

The surface wind system in the land-breeze phase is simpler in structure (Figure 5.4), and consists mainly of northerly winds over most of Hong Kong and an easterly wind over the northwestern part. Several convergence zones are revealed. (a) A relatively weak convergence zone is produced at Deep Bay by the land breeze over Shekou and the northwestern part of New Territories. (b) There is also a convergence zone near the West Lamma Channel produced by the land breeze over northeastern part of Lantau Island and the western part of Kowloon. (c) The land breeze over Tuen Mun and the northern part of Lantau island also produce a small convergence zone.

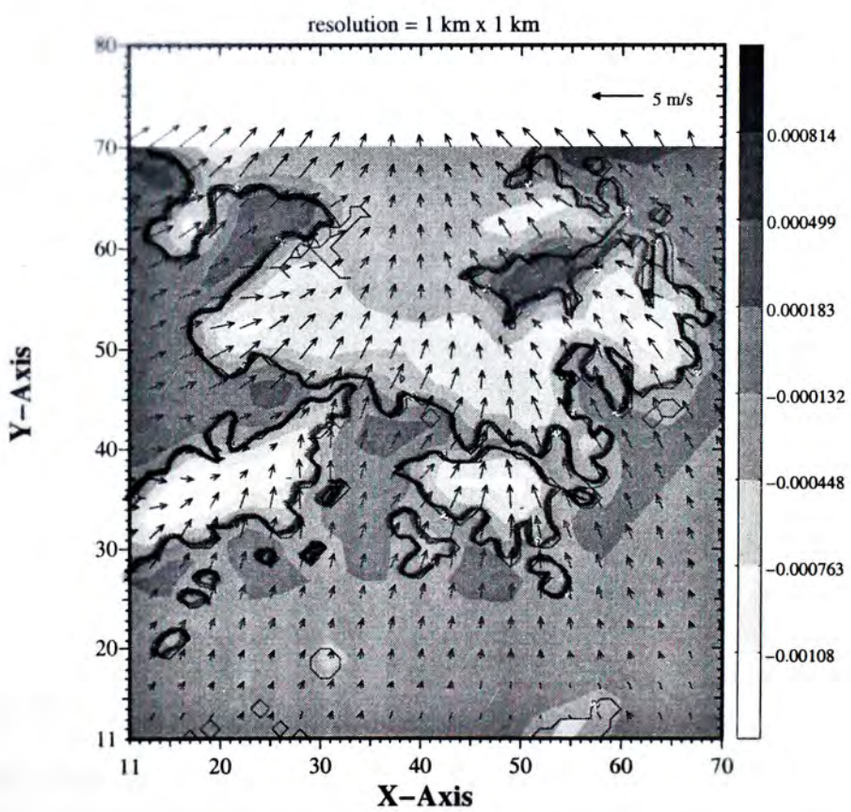

Figure 5.3. Surface wind (arrow) and divergence field (grey scale in s^{-1}) in Hong Kong during the sea-breeze phase. The wind system roughly consists of three main branches: (a) westerly winds from Deep Bay; (b) southeasterly winds from Mirs Bay; and (c) southerly winds passing over Hong Kong Island and the Lamma Channel.

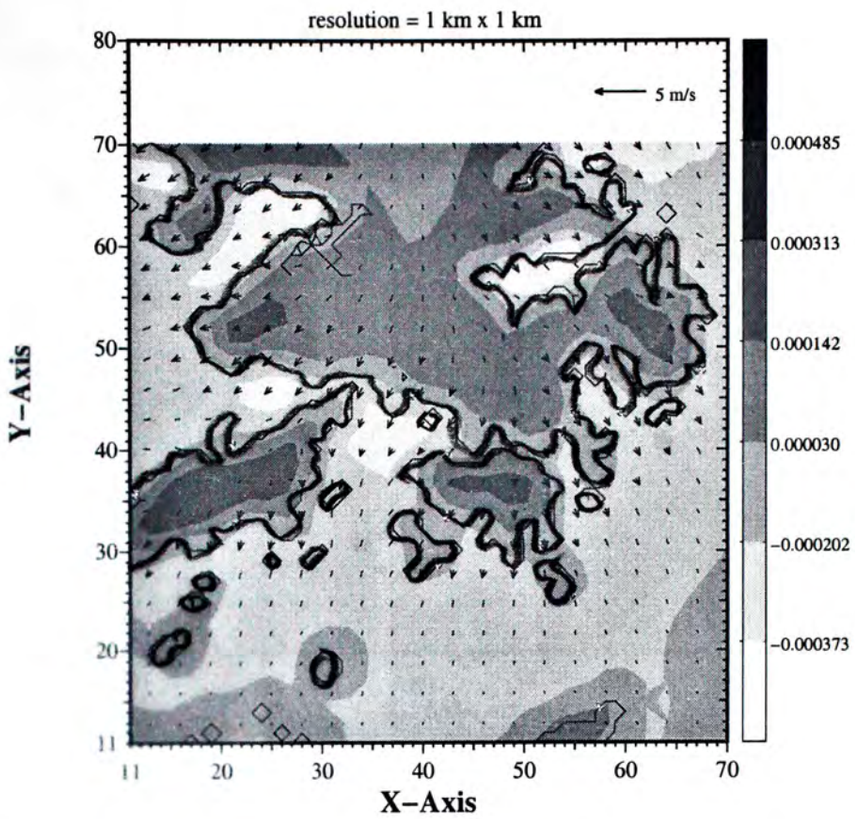

Figure 5.4. Surface wind (arrow) and divergence field (grey scale in s^{-1}) in Hong Kong during the land-breeze phase. The wind system consists mainly of two main branches: (a) northerly winds over most of Hong Kong; and (b) easterly winds over the northwestern part.

5.3 Effects of urban heat islands and sun-facing slopes

In order to obtain a more realistic picture of the wind system and the convergence zones, it is necessary to incorporate the sun-facing slope effect and the urban heat island effect. The clearest way to exhibit these effects is to analyse the divergence field.

Sun-facing slopes

The different aspects of a mountain will receive different amounts of solar radiation, leading to different heating rates over the terrain. This effect is quite important for Hong Kong in view of its hilly terrain (Figure 5.5), and should be included in the model.

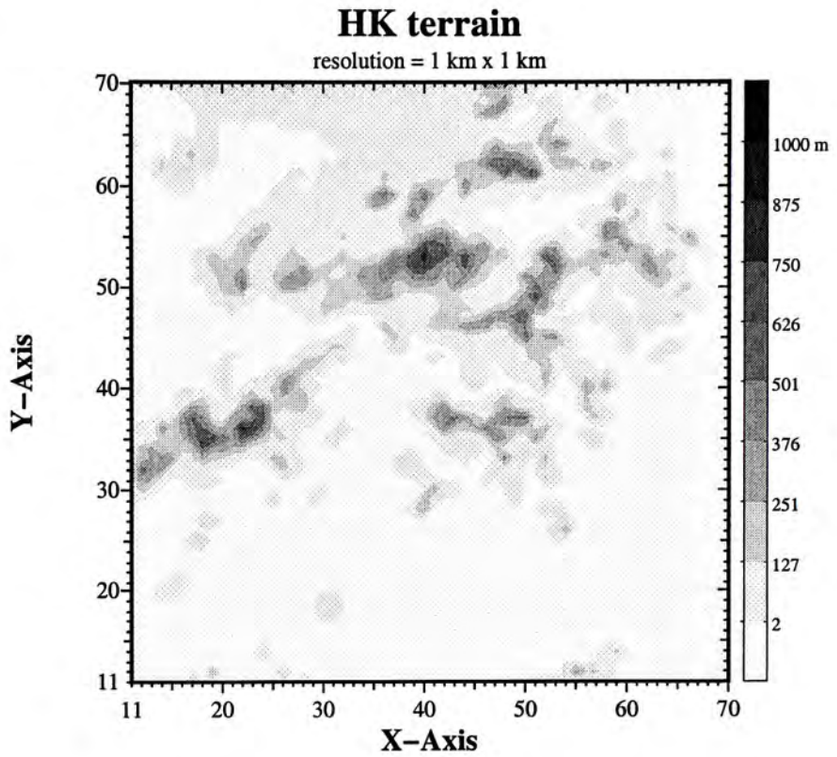

Figure 5.5. A map showing the terrain of Hong Kong. The terrain height is represented by the gray scale

For simplicity, the southern slope of any mountain is assumed to be sun-facing, and is assigned double the normal heating rate during the day; the opposite shaded slope is assigned the normal heating rate. The cooling rates at night are assumed to be identical.

Urban heat islands

Kowloon Peninsula and Hong Kong Island are developed urban areas, with tall buildings and a dense population, leading to fairly prominent urban heat islands, not only in the daytime, but also at night; it is well known that the temperature in these urban areas is often higher than that in the surrounding areas (Stanhill, 1995).

Since the sea-land breeze is thermally forced, the urban heat island effect must be incorporated. In the present model, the areas of Kowloon Peninsula and Hong

Kong Island (shaded box in Figure 5.1) are assumed to be urban heat islands; in the daytime, the heating rate is assumed to be double the normal value, while at night, the cooling rate is assumed to be 20% less than the normal value.

Wind system modification

For the sea-breeze phase (1400 LST), Figure 5.6 shows the divergence field with both the sun-facing slope effect and the urban heat island effect. The urban heat island effect is seen more clearly when compared with Figure 5.3. Three main features are worthy of note. (a) The three main branches remain qualitatively unaffected. (b) The convergence over Lantau Island and at the confluence of the three wind branches over the southern part of the New Territories is strengthened principally because of the sun-facing slope effect. (c) The convergence over Kowloon Peninsula and Hong Kong Island is enhanced in intensity and in extent,

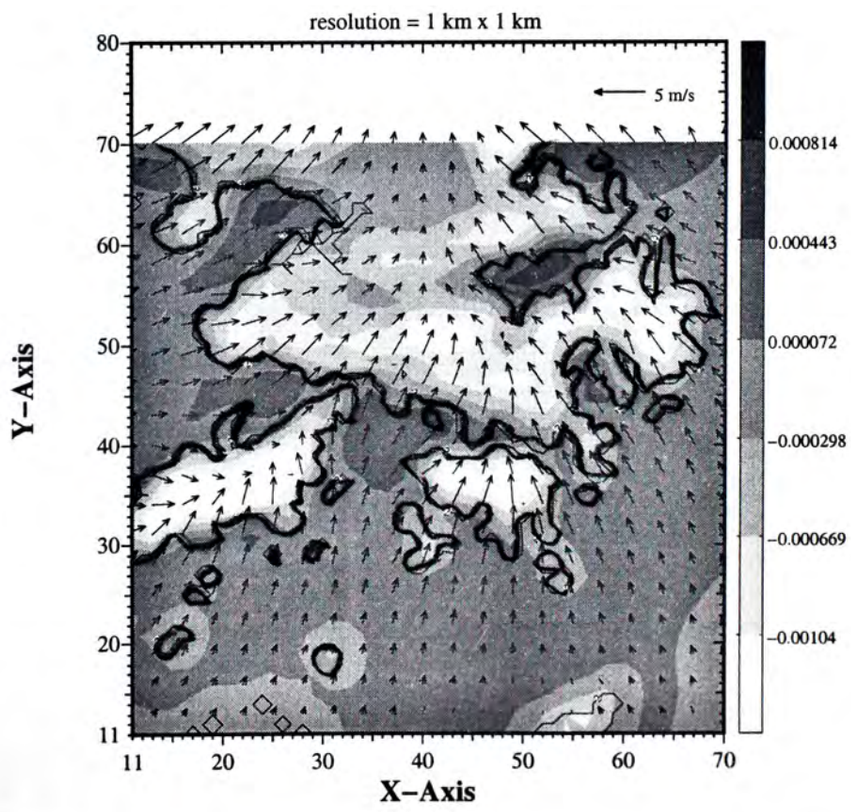

Figure 5.6. The flow field and the divergence field during sea-breeze phase incoporating the sun-facing slope effect and the urban heat island effect

principally because of the urban heat island effect.

5.4 Static heating mode

In expanding the functions as Fourier series in time t, there is a term with $n = 0$, which is the static harmonic, constant during a day. It exists because there is unequal heating in the daytime and cooling at night, so that excess heating occurs, as indicated by the different areas enclosed by the curve in the two phases of a day (See Figure 3.16). This harmonic is a mode with heating rate over land always larger than over sea throughout the day. The static harmonic brings along with it a static flow, in which the wind direction and the wind strength are constant in time. Therefore, strictly speaking, the harmonic does not qualify as a sea-land breeze.

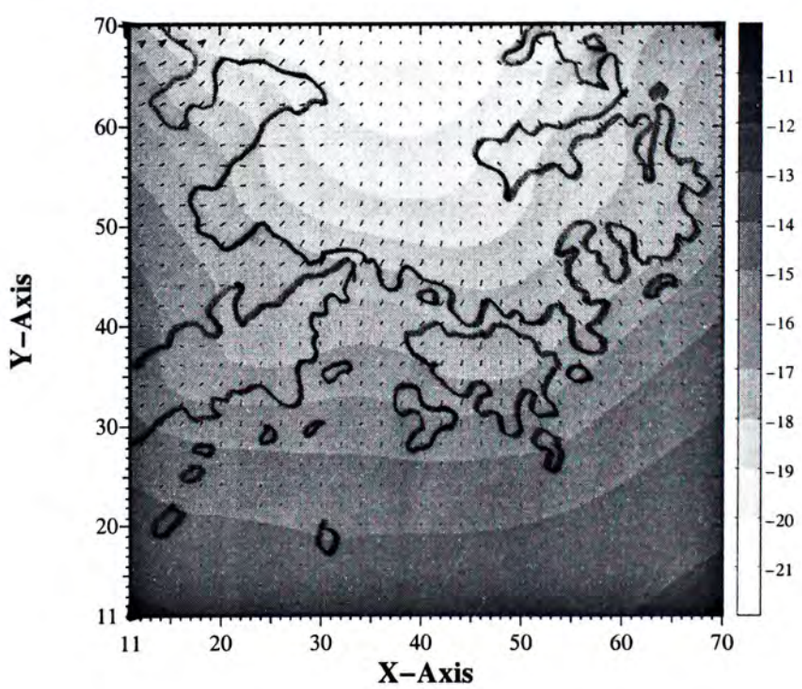

Figure 5.7. The flow pattern (arrows) and the pressure perturbation (grey scale in $m^2\ s^{-2}$) of the static harmonic in the sea-breeze phase. The pressure field is not very sensitive to the shape of coastline, though the influence of Lantau island to the East and the Tolo Harbour near the North-East can still be recognized.

Figure 5.7 shows the surface wind field and the pressure field of the static harmonic in Hong Kong. The figure indicates that the pressure field is not very sensitive to the shape of coastline, though the influence of Lantau island to the East and the Tolo Harbour near the North-East can still be recognized.

For the vertical motion, the $n = 0$ harmonic dominates. Interestingly, the static harmonic in the vertical motion has a good correlation to the 30-year spatial mean October rainfall pattern as recorded by the Hong Kong Observatory. This is probably because the uplifting air mass of the warm, humid sea breeze brings the moisture to the cooler upper levels, promoting condensation. The correlation is further studied in Chapter 6.

5.5 Effect of model height

The model parameter H, which represents the height of the mixing layer, has an influence on the resultant flow field. Figure 5.8 presents the surface flow and the pressure field when H is taken to be 10 km, the tropopause extent. A comparison with Figure 5.3 ($H = 3$ km) shows that with large H, the flow is less sensitive to the shape of the coast, and systems with small length scales are filtered out. Therefore the fine adjustment of the value of H depends on the resolution of the horizontal scale. In this case, we suggest H to be taken as about 3 km, in agreement with previous studies (Anthes, 1978).

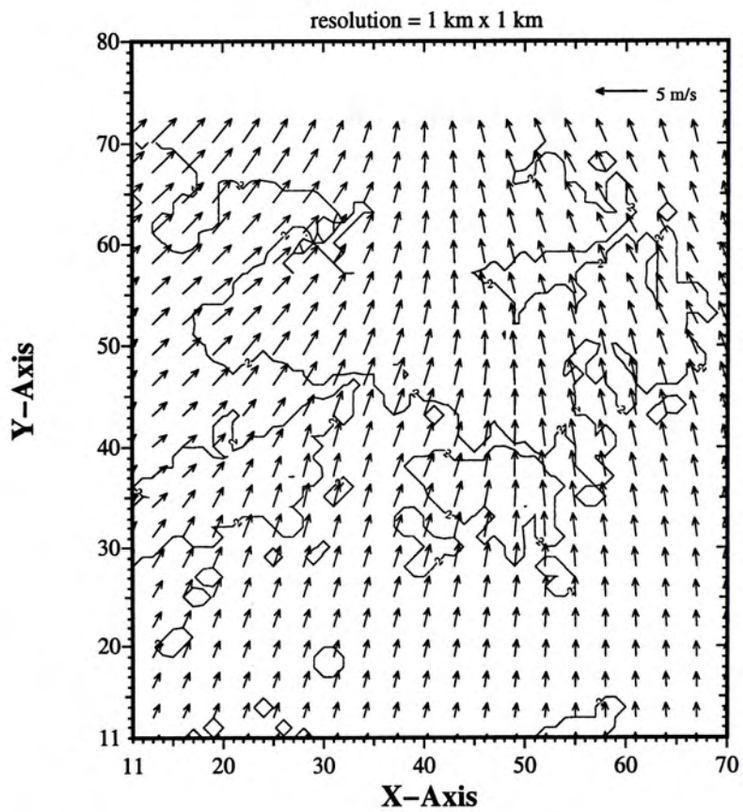

Figure 5.8. Surface wind field in Hong Kong during the sea-breeze phase taking the model height to be 10 km

Chapter 6

Association of sea-land breeze with spatial rainfall pattern

Introduction

Sea-land breezes are thermally driven convections, commonly found in the coastal areas. The uplift airflow of the circulation might cause heavier precipitation if the atmospheric conditions are unsettled.

In particular, sea-land breezes are frequently observed in Hong Kong, especially with clear sky conditions under light synoptic wind. For example, in 1980, sea-land breezes were reported on more than 100 days in that year. (See Chapter 1.) Wai et al. (1995) pointed out that in Hong Kong the sea-land breeze convection is one triggering mechanism that initiates the summer storms apart from tropical cyclones.

In Hong Kong, the spatial distribution of rainfall is highly uneven; the annual spatial distribution is given in Figure 6.1. The total annual rainfall in Hong Kong ranges from below 1400 mm in the northwest and southeast to over 3100 mm at Tai Mo Shan. The Observatory, situated near the centre of the territory, receives an amount very close to the mean of the two extremes. (Ng and Wong, 1996)

In this statistical study, we shall investigate the extent to which the spatial rainfall pattern of Hong Kong is associated with the vertical motion of sea-land breeze circulation as well as the terrain height. The terrain height is also included

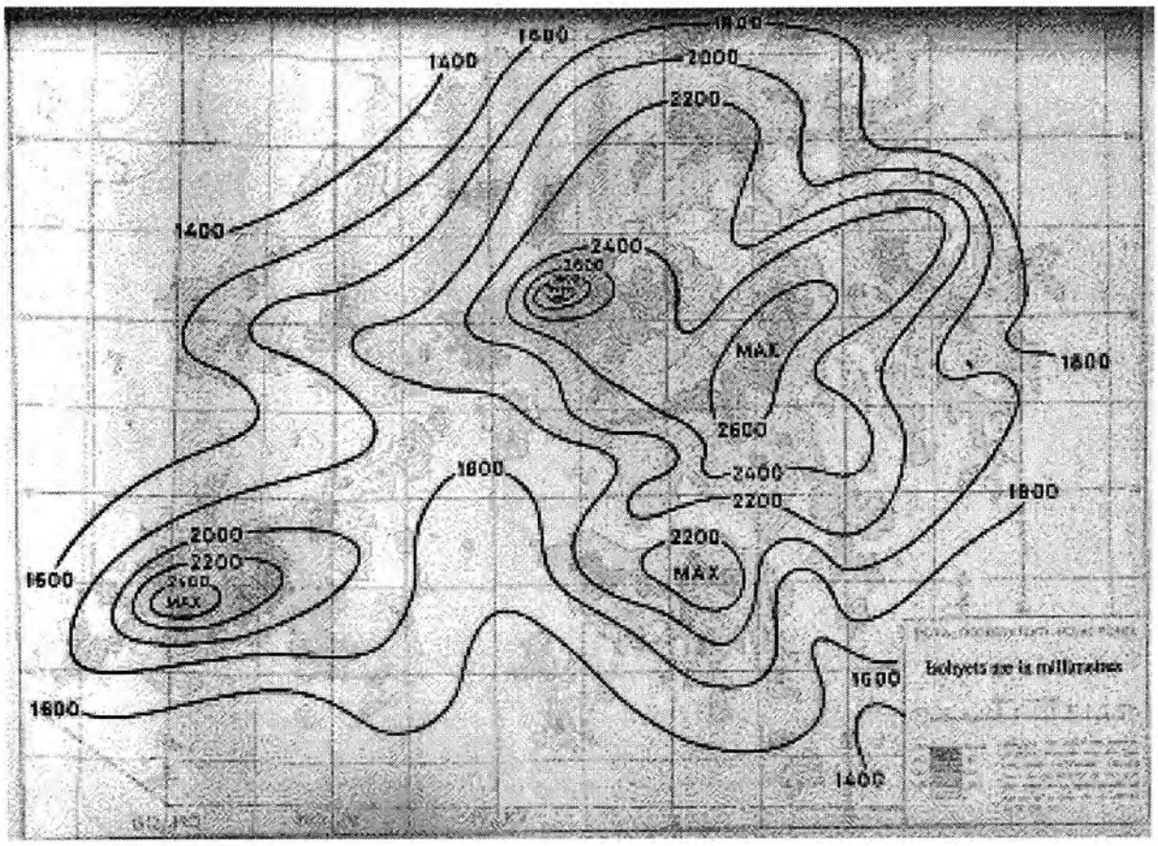

Figure 6.1. Mean annual rainfall distribution map (1961–1990). The rainfall contour is in millimetres. The altitude is shown by grey scale, ranging from 0 m to 1000 m. [From Ng and Wong (1996)]

as a factor since it is known that more rain is generally recorded over higher grounds than over lowlands (Ng and Wong, 1996). A comparison with the effect of the height gives us a relative weighting for the significance of the vertical motion. A map showing the terrain of Hong Kong is available in Figure 5.5 for reference.

There are at least two ways for the study to proceed.

Temporal. — One is to trace how the rainfall collected varies at a station during the occurrence of a sea-land breeze, and see whether a similar pattern can be recognized at nearby stations in the coastal area concerned in a number of sea-land breeze days. However, this requires massive and detailed temporal records that make it difficult to carry out.

Spatial. — Another is to analyze the correlation between the averaged spatial rainfall pattern and the net motion of the circulation, making an attempt to discover the association in general.

Because of the limitation of data available, the latter method is employed.

6.1 Regression analysis

Linear regressions were carried out associating the mean monthly rainfall r within 1961–1990 with the vertical wind component w at 1000 m and the height of the station h above the mean sea-level, i.e., a fit was carried out.

$$r \sim \hat{r} = \alpha w + \beta h + \gamma$$

where $\hat{r}$ is the estimated rainfall, and γ is the intercept, the value of $\hat{r}$ when both w and h equal zero. The slopes α and β are the rate of change in $\hat{r}$ for a unit change in w and h, respectively. The parameters (α, β, γ) are all to be determined by fitting the data.

The residuals

$$e_i \equiv r_i - \hat{r}_i = r_i - (\alpha w_i + \beta h_i + \gamma)$$

are random errors that express the deviation of the observed values from a straight line. The random errors can arise from measurements or from factors that are not included.

The residual sum of square $E = \sum e_i^2$ is thus an indication of how well the model fit the data overall. The smaller the quantity, the smaller the deviation of the actual readings from the regression line. The parameters, α, β, γ are hance chosen so that E is minimized.

We emphasize two quantities in the following study, in order to see the extent to which the sea-land breeze system affects the rainfall distribution in Hong Kong.

The first one is *the coefficient of determination* (denoted by Rsq), which ranges from zero to one. In our case,

$$Rsq = 1 - \frac{\sum(r_i - \hat{r}_i)^2}{\sum(r_i - \bar{r})^2}$$

$$= 1 - \frac{\sum e_i^2}{\sum (r_i - \bar{r})^2}$$

It indicates the portion of variability of the rainfall explained by the independent variables suggested. When $Rsq = 1$, all data points fall exactly on the regression line[1]; when $Rsq = 0$, the fitting fails completely[2].

The second one is *the standardized coefficient*, which reveals the relative significance of these variables, or the sensitivity of the variation of the rainfall with that of the independent ones. It is obtained by the standardization of the regression equation, which scales each variable by subtracting its sample average and dividing by its sample standard deviation, e.g.,

$$Z_w = \frac{w - \bar{w}}{\sigma_w}$$

The standardized coefficient of an independent variable thus indicates that an increase in that variable by one standard deviation could result in an increase in the rainfall by how many standard deviations. In our case, the standardized coefficients α' and β' are given by a fit of

$$Z_r \sim Z_{\hat{r}} = \alpha' Z_w + \beta' Z_h$$

where Z's are the corresponding standardized variables.

6.2 Source of data

The Hong Kong Observatory places much effort on the observation of rainfall in the territory. About 120 rainfall stations had been set up by 1982 in the area of only about 1000 km^2. Ng and Wong (1996) have made a detailed analysis on the 30-year mean rainfall for the standard reference period 1961–1990. That work computed the mean monthly and annual rainfall at 95 rainfall stations in Hong

[1]Mathematically, $Rsq = 1$ if and only if all of the residuals e_i equal zero

[2]This means $\sum e_i^2 = \sum (r_i - \bar{r})^2$, that is, the model gives no better estimate than merely taking the mean rainfall whatever the value of the independent variables are.

Kong, and presented a list of monthly and annual spatial distributions of rainfall, which made the present study possible.

All 95 rainfall stations covered are included as sample points.

The net vertical motion of a sea-land breeze system is a result of unequal amounts of heating in the daytime and cooling at night. The net motion due to the excess heating over a sea-land breeze day corresponds to the static harmonic in a Fourier analysis of the circulation. The averaged flow concerned here is prepared by means of the model in Chapter 5 under calm prevailing synoptic winds. No terrain-driven convection is involved in the present study, as the flow is computed in a model with flat terrain.

6.3 Annual rainfall

The result of a linear regression shows that the contribution of the sea-land breeze vertical motion is negligible on the annual spatial pattern of rainfall.

However a marked correlation between if attention is restricted to the month of October, in which sea-land breezes usually occur on sunny days under weak synoptic winds.

6.4 October

Comparing the map showing the uplift flow (Figure 6.2) with the spatial rainfall pattern in October (Figure 6.3), it can be seen that the most local rainfall maxima are recorded around these upflux zones.

The regression line obtained between r in m, w in m $s^{-1}$and h in m is

$$\hat{r} = 61000w + 0.9h + 110$$

or standardized as

$$Z_{\hat{r}} = 0.17Z_w + 0.47Z_h$$

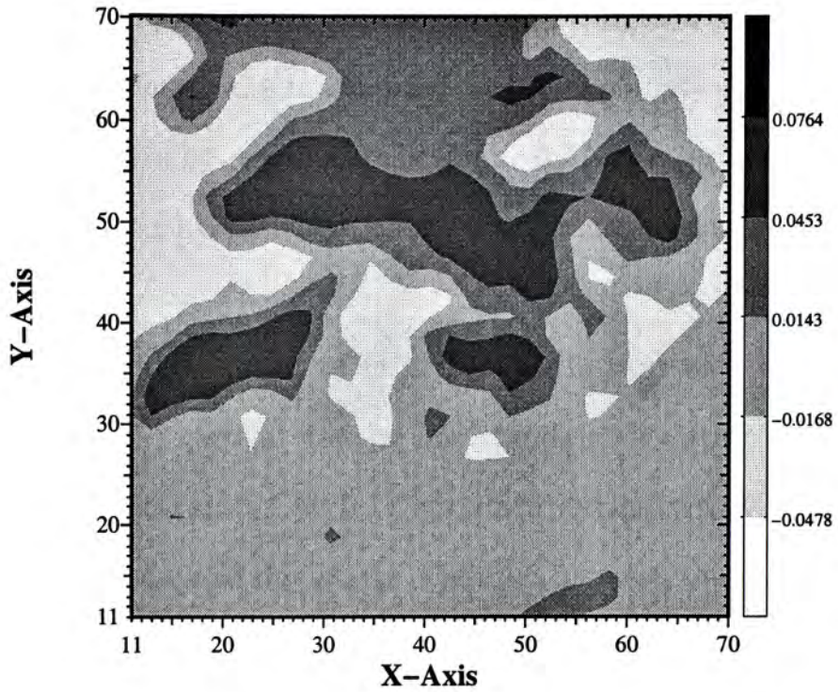

Figure 6.2. Average vertical motion of sea-land breeze circulation in Hong Kong. The contour is the vertical velocity in m s^{-1}.

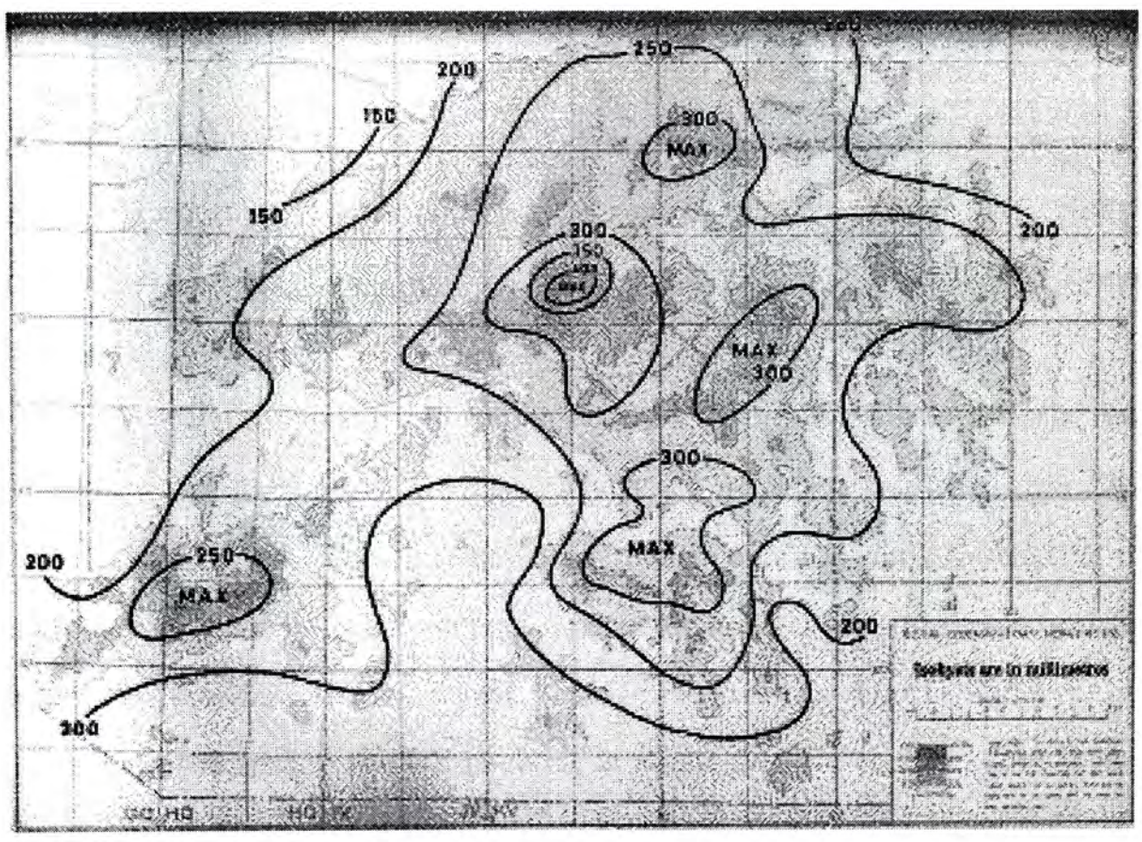

Figure 6.3. Mean October rainfall distribution map (1961–1990). The rainfall contour is in millimetres. The altitude is shown by the grey scale, ranging from 0 m to 1000 m. [From Ng and Wong (1996)]

Figure 6.4 shows a graph of r against the estimated value $\hat{r}$. For a perfect estimation, all sample points should fall on the straight line on the graph. The deviation, however, shows the inadequacy in the explanation. Read off from the graph, the coefficient of determination is $Rsq = 0.317$, i.e., 31.7% of the variations of rainfall is explained by variation of the independent variables w and h in the model.

The standardized coefficient of w is 0.17 while that of h is 0.47, indicating that an increase in the vertical flow by one standard deviation could result in an increase in the annual rainfall by 0.17 standard deviations, while an increase in the height by 0.47 standard deviation. Figure 6.5 shows the rainfall distribution estimated based on this regression model, which is similar to the spatial pattern observed (Figure 6.3).

6.5 Seasonal Changes

Figure 6.6 shows the monthly changes of the coefficient of determination. The w-line shows the proportion of variability of the rainfall explained by the vertical motion ignoring h. The correlation is in general higher in early winter than in summer, which broadly agrees with the seasonal changes of the sea-land breeze occurrence[3].

In winter the atmosphere is generally stable. Fine weather is brought under the influence of high pressure ridges, which are usually established over South China in this period. The clear sky condition favours the diabatic heating process and precipitation usually occurs as drizzles or light rain (Jackson and Hsu, 1996). The standardized coefficient, which indicates the relative significance of determining the spatial rainfall pattern, is about 0.15 for w and about 0.45 for h, as shown in Figure 6.7.

[3]See the monthly mean number of sea-land breeze day for the period 1980-1989, tabulated in Table 1.3.

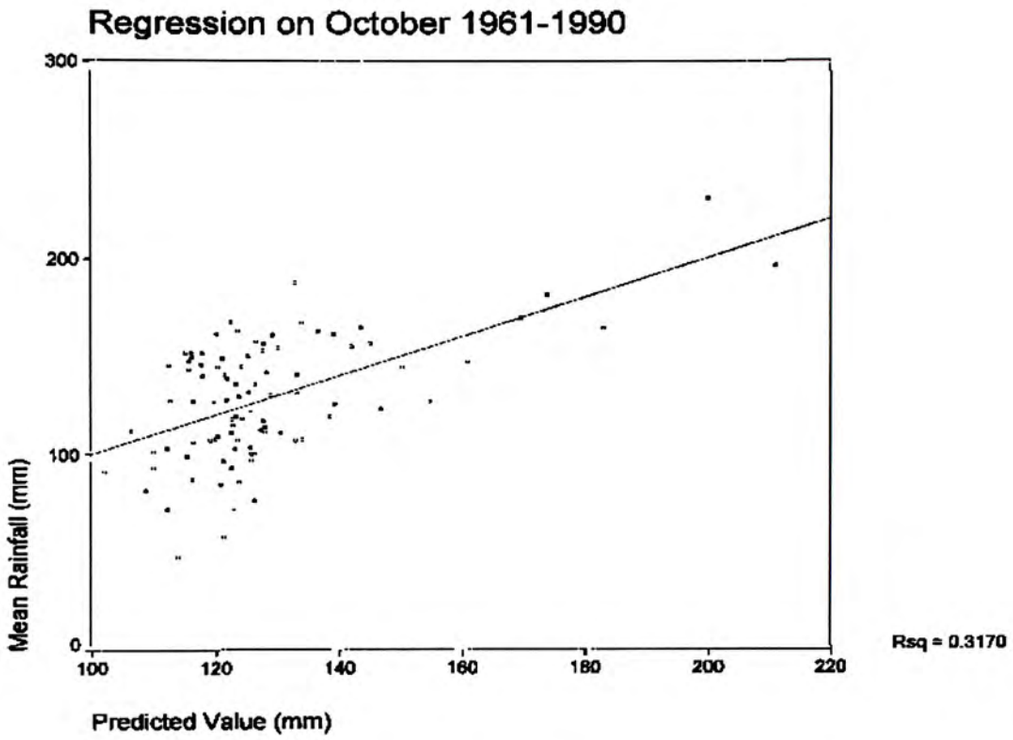

Figure 6.4. Linear regression of the mean recorded October rainfall against the estimated

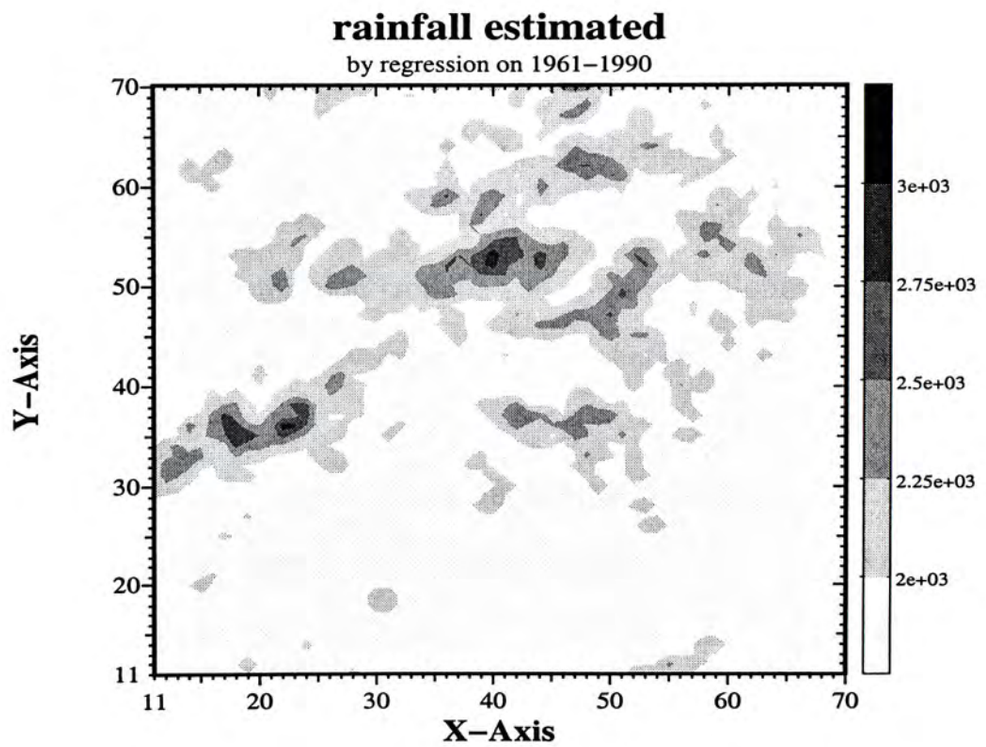

Figure 6.5. Spatial rainfall distribution estimated based on the regression model. The contour is the rainfall in millimetres.

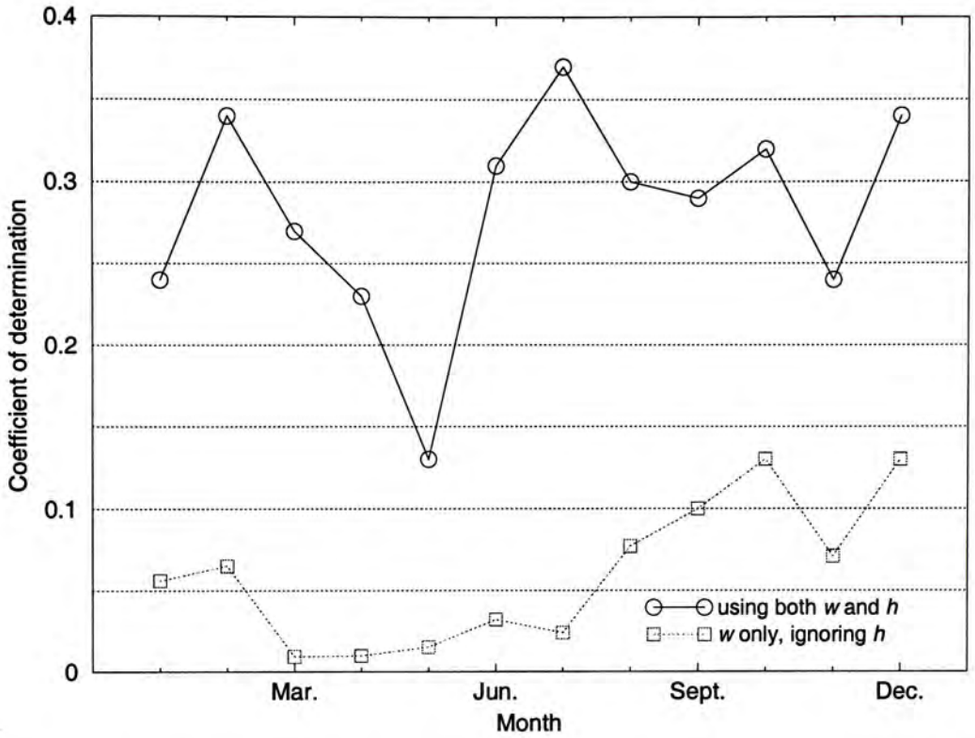

Figure 6.6. Seasonal changes of the coefficient of determination. The solid line shows the proportion of variability of the rainfall explained by both independent variables h and w, while the dashed line shows that by w ignoring h. The effect of terrain height is in general more significant than the uplift flow of sea-land breeze system, especially in summer.

However in summer the atmosphere is nearly always conditionally unstable (Jackson and Hsu, 1996). Sea-land breeze rarely occurs, only 1–3 days in a month, giving nearly insignificant contribution to the total rainfall. The heavy rains are mainly contributed by monsoon troughs and tropical cyclones, which overshadow the effect of the sea-land convection, so that the standardized coefficient of w even becomes negative.

The effect of terrain height is in general more significant than the uplift flow of the sea-land breeze system, especially in summer. The seasonal changes in the association is also revealed in Figure 6.6, by the monthly variation of the coefficient of determination. Here the upper line shows the proportion of the variability of the rainfall explained by both independent variables h and w together, while the lower line shows that explained by w ignoring h. The effect by h and w is roughly suppressed in spring and early summer, and rises in autumn and winter.

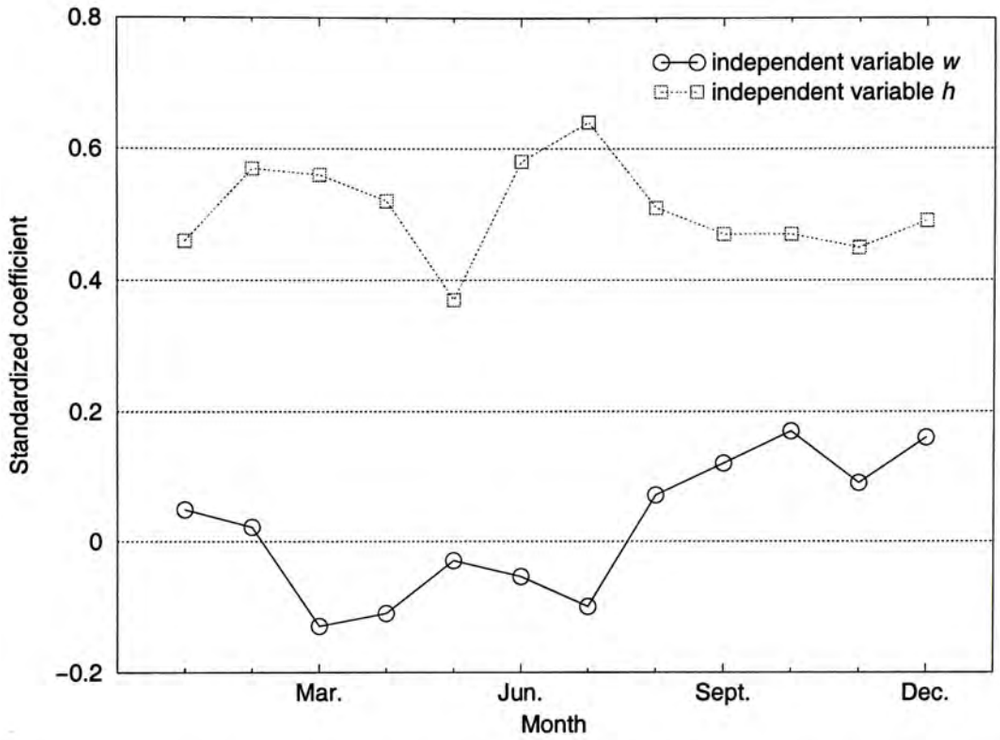

Figure 6.7. Seasonal changes of standardized coefficients referring to the model with both w and h as independent variables. The standardized coefficient shows the relative importance of the independent variable, by indicating the amount of standard deviation by which an increase in the vertical flow by one standard deviation could result in an increase in the annual rainfall. The contribution of the sea-land breeze system is relatively higher in winter than in summer, which is consistent with the seasonal changes in its frequency of occurrence.

It is of interest to point that the effect of terrain height is comparably dominant in February and July. The underlying factors are yet unclear and would require further studies.

6.6 Conclusion

The spatial rainfall distribution in Hong Kong is to some extent correlated with the vertical motion of the sea-land breeze circulation in autumn and in winter.

Chapter 7

Conclusion

Sea-land breeze circulation can be regarded as a kind of forced inertio-gravity oscillation, thermally driven by the uneven distribution of heating which varies in time with a period of a day.

In light of this, a three-dimensional linear model is developed, which starts with the different heating rates over land and sea, which attempts to capture the influence of the coastline pattern on the wind system.

Using the model, we have performed a semi-analytic harmonic analysis, in which the sea-land breeze circulation is viewed as a resultant flow of modes with different time and vertical length scales.

We see that the different heating rates over the land and the sea drive the entire effect, and all measures of the sea-land breeze circulation are proportional to the differential heating. The latitude, the stability of the atmosphere and the different frictional forces all play some role in controlling the extent of the penetration landwards and seawards.

We also see that the fundamental spatial mode (m=1) primarily determines the horizontal structure of the sea-land breeze system. The vertical structure is mainly related to the first three spatial modes (m=1, 2, 3).

From the result, we also found that the presence of the higher temporal harmonics (with frequencies higher than $2\pi/T$, where $T = 24$ hours) (a) breaks the symmetry between the sea-breeze phase and the land-breeze phase, (b) causes a

shorter horizontal extent, and (c) causes a larger normal component across the coastline.

It is worthwhile to note that the model reveals that the onset of the sea-breeze is characterised by the sinking of the offshore flow above surface wind.

Furthermore, we also see that the sub-circulation of each mode from different parts of the coast interact, when the radius of coastline curvature is less than the horizontal extent of the mode. When applied to the case of a circular island, the model reveals that the sea-breeze phase onsets earlier and persists longer for small islands. In the sea-breeze phase, the interaction of the horizontal flow gives rise to a strong ascending flow, when the island size is comparable to the horizontal extent of the sea breeze circulation. The intensification of the vertical velocity weakens rapidly as the radius increases.

When we apply the model to the case of Hong Kong, the following conclusion are drawn.

According to the meteorological statistics, Hong Kong is often subject to the influence of sea-land breezes, with the highest frequency in winter and autumn. The modeling results confirm that in the sea-breeze phase, there are three wind branches, leading to various convergence zones. In the land-breeze phase, the wind system is much simpler. The main features of the sea-land breeze system are determined by the coastline, the sun-facing slopes and the urban heat islands only weakly modify the wind system.

A statistical study on the association of the spatial rainfall distribution in Hong Kong and the average vertical motion due to sea-land breeze circulation is performed. It shows that they are correlated in autumn and in winter.

The treatment and the mathematical approach of the model go beyond the sea-land breeze application; it can be used to study other thermally driven secondary circulation.

However, beyond the factors explored in this work, the sea-land breeze system

is further complicated by the following factors.

1. The blocking and the lifting of the flow by the orography. The lifting and blocking effect to the flow are especially important to the situation of Hong Kong, since the landscape of Hong Kong is dominated by low mountains and hills. For example, the land breeze is observed to be enhanced over the lee side of Lantau island (Wai et al., 1995).

2. The precipation processes and the attendant condensational heating associated with land-sea breeze circulation. The moisture flux carried by the sea breeze is one of the important source of heating in the storm development (Wai et al., 1995; Jackson and Hsu, 1996).

3. The effect of synoptic-scale circulation, such as monsoons and frontal passages, on the system. The background wind modifies both the strength and coverage of the wind branches developed by the sea-land breeze system (Zhang and Zhang, 1997).The deflection of the breeze by the terrain is also found stronger in the presence of light synoptic winds (Yeung et al., 1991).

However, since the sea-land breeze system is driven by the diurnal cycle of differential heating, it depends mainly on the physical features of the coastline. This is already captured in this simple model.

Appendix A

Linearisation of the basic equations

The basic equations[1] for a three-dimensional motion of an incompressible atmosphere may be written as follows:

$$\partial_t u_* + (\mathbf{v}_* \cdot \nabla) u_* - f v_* + \frac{1}{\rho_*} \partial_x p_* + F_x = 0 \tag{A.1}$$

$$\partial_t v_* + (\mathbf{v}_* \cdot \nabla) v_* + f u_* + \frac{1}{\rho_*} \partial_y p_* + F_y = 0 \tag{A.2}$$

$$\partial_t w_* + (\mathbf{v}_* \cdot \nabla) w_* + g + \frac{1}{\rho_*} \partial_z p_* + F_z = 0 \tag{A.3}$$

$$\partial_t \theta_* + (\mathbf{v}_* \cdot \nabla) \theta_* = \frac{J}{c_p T_*} \tag{A.4}$$

$$\partial_x u_* + \partial_y v_* + \partial_z w_* = 0 \tag{A.5}$$

where $\mathbf{v}_* = (u_*, v_*, w_*)$ denotes the velocity vector field, and J the rate of heating per unit mass owing to radiation, conduction, and latent heat release. Other symbols carry their conventional meaning.

The potential temperature θ is related to pressure and density by

$$\theta_* = T_* \left(\frac{p_s}{p_*} \right)^{R/c_p} = \frac{p_*}{\rho_* R} \left(\frac{p_s}{p_*} \right)^{R/c_p} \tag{A.6}$$

where the equation of state of ideal gas is assumed. We now linearise (A.2)–(A.6) by letting

$$u_* = \overline{u} + u, \qquad v_* = \overline{v} + v$$

$$w_* = w, \qquad p_* = \overline{p}(z) + p$$

[1]The derivation is an extention of the work of Holton (1992).

$$\rho_* = \rho_0 + \rho', \qquad \theta_* = \theta_0(z) + \theta' \tag{A.7}$$

where the basic state air flow and the density ρ_0 are both assumed to be constant. The basic state pressure field must satisfy the hydrostatic equation

$$\partial_z \overline{p} = -\rho_0 g \tag{A.8}$$

while the basic state potential temperature must satisfy (A.6), so that

$$\ln \theta_0 = \frac{c_p}{R} \ln \overline{p} - \ln \rho_0 + \text{const} \tag{A.9}$$

The linearized equations are obtained by substituting (A.7) into (A.2)–(A.6) and neglecting all terms that are products of the perturbation variables. For example, the last two terms in (A.4) are approximated as follows:

$$\begin{aligned} \frac{1}{\rho_*}\partial_z p_* + g &= \frac{1}{\rho_0 + \rho'}\left(\partial_z \overline{p} + \partial_z p\right) + g \\ &\approx \frac{1}{\rho_0}\partial_z \overline{p}\left(1 - \frac{\rho'}{\rho_0}\right) + \frac{1}{\rho_0} + g = \frac{1}{\rho_0}\partial_z p + \frac{\rho'}{\rho_0} g \end{aligned} \tag{A.10}$$

where (A.8) has been used to eliminate $\overline{p}$. The perturbation form of (A.6) is obtained by noting that

$$\ln\left[\theta_0\left(1 + \frac{\theta'}{\theta_0}\right)\right] = \frac{c_p}{R} \ln\left[\overline{p}\left(1 + \frac{p}{\overline{p}}\right)\right] - \ln\left[\rho_0\left(1 + \frac{\rho'}{\rho_0}\right)\right] + \text{const} \tag{A.11}$$

Note that

$$\ln\left[\theta_0\left(1 + \frac{\theta'}{\theta_0}\right)\right] = \ln \theta_0 + \ln\left(1 + \frac{\theta'}{\theta_0}\right)$$

and that

$$\ln\left(1 + \frac{\theta'}{\theta_0}\right) \approx \frac{\theta'}{\theta_0}$$

for $\frac{\theta'}{\theta_0} \ll 1$. With the aid of (A.9), (A.11) may be approximated by

$$\frac{\theta'}{\theta_0} \approx \frac{c_p}{R}\frac{p}{\overline{p}} - \frac{\rho'}{\rho_0} \tag{A.12}$$

Solving for ρ' yields

$$\rho' \approx -\rho_0 \frac{\theta'}{\theta_0} + \frac{p}{c_s^2} \tag{A.13}$$

where $c_s^2 = \overline{p}R/c_p\rho_0$ is the square of the speed of sound. For buoyancy wave motions $|\rho_0\theta'/\theta_0| \gg |p/c_s^2|$; i.e., density fluctuations due to pressure changes are small compared with those due to temperature changes. Therefore, to a first approximation,

$$\frac{\theta'}{\theta_0} = -\frac{\rho'}{\rho_0} \tag{A.14}$$

Using (A.10)–(A.14) and defining $\theta = g\theta'/\theta_0$, the linearized version of the set (A.2)–(A.5) can be written as[2]

$$(\partial_t + \overline{\mathbf{v}} \cdot \nabla)\, u - fv + \frac{1}{\rho_0}\partial_x p + F_x = 0 \tag{A.15}$$

$$(\partial_t + \overline{\mathbf{v}} \cdot \nabla)\, v + fu + \frac{1}{\rho_0}\partial_x p + F_y = 0 \tag{A.16}$$

$$(\partial_t + \overline{\mathbf{v}} \cdot \nabla)\, w - \theta + \frac{1}{\rho_0}\partial_z p + F_z = 0 \tag{A.17}$$

$$(\partial_t + \overline{\mathbf{v}} \cdot \nabla)\, \theta + N^2 w = \frac{gJ}{c_p T_0} \tag{A.18}$$

$$\partial_x u + \partial_y v + \partial_z w = 0 \tag{A.19}$$

where $T_0 = \overline{p}/R\rho_0$ is the basic state temperature, and $N^2 = g\partial_z\theta_0$ is the square of the buoyancy frequency, which is assumed to be constant. Strictly speaking, N^2 cannot be exactly constant if ρ_0 is constant. However, for shallow disturbance the variation of N^2 with height is unimportant.

To conclude, it is noted that the linearization assumes the validity of the ideal gas condition and the Boussineq approximation. In this approximation the atmosphere is considered to be incompressible and the vertical variation of density is neglected except where coupled with gravity. It also requires that the vertical scale of motion is less than the atmospheric scale height (about 8 km) for the approximation to be valid.

[2]For the linearization to be valid, it is required that the quadratic terms in the perturbation variables be small compared to the dominant linear terms; however, not necessary that the perturbation quantities be small compared to the mean values.

Bibliography

Abbs, D. J., 1986: Sea-breeze interactions along a concave coastline in southern australia: Observations and numerical modeling study. *Mon. Weather Rev.*, **114**, 831–848.

Abe, S. and Yoshida, T., 1982: The effect of the width of a peninsula on the sea breeze. *J. Meteor. Soc. Japan*, **60**, 1074–1084.

Anthes, R. A., 1978: The height of the planetary boundary layer and the production of circulation in a sea breeze model. *J. Atmos. Sci.*, **35**, 1231–1239.

Anthes, R. A., 1984: Enhancement of convective precipation by mesoscale variations in vegetative covering in semiarid regions. *J. Appl. Meteor.*, **23**, 541–554.

Arritt, R. W., 1989: Numerical modeling of the offshore extent of sea breezes. *Q. J. R. Meteorol. Soc.*, **115**, 547–570.

Atkinson, B. W., 1984: *Meso-scale Atmospheric Circulations.* Academic Press, London.

Buchan, A., 1860: *Handy book of meteorology.* Blackwood and Sons.

Chan, J. C. and Ng, M. H., 1993: Morning showers over Hong Kong in summer. *HKMets BULLETIN*, **3**(1), 14–25.

Chin, P. C., 1963: Diurnal variation of winds over Hong Kong. *Journal of Tropical Geography*, **17**, 46–56.

Dalu, G. A. and Pielke, R. A., 1998: An analytical study of the sea breeze. *J. Atmos. Sci.*, **46**, 1815–1825.

Davis, W. M., Schultz, L. G., and Pearson, C. E., 1889: An investigation of the sea-breeze. *New Engl. Meteor. Soc. Obser.*, **21**, 214–264.

Defant, F., 1951: Local winds. In *Compendium of Meteorology*, pages 655–672. American Meteorology Society.

Fisher, E. L., 1960: An observational study of the sea breeze. *J. Meteorol.*, **17**, 645–660.

Halley, E., 1686: An historical account of the trade-winds and monsoons observable in the seas between and near the tropics with an attempt to assign the physical cause of said winds. *Phil. Trans. R. Soc. London*, **26**(153–168).

Haurwitz, B., 1947: Comments on the sea-breeze circulation. *J. Meteor.*, **4**, 1–8.

Holton, J. R., 1992: *An introduction to Dynamical Meteorology.* Academic Press, California.

Jackson, I. and Hsu, S. I., 1996: Aspects of rainfall and water balance of Hong Kong. Occasional Paper 115, Department of Geography, the Chinese University of Hong Kong.

Jeffreys, H., 1922: On the dynamics of wind. *Q. J. R. Meteorol. Soc.*, **48**, 29–46.

Lu, R. and Turco, R. P., 1994: Air pollutant transport in a coastal environment. Part I: Two-dimensional simulations of sea-breeze and mountain effects. *J. Atmos. Sci.*, **51**, 2285–2308.

Mahrer, Y. and Segal, M., 1985: On the effects of islands' geometry and size on inducing sea breeze circulation. *Mon. Weather Rev.*, **333**, 170–174.

Man, K. M. and Walsh, J. E., 1976: On the relative intensities of sea and land breezes. *J. Atmos. Sci.*, **33**, 242–251.

Mass, C. and Dempsey, D. P., 1985: A one-level, mesoscale model for diagnosing surface winds in mountainous and coastal regions. *Mon. Weather Rev.*, **113**.

McPherson, R. D., 1970: A numerical study of the effect of a coastal irregularity on the sea breeze. *J. Appl. Meteor.*, **9**, 767–777.

Neumann, J., 1951: Land breezes and nocturnal thunderstorms. *J. Meteorl.*, **8**, 60–67.

Neumann, J., 1973: The sea and land breezes in the classical Greek literature. *Bull. Amer. Meteor. Soc.*, **54**, 5–8.

Neumann, J., 1984: The coriolis force in relation to the sea and land breezes–a historical note. *Bull. Amer. Meteor. Soc.*, **65**(1), 24–26.

Ng, M. C. and Wong, K. P., 1996: 30-years mean rainfall in Hong Kong 1961–1990. Technical Note 88, Observatory of Hong Kong.

Niino, H., 1987: The linear theory of land and sea breeze circulation. *J. Meteor. Soc. Japan*, **65**, 901–920.

Ogura, Y. and Phillips, N. A., 1962: Scale analysis of deep and shallow convection. *J. Atmos. Sci.*, **19**, 173–179.

Press, W. H., Flannery, B. P., Teukolsky, S. A., and Vetterling, W. T., 1987: *Numerical Recipes: the art of scientific computing.* Cambridge University Press, London, 1st edition.

Rotunno, R., 1983: On the linear theory of land and sea breeze. *J. Meteor. Soc. Japan*, **40**, 1999–2009.

Schmidt, F. H., 1947: An elementary theory of the land- and sea-breeze circulation. *J. Meteorol.*, **4**, 9–15.

Simpson, J. E., 1994: *Sea Breeze and Local Winds.* Cambridge University Press, New York, 1st edition.

Smith, R. K., Crook, N., and Roff, G., 1982: The morning glory: an extraordinary atmospheric undular bore. *Q. J. R. Meteorol. Soc.*, **108**, 937–956.

Stanhill, G., 1995: Solar dimming and urban heating at Hong Kong. *Int. J. Climatol.*, **15**, 933–941.

Sun, W. Y. and Orlanski, I., 1981: Large mesoscale convection and sea breeze circulation. Part II: Nonlinear numerical model. *J. Atmos. Sci.*, **38**, 1694–1706.

Wai, M. M. K., 1993: Diurnal atmospheric secondary circulations over Hong Kong. *HKMets BULLETIN*, **3**(2), 9–20.

Wai, M. M. K., Welsh, P. T., and Ma, W. M., 1995: The timing and distribution of summer convective rainfall over Hong Kong and South China. *HKMets BULLETIN*, **5**, 3–21.

Walsh, J. E., 1974: Sea breeze theory and application. *J. Atmos. Sci.*, **31**, 2012–2026.

Xian, Z. and Pielke, R. A., 1991: The effects of width of landmasses on the development of sea breezes. *J. Appl. Meteor.*, **30**, 1280–1304.

Yan, H. and Anthes, R. A., 1987: The effect of latitude on the sea breeze. *Mon. Weather Rev.*, **115**, 939–956.

Yeung, K. K., Chan, W. L., Wan, B., Kimura, F., and Yoshikawa, T., 1991: Simulation of boundary layer flow in Hong Kong. *Atmospheric Environment*, **25A**, 2161–2172.

Young, K. and Zhang, M., 1999: Analytic study of sea-land breezes. *Advances in Atmospheric Sciences*, **16**, 263–278.

Zhang, L. F. and Zhang, M., 1999: Study of sea-land breeze system in the Zhujiang Delta. *Chinese Journal of Atmospheric Sciences*, **23**, 581–589.

Zhang, M. and Lam, W. Y., 1996: Observational study of sea-land breezes in Zhujiang Estuary. To be published.

Zhang, M., Zhang, L., Ngan, S. F., and Young, K., 1997: Diagnosis of secondary circulations driven by periodic diabatic forcing. In *The 4th Chinese National Conference of Dynamical Meteorology.*

Zhang, M. and Zhang, L. F., 1997: Study of the sea-land breeze system in Hong Kong. *HKMets BULLETIN*, **7**, 22–43.

Zhang, M., Zhang, L. F., Ngan, S. F., and Young, K., 1999: A calculation method on the sea breeze circulation. *Chinese Journal of Atmospheric Sciences*, **23**, 693–702.